Nemesis

TEAM 06 Technical Report to the 2025 EuRoC

Alfieri Gabriele [1)], Antonelli Giacomo [2)], Bandini Daniele [3)], Bacchini Giovanni [4)], Basso Nicolò [5)], Benelkaid Amira [6)], Bernabei Anna [7)], Bevoni Riccardo Alessandro [8)], Biondi Sara [9)], Braglia Davide [10)], Brino Valeria [11)], Bruzzi Edoardo [12)], Cantero Pedro Vico [13)], Capizzi Matteo [14)], Capozucca Giorgia [15)], Cappetti Leonardo [16)], Casadei Christian [17)], Cecchini Andrea [18)], Cirulli Greta [19)], Collaone Damiano [20)], Dascola Diego [21)], Donà Maria [22)], Fantoni Simone [23)], Farini Giacomo [24)], Ferrari Sara [25)], Iannì Sara [26)], Iuretta Matilde [27)], Kostner Lois [28)], Laghi Caterina [29)], Latufara Miriam [30)], Laroussi Zinedine [31)], Matti Lorenzo [32)], Mattucci Mattia [33)], Monticelli Alessandro [34)], Neri Leonardo Francesco [35)], Nicoletti Alessandro [36)], Mrass Alessio [37)], Olmi Leonardo [38)], Paoletti Andrea [39)], Pedicini Federico [40)], Pedretti Tobia [41)], Perugini Giammarco [42)], Petrani Alex [43)], Piccinini Lorenzo [44)], Piersanti Luca [45)], Pintauro Lorenzo [46)], Poncato Flavia [47)], Ravaioli Lorenzo [48)], Romagnolo Maurizio [49)], Rosati Matilde [50)], Rossi Emanuele [51)], Sberlati Thomas [52)], Scattolini Caio [53)], Souza Caio Eduardo [54)], and Trerè Filippo [55)]

[5)] President, Aurora Rocketry, University of Bologna, Forlì - FC
[28)] Vice president, Aurora Rocketry, University of Bologna, Bologna - FC
[44)] Nemesis Project Manager, Aurora Rocketry, University of Bologna, Forlì - FC
[3, 4, 35, 37, 40, 43, 46, 53)] Mission Analysis, Aurora Rocketry, University of Bologna, Forlì - FC
[1, 9, 12, 14, 20, 21, 31, 41, 50, 51, 52, 55)] Aerodynamics Department, Aurora Rocketry, University of Bologna, Forlì - FC
[6, 15, 16, 22, 25, 29, 39)] Recovery Department, Aurora Rocketry, University of Bologna, Forlì - FC
[8, 23, 30, 32, 33, 48)] Electronics Department, Aurora Rocketry, University of Bologna, Forlì - FC
[7, 10, 11, 18, 19, 24, 38, 42, 45, 47, 49)] Structure Department, Aurora Rocketry, University of Bologna, Forlì - FC
[2, 13, 34)] Software Department, Aurora Rocketry, University of Bologna, Cesena - FC
[26, 27)] Media & Logistics, Aurora Rocketry, University of Bologna, Bologna - FC
[36, 54)] Propulsion, Aurora Rocketry, University of Bologna, Bologna - FC
[17)] Guidance, Navigation & Control, Aurora Rocketry, University of Bologna, Bologna - FC

ABSTRACT

Nemesis is the first competition rocket developed by Aurora, the University of Bologna's rocketry team. The rocket features an aerostructure manufactured from aluminum and composite materials, and is powered by a Cesaroni Pro75 6GXL-8187M1545 COTS solid rocket motor. Its payload, a 1U CubeSat named Aether, is equipped with a Software-Defined Radio capable of receiving L-band satellite data during the ascension phase. The project has a scientific purpose to demonstrate the applicability of the payload in the aerospace sector. Nemesis involves a dual-event recovery system without separation.

Symbols and Acronyms

1U	One Unit
3 D	Tridimensional
A	Amperes/ Area [m^2]
ABS	Acrilonitrile butadiene stirene
ACARS	Aircraft Communications Addressing and Reporting System
ADS	Automatic Dependent Surveillance
AGL	Above Ground Level
Ah	Amper per hour

APCP	Ammonium Perclorate Composite Propellant
AR	Aspect Ratio [-]
a	Speed of sound [m/s]
C	Design parameter of the nosecone [-]/ Generic coefficient [-]/ Battery capacity [Ah]/ Celsius
CAD	Computer Assisted Design
CFD	Computational Fluid Dynamic
CG	Center of Gravity
CNC	Computer Numerical Control
CO_2	Carbon dioxide
COTS	Commercial Of-The-Shelf
c	Chord [m]/ Speed of light [m/s]
D	Rocket diameter [m]
DC	Direct Current
DN	Denominator constant [Pa]
DoD	Depth of Discharge [-]
d	Diameter [m]
E	Energy [Wh]
EGC	Enhanced Group Call
F	Force [N]
FRR	Flight Readiness Review
f	Frequency [1/s]
ft	Feets
G	Shear modulus [Pa]
GNC	Guidance, Navigation and Control
GPS	Global Positionins System
GSE	Ground Support Equipement
g	Grams/ Gravitational acceleration [m/s^2]
Hz	Hertz
I	Turbolence intensity [-]/ Geometric inertia [m^4]/ Moment of inertia [kg*mm^2]
I2C	Inter-Integrated Circuit
IMU	Inertial Measurement Unit
J	Geometric rotational inertia [mm^4]
K	Kelvin
k	Turbolent kinetic energy [m^2*s^-2]
kg	Kilograms
L	Nosecone length [m]/ Rocket length [m]/ Antenna length [m]/ Lift [N]
LED	Light Emitting Diode
$LiFePo_4$	Lithium Iron Phosphate

LNA	Low Noise Amplifier
LRR	Launch Readiness Review
l	Litres
M	Mach number [-]/ Moment [N*m]
MOSFET	Metal-Oxide-Semiconductor Field-Effect Transistor
m	Meters
min	Minutes
N	Newtons/ Number of batteries [-]/ Axial force [N]
NACA	National Advisory Committee for Aeronautics
F	Farads
P	Power [W]/ Pressure [Pa]
Pa	Pascal
PCB	Printed Computer Board
PET	Polyethylene terephthalate
PVC	Polyvinyl chloride
p	Pressure
R	Raius parameter of the nosecone design
RANS	Reynolds-Averaged Navier-Stokes
Re	Reynolds number [-]
RF	Radio Frequency
S	Surface [m^2]
SD	Secure Digital
SDR	Software-Defined Radio
SF	Safety Factor [-]
SMA	SubMiniature Version A
SNR	Signal-to-Noise Ratio [-]
SRD	System Reference Document
SRAD	Student Researched And Developed
SST	Shear Stress Transport
s	Seconds
T	Temeprature [K]/ Transverse force [N]
t	Local fin thickness [m]/ Time [s]
tpu	Thermoplastic Polyurethane
USB	Universal Serial Bus
V	Effective velocity [m/s]/ Volts
v	Velocity [m/s]
W	Watts
x	Horizontale coordinate [m]
y	Vertical coordinate [m]

y+	Non-dimensional wall distance [-]
α	Angle of attach [deg]
δ	Boundary layer thickness [m]
ε	Permittivity [-]
γ	Heat capacity ratio [-]
λ	Taper ratio [-]/ Wave length [m]
η	Efficiency [-]
ρ	Density [kg/m^3]
θ	Angular coordinate of the nosecon profile [rad]
Ω	Ohms
ω	Specific dissipation rate [1/s]

Table of Contents

1 Introduction

1.1 Overview

Aurora Rocketry is an undergraduate student-run rocket design group from the University of Bologna, founded in 2024. The team provides its members with an enriching opportunity to deeply engage with aerospace engineering through the design, construction, and experimentation of rockets from the ground up. In addition to the students' efforts, this project was made possible by the kind assistance of the faculty, researchers, and technicians who are all passionate about forming the future of aerospace professionals. Aurora Rocketry is essentially built on a holistic learning methodology. Our team cares about its members' professional growth at each step of the rocket development process: from the design, to the simulation, production, testing and launch. The team's offering extends beyond technical proficiency to include problem-solving, teamwork, communication, and the application of both theoretical and practical knowledge. The team aims to prepare its members for professional careers in engineering, aerospace, and other fields by offering them real-world applications and hands-on experience.

Since the team's founding, Aurora Rocketry has designed two rockets and tested all their parts; it also supports a variety of technology conferences, meetings and round tables. All of these endeavors have provided the team with copious exposure and experience and enabled its members to identify themselves and challenge one another to ever-higher accomplishments. Borealis and Nemesis are two notable rockets that the team has successfully designed and constructed over the years. Our team also challenged our projects by experimenting with novel materials, technologies, and rocket-building methods.

1.2 Stakeholders

A crucial component of Aurora Rocketry success is the inspiration and motivation from its stakeholders thanks to whom the team's enthusiasm for innovation and exploration in the field of aerospace engineering is implemented. Aurora Rocketry program includes two of its main goals: the enchantment of society's understanding of science and engineering and taking them in everyday life, encouraging all the students and others passionate about aerospace to follow their dreams. The most important parties involved are:

A. The Team's Students: In Aurora Rocketry, the students are the biggest assets. The team gives students a chance to utilize their academic foundation to provide solutions to real engineering challenges, sparking potential personal and professional development. Students, through involvement, have the opportunity to sharpen their skills in multiple disciplines of engineering all while being part of a team that is designing, developing, and testing new technologies.

B. External Audiences and Students: The group's communication and outreach practices encourage and inspire a larger audience from other students at the University of Bologna to those outside the confines of the university.

C. The University of Bologna: The University of Bologna is a respected institution and its reputation as a leader in engineering and innovation is supported by its participation in national and international competitions, conferences, and other events.

D. Sponsors and Partners: Sponsor partnerships at Aurora Rocketry are win-win scenarios. Sponsors have high-quality exposure through their association with such cutting-edge, high-profile leadership in the field of rocketry, and the team at Aurora Rocketry gets tremendous gains from access to the financial,

materials, and expertise for their work. Both parties can use these partnerships to do more advanced research and development that advances the aerospace community as a whole. Our team has already received support from a few sponsors, including:

- Regione Emilia Romagna;
- Ansys and Solidworks, who together provide us with software programs;
- Cobalm SRL, who offers a waterjet system to cut carbon fibre;
- Basso PB SRL, who has offered our team a high-performance computing server;
- C.L.V. SRL, which performed high-precision CNC machining on the rocket tubes and flanges;
- BCC Ravennate Forlivese, who granted financial contributions to our team;
- WD-40 Company, which has gifted some products to our team.

1.3 Team structure

Aurora Rocketry employs 95 members on its staff, recruited from various faculties at the University of Bologna, including engineering, math, architecture, audiovisual communication, and modern languages. This is aimed at providing a rich, multidisciplinary setup where lots of individuals get together and place varying ideas on the table, making the work of the team more powerful and creative. There are some specialized groups in the team, with a specific area of rocket development:

- Aerodynamics;
- Electronics;
- Guidance, Navigation & Control (GNC);
- Recovery Systems;
- Propulsion;
- Mission Analysis;
- Software;
- Structural Design;
- Public Relations;
- Marketing.

Each and every one of these groups plays a very crucial role in the designing and development of the rockets, contributing its part to make each project successful. The company is managed by a president, with a vice president as his second in command, whereas each technical group and committee is managed by a head. Their university advisor, Professor Fabrizio Ponti, a highly esteemed member of the University of Bologna, provides guidance and mentorship to ensure that the project is based on fundamental scientific principles. The organizational structure of Aurora Rocketry is to encourage responsibility, unity, and creativity. The members are pushed to be responsible for their own projects as they work towards the greater goals of the team. The company ensures every member is listened to, thus the team is lively and inclusive where the thoughts and opinions are treated equally with respect. There are also weekly communications and coordination meetings, along with the technical teams which keep project goals in line for everybody. At each meeting's end, the coordinator writes a report where everyone can read the progress made, the decisions taken, and the next steps for the project. This process-focused approach keeps everybody aligned, enabling good decision-making and successful project execution.

1.4 Team management strategies

Good organizational and communication openness are crucial to ensure smooth operations and high levels of productivity in Aurora Rocketry. The team employs many computer softwares to facilitate ease of collaboration and ensure that all members are well aware and punctual. The main management strategies are:

Communication Tools: Slack and WhatsApp are the fundamental communication tools that facilitate the members to provide real-time and asynchronous feedback. The tools provide a direct channel whereby the members can exchange ideas, clarify problems, and exchange information in real-time.

3D Modeling and Collaboration in Teams: The team employs SolidWorks as its CAD program of choice for accurate design and simulation. This aspect allows team members to collaborate while they brainstorm and imagine components of the rocket in a way that each component simply fits into the final product. A number of team members can work on a single project at once, making it time-efficient and promoting in-session collaboration.

Document and Data Management: All project documents, team documents, and research data are stored in Google Drive and it is therefore a sharable and centralized repository and is accessible to all.Sharing of resources, technical data, and previous project documents is hence made convenient across groups and committees.

Project Tracking and Management: Microsoft Excel is utilized by the team for a number of organizational activities such as tracking the members' work, task checklists, and calculating essential project parameters. This puts the team ahead of time and delivers quality results, as well as identifying potential project development timeline chokepoints.

Applying these tools and methods, Aurora Rocketry has established a solid and successful approach to the management of complex projects. Through open communication and collaboration, the team can address challenges and accomplish its mandate. This dynamic organizational and management system have endeared Aurora Rocketry as a successful student club not only in promoting members' academic and professional growth but also in venturing beyond the limits of experimental rocketry. The team's success is proof of unity in strength, commitment, and common passion for innovation.

2 System architecture

2.1 Overview

Nemesis is a single-stage rocket propelled by a COTS solid motor designed to carry a 1kg payload up to an apogee of 3000 m and to return safely to the ground thanks to a recovery system. The rocket was especially designed for the competition with reliability, ease of maintenance and assembly in mind. Its architecture is divided into 5 main subsystems: Propulsion, Aerostructure, Recovery, Payload and Electronics.

The aerostructure subsystem is the one responsible for the organisation, stability and integrity of the rocket; in fact, the airframe divides Nemesis into 4 subsections: the lower tube, which contains the propulsion system, the electronics bay, the higher tube, which includes the recovery system, and the nosecone, where the payload is located.

The propulsion is, as already mentioned, based on a COTS motor, which is positioned in the lower tube, at the bottom of the rocket. The Recovery subsystem is a redundant dual-event system, where the separation is powered by CO2 and black powder. The detection of the events is responsibility of the Electronics subsystem, a fully redundant SRAD and COTS system positioned in the electronics bay. Finally, the last subsystem is the Payload, a satellite communication electronic system positioned in the nosecone and made for testing the effect of speed, vibrations and acceleration on wireless data transfer.

2.2 Propulsion subsystem

1 Motor

The heart of the propulsion subsystem is a Pro75 6GXL-8187M1545-P-GR commercial off-the-shelf solid rocket motor produced by Cesaroni Technologies Inc. [1]. It uses an non-toxic APCP-based solid propellant commercially known as Green3 and produces 8187 Ns of total impulse in 5.3 seconds. Like most solid rocket motors, this model generally uses an electrically operated pyrotechnic igniter to initiate the combustion of the propellant in the combustion chamber. In this case the electronic ignition system will be provided by EuRoC, as determined by the SRD [2]. This igniter is to be inserted in the motor only after explicit authorization is given during launch preparations, according to the dedicated checklist (See Appendix F, Checklist #11). From this moment onwards, motor arming and ignition depends only on the EuRoC-provided launch support equipment and ground station.

2 Motor centering

The external diameter of the motor is far inferior to that of the rocket body tube; consequentially, structural elements have been implemented to make sure the motor stays centered during all phases of flight. The rocket's aftmost aluminum body tube hosts the thrust-bearing motor bulkhead. Its center section is designed to have room for the first few centimeters of the front end of the phenolic tube in which the motor tube is to be inserted, to contribute to a better fit inside the centering rings system.

Connection between the motor casing and the phenolic tube is guaranteed by the Aeropack motor retainer in the rear: the foremost part of the retainer is glued to the phenolic tube, while the aftmost is screwed to the other, enclosing the motor's aft closure between them as in Figure 2.1.

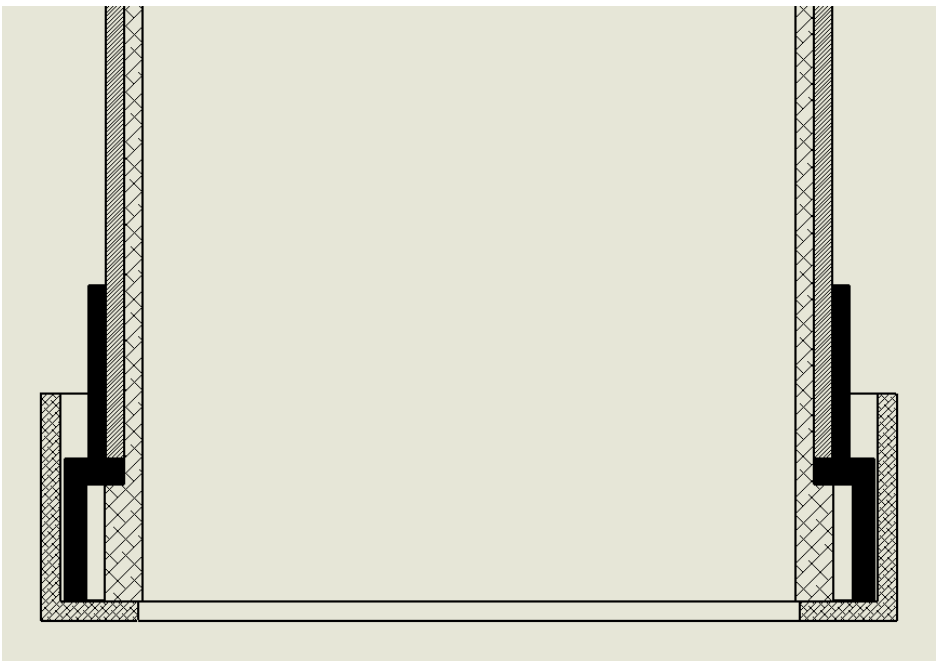

Fig. 2.1: Section view of the Aeropack motor retainer parts, that shows how they interact with the motor tube to hold it in place.

To keep the motor centered further and further towards its nozzle, the phenolic board tube that contains the motor casing is glued to four aluminum centering rings; these centering rings are connected with three screws each to the rocket's body tube, to prevent the tube-and-rings assembly from falling from the rear end of the rocket (See Figure 2.2).

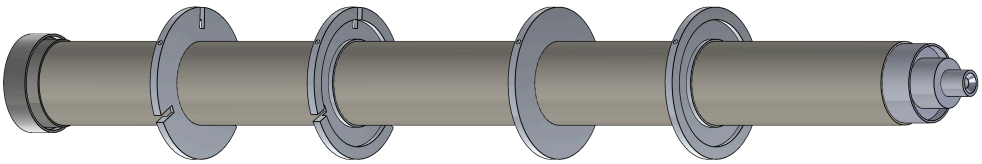

Fig. 2.2: Phenolic tube-centering rings assembly, with motor tube inserted and Aeropack retainer.

3 Thermic isolation

While not being a major concern (due to it being mostly addressed by the designers of the COTS system), thermic isolation of the motor has been improved by the presence of the phenolic board tube outside of the aluminum motor casing.

4 Thrust-transferring bodies and motor retention

The structural element that is mainly responsible for bearing the thrust of the motor is the front bulkhead, a thick aluminum component linked to the main rocket tube with seven M8 screws, and one M5 screw (intended for the attachment of a rail button), and that poses a solid obstacle to the thrust of the motor. Simulations show (see Appendix I) that this constitutes a safe and reliable architecture.

This component is also responsible for motor retention, as a hole in its top section (see Figure 2.3) allows a single 3/8″ screw to hold the motor from its forward closure. The thread in the forward closure used for this purpose is designed to be used as an anchorage point for recovery systems in full-diameter rocket designs, so it is expected to withstand the weight of the motor easily. Both thrust transfer and motor retention benefit from redundancy: the Aeropack retainer, together with the phenolic tube and the centering rings, provide an additional mean of stress bearing in both applications.

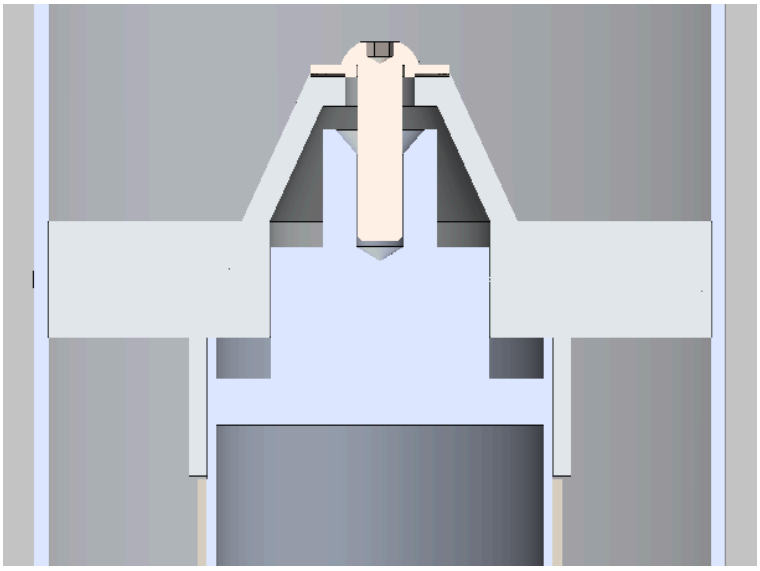

Fig. 2.3: Section view of the main thrust transferring bodies.

2.3 Aerostructure subsystem

Regarding the aerodynamic surfaces, the design method adopted aimed to maximize the apogee based on the initial conditions, such as the motor configuration and the baseline structure of the rocket's main body. In order to achieve this objective, advanced software tools tailored for these tasks, along with studies on the subject, were employed.

1 Nose cone

The nose-cone geometry (see Figure 2.6) was selected to maximize apogee while satisfying a design constraint: the aft portion of the nose cone had to be tangent to the body tube, enabling it to house the CubeSat (see Figure 2.4) and to allow radio communication through the radio-transparent fiberglass of the nose.

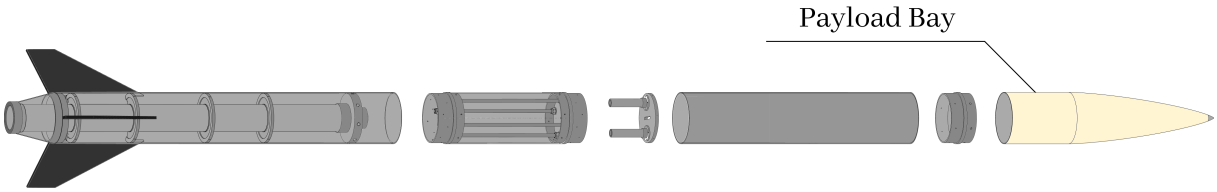

Fig. 2.4: Nose cone in the assembly.

Two nose-cone profiles commonly used at transonic speeds were evaluated: the tangent ogive and the Von Kármán ogive. For each nose-cone shape, a dedicated fin set was generated using an in-house script (MatFins.m, see Appendix J). The fin sets were iteratively optimized to maximize apogee while maintaining the required static margin, taking into account the combined mass properties (mass and center of mass) of the rocket tube, nose cone, and boat tail. This ensured that each nose-cone configuration was assessed under equivalent stability conditions.

The resulting configurations were simulated in RASAero, and the Von Kármán ogive was selected for Nemesis based on its superior apogee performance. This profile corresponds to the Haack series with $C = 0$, whose general equation for the nose radius is given by:

$$\begin{cases} x(\theta) = \frac{L}{2}(1 - \cos\theta) \\ y(\theta, C) = \frac{R}{\sqrt{\pi}}\sqrt{\theta - \frac{\sin(2\theta)}{2} + C\sin^3(\theta)} \end{cases} \tag{2.1}$$

Nosecone manufacturing used the wet lay-up method. Procedures:

- Mold making: a positive and a negative mold were designed and 3D-printed in ABS.
- Mold coating (release): to prevent epoxy from adhering to the mold surface, multiple layers of Zyvax Sealer GP and Zyvax Composite Shield were applied.
- Fiberglass lay-up: the mold was laminated with fiberglass fabric (E-glass 390 g/m², 2/2 twill, h 1250) and a two-component epoxy resin (SX10 EVO/M).
- Mold clamping: the positive mold was clamped onto the negative mold to squeeze out excess resin and achieve the correct fiber-to-epoxy ratio.
- Trimming and finishing: excess material was cut with a Dremel; the nosecone was sanded, coated with fiberglass bond, sanded again, sprayed with a filler base, and painted the final color.

2 Finset

The fin set comprises three swept fins (see Figure 2.7). The planform geometry was optimized with our in-house MatFins code through successive iterations to maximize apogee while meeting the prescribed static-margin and flutter-velocity constraints (Appendix J). The fin is a composite sandwich panel with the following layout (from one outer surface to the other): 0.6 mm carbon fiber / 3.0 mm Nomex / 0.4 mm carbon fiber / 3.0 mm Nomex / 0.6 mm carbon fiber (total thickness 7.6 mm).

During thickness sizing we balanced the influence of fin thickness on both peak altitude and aeroelastic safety. Apogee was verified with OpenRocket and RASAero, while aeroelastic screening relied on the conservative rapid-estimate criterion of Martin (NACA TN 4197) as implemented in Apogee (Peak-of-Flight Newsletter 615). The TN-4197/Apogee criterion is an empirical, conservative screening method suitable for subsonic to moderately transonic conditions, which correspond to the expected flight regime of Nemesis.

The flutter boundary speed was estimated with the semi-empirical expression:

$$v_f = a \sqrt{\frac{G_E}{\left(\frac{\mathrm{DN}\ \mathrm{AR}^3}{\left(\frac{t}{c_r}\right)^3 (\mathrm{AR}+2)}\right)\left(\frac{\lambda+1}{2}\right)\left(\frac{p}{p_0}\right)}} \tag{2.2}$$

The symbols represent:

- v_f flutter boundary speed (m/s).
- a local speed of sound (m/s), computed from ambient temperature.
- G_E shear modulus of the fin material (must be expressed in the same pressure units as DN).
- DN denominator constant (pressure units) computed from the centroid offset.
- AR aspect ratio.
- t local fin thickness (same length units as the chords).
- c_r root chord (ct denotes the tip chord and xr the sweep distance).
- λ taper ratio (ct / cr).
- p static ambient pressure at the evaluation altitude (same units as p0).
- p_0 reference sea-level pressure (e.g., 101.325 kPa).

The denominator constant has been calculated with:

$$\mathrm{DN} = \frac{24\,\varepsilon\,k\,p_0}{\pi} \tag{2.3}$$

Where:

$$\varepsilon = \frac{C_x}{c_r} - 0.25, \qquad C_x = \frac{2c_t x_r + c_t^2 + x_r c_r + c_t c_r + c_r^2}{3(c_r + c_t)} \tag{2.4}$$

Because the fin is a composite sandwich panel made of carbon-fiber skins and Nomex cores, it is necessary to compute an effective shear modulus GE - calculating a single-layer modulus would not be meaningful.

To obtain the GE we followed the homogenization approach from the report "*Calculation of the Effective Shear Modulus of Composite Sandwich Panels*" Rebhi et al. (2017) [3]. Assuming the shear strain is approximately uniform through the panel thickness, the effective shear modulus is obtained as a thickness-weighted average of the individual layer shear moduli:

$$G_E = \frac{\sum_{i=1}^{n} G_i t_i}{\sum_{i=1}^{n} t_i} \tag{2.5}$$

Where G_i and t_i are respectively the shear modulus and the thickness of the individual layer i. This expression corresponds to conservation of shear energy integrated over the entire thickness and is the relation proposed and validated in the cited literature for analogous cases.

Ultimately, we selected a final fin thickness of 7.6 mm. Under the worst-case conditions considered (altitude 750 m, maximum speed 256 m/s) the calculated flutter speed is $v_f = 775$ m/s, yielding a more than adequate flutter margin for the flight condition. The modelling prioritized achieving the target apogee, which accounts for the large flutter margin. The following graph shows the flutter velocity and the rocket velocity on the ordinate axis, plotted against altitude on the abscissa. The maximum flow velocity near the fins, obtained from CFD analysis (0.893 Mach, 2.5), is also included for comparison with the flutter velocity:

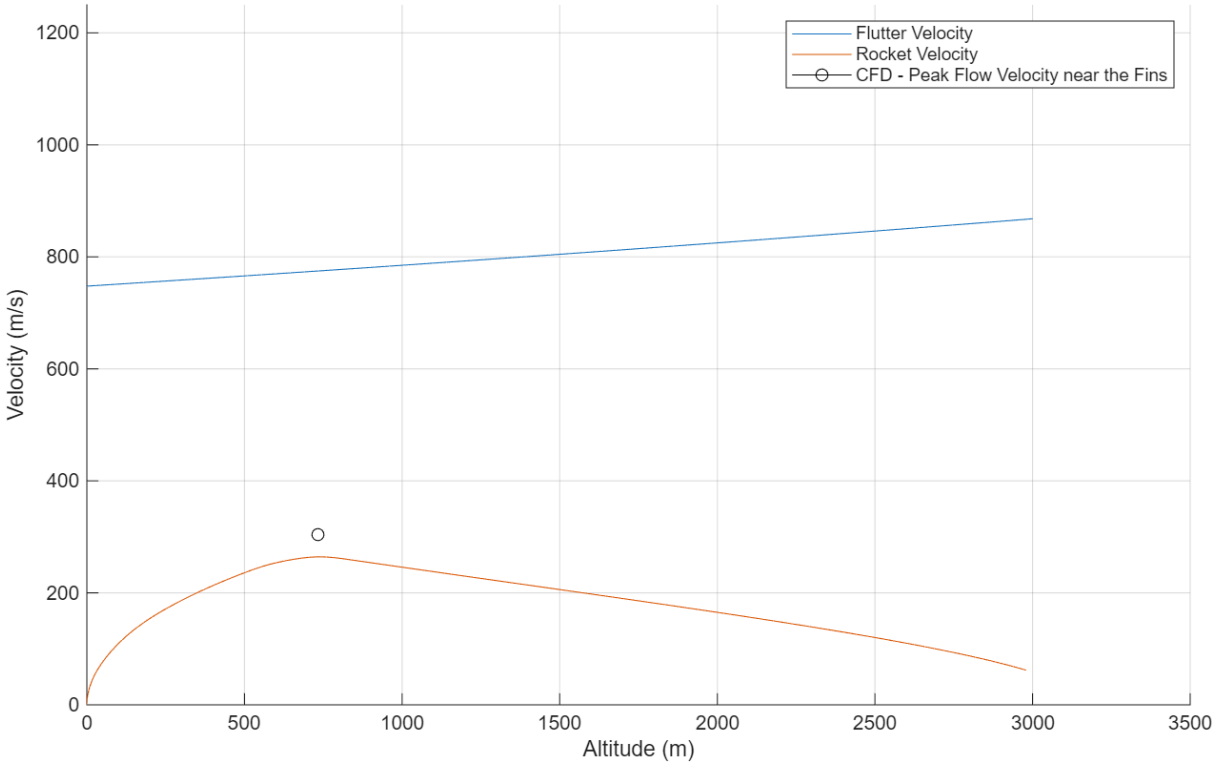

Fig. 2.5: Flutter velocity with respect to altitude.

The fins were fabricated as a sandwich made of carbon-fiber and Nomex, curated in a autoclave. After, the sandwich was cut through a computer controlled waterjet. The leading edge, trailing edge and side closure are made of 3d printed PET-CF material, which is inserted inside the carbon-fiber body and glued, for safety reasons.

3 Boat tail

A boat tail (see Figure 2.8) was incorporated into Nemesis to minimize base drag and to limit disturbed flow that could affect motor performance. Boat tail manufacturing used the vacuum casting method. Below are the procedures of such method:

- Mold making: a positive mold was designed and 3D-printed in ABS.
- Mold coating (release): to prevent epoxy from adhering to the mold surface, multiple layers of Zyvax Sealer GP and Zyvax Composite Shield were applied.
- Fiberglass lay-up: the mold was laminated with fiberglass fabric (E 390 g/m², 2/2 twill, h 1250) and a two-component epoxy resin (SX10 EVO/M).
- Bag preparation: due to the boat tail geometry, a toroidal bag was formed using HT15090T bags and M-SEAL 10×2 sealer.
- Vacuum: the laminate was wrapped in ELA20100/P1 release film and AER 160 breather felt, placed in the bag, fitted with a vacuum valve, sealed, and evacuated.
- Trimming and finishing: excess was cut with a Dremel; the part was sanded, coated with fiberglass bond, sanded again, sprayed with a filler base, and painted in the final color.

Fig. 2.6: The nose cone.

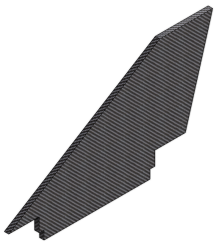

Fig. 2.7: One of the three fins.

Fig. 2.8: Nemesis boat tail.

4 CFD Setup

A set of CFD simulations were carried out in ANSYS Fluent on the full body configuration of the rocket, modeled as a clean and simplified geometry. This approach neglects small features such as screws and bolts, which would only complicate the meshing process and increase computational cost. The main objective was to determine the overall drag acting on the vehicle and, only qualitatively, to identify the regions of the rocket subjected to the highest aerodynamic loads, since more detailed studies will address this aspect. As a secondary outcome, a comparison with the data provided by RASAero was performed, allowing the validity of the software to be assessed.

For the CFD setup, a pressure-based coupled solver was used due to its robustness in the subsonic–transonic regime, while the k–ω SST turbulence model was selected for its proven accuracy in capturing near-wall phenomena. The results demonstrated good agreement with RASAero. Given this consistency, and considering the efficiency of RASAero in generating aerodynamic data across a wide range of conditions, the mission analysis was ultimately based on the RASAero dataset, with CFD serving as a high-fidelity validation step. Furthermore, the simulations highlighted that the fins are the most stressed components and the main contributors to aerodynamic drag, underlining their critical role in the overall aerodynamic behavior of the vehicle.

Regarding CFD analysis, the entire rocket geometry was modeled in a clean aerodynamic configuration,retaining only the main external surfaces of interest (nosecone, fuselage, fins and boat tail). All secondary mechanical additions such as fasteners, protuberances, and small fittings, were removed.

This simplification was introduced to isolate the contribution of the primary aerodynamic surfaces and to avoid spurious local effects that would not significantly influence the global aerodynamic coefficients but could unnecessarily increase mesh complexity and computational cost.

Surface roughness was also neglected, and the external surfaces were assumed to be ideally smooth. This assumption is consistent with standard practices in preliminary aerodynamic studies, as small-scale surface irregularities have a second-order influence on the global aerodynamic behavior compared to the effects of geometry and flow regime. Similarly, minor geometric details (e.g., fillets, chamfers, etc…) were omitted, as their inclusion would not materially change the aerodynamic coefficients at the accuracy level sought for this study.The resulting simplified configuration used for the CFD simulations is shown in Figure 2.9.

Fig. 2.9: Simplified model for CFD analysis.

Domain

The computational domain was designed with specific dimensions to ensure that the flow around the rocket was not artificially affected by the proximity of the boundaries. The domain was constructed as a semicylindrical volume (as illustrated in Figure 2), with its geometry scaled relative to the rocket's length L and diameter D. A representative view of the domain in the X–Y planes is shown in Figure 2.10.

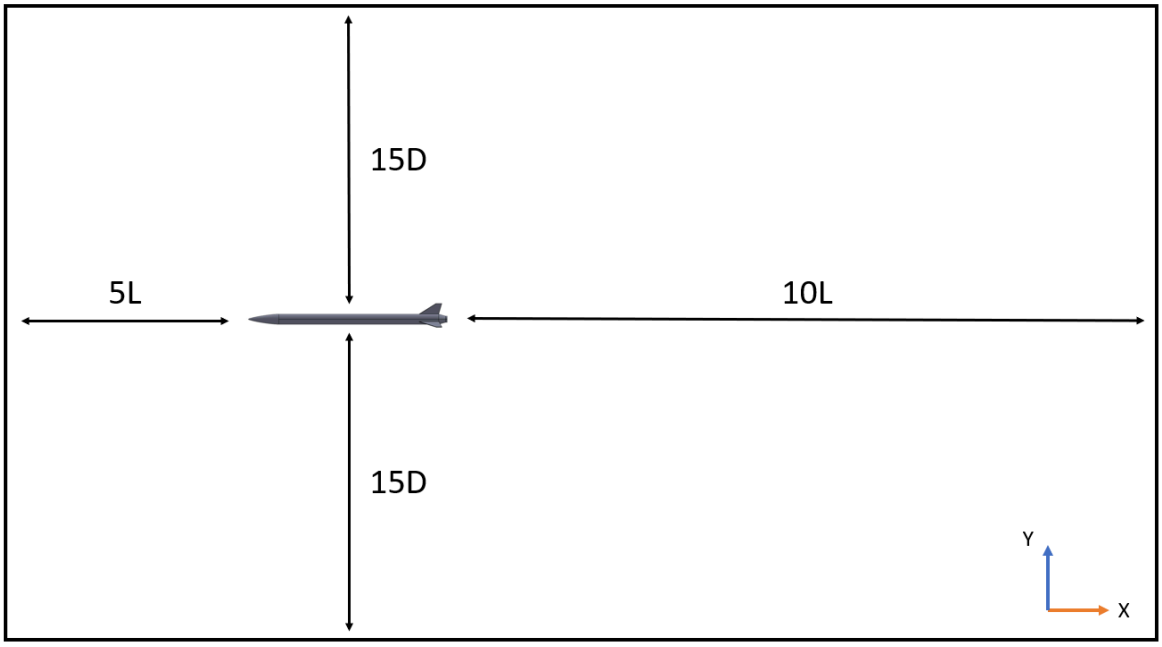

Fig. 2.10: Computational domain used in CFD.

To reduce computational cost, only half of the configuration was simulated, exploiting the symmetry of the rocket with respect to its longitudinal plane. This allowed a significant reduction in mesh size while maintaining the physical accuracy of the results.

The downstream length of the domain was set sufficiently large to capture the full development of the wake and to ensure an accurate prediction of the base drag contribution, without interference from the outlet boundary. Similarly, the upstream distance was chosen to allow proper flow development before interacting with the nosecone.

The computational domain was discretized using an unstructured mesh consisting of approximately 4 million cells. Based on an estimated maximum boundary-layer thickness of $3 \cdot 10^{-2}\mathrm{m}$ from prior CFD simulations, inflation layers were applied along all rocket wall surfaces to properly resolve the boundary layer, as shown in Figure 2.11 and Figure 2.12. The height of the first cell was set to $7 \cdot 10^{-4}$ m, with a surface element size of $7 \cdot 10^{-3}$ m. These values were chosen to achieve a target non-dimensional wall distance y+ in the range of 30-300, which is consistent with the use of wall functions and allowed a reduction in computational cost compared to fully resolving the viscous sublayer. In addition, two refinement boxes were introduced to capture critical flow features, as illustrated in Figure 2. Post-processing confirmed the estimated boundary-layer thickness and the y+ range. The y+ remained entirely below 300 and, over 99% of the surface, above 30; only small areas in the fin region dropped to values around 10.

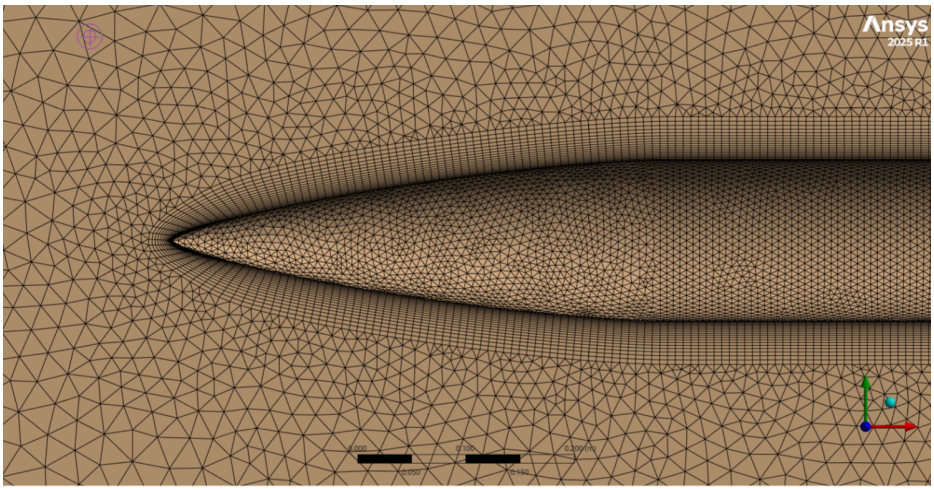

Fig. 2.11: Mesh at the top of the rocket.

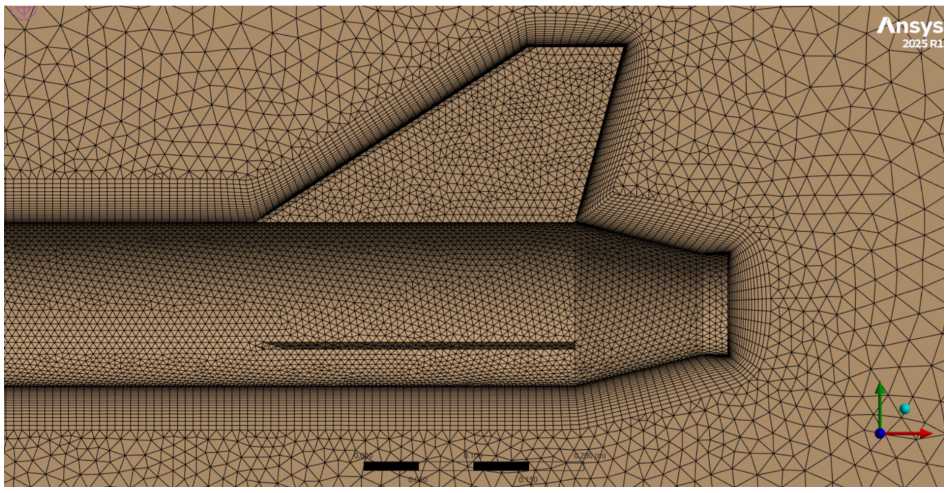

Fig. 2.12: Mesh at the bottom of the rocket.

Furthermore, the mesh generated for the simulations meets the imposed quality requirements, as shown in Table 2.1.

Table 2.1: Table of acceptance criteria and effective values.

Quality Parameter	Acceptance Criteria	Effective	Mean Value
Skewness	95% SKW < 0.9 $\mathrm{SKW}_{\max} < 0.95$	100% SKW < 0.9 $\mathrm{SKW}_{\max} = 0.89$	0.221
Aspect Ratio	95% AR < 50 $\mathrm{AR}_{\max} < 75$	100% AR < 50 $\mathrm{AR}_{\max} = 37.9$	2.554
Orthogonal Quality	95% OQ > 0.1 $\mathrm{OQ}_{\min} > 0.05$	99% OQ > 0 $\mathrm{OQ}_{\min} = 0.100$	0.778

5 Simulations

The CFD simulations were carried out in ANSYS Fluent using a pressure-based solver with pressure–velocity coupling, a formulation well suited for subsonic and transonic flows and known for its numerical robustness. A steady-state Reynolds-Averaged Navier–Stokes (RANS) approach was adopted. For turbulence modeling, the k–ω SST (Shear Stress Transport) model was selected, as it combines reliable near-wall accuracy with robust predictions of flow separation.

Viscosity was modeled using Sutherland's law, and the turbulence-model parameters were computed as follows:

$$k = \frac{3}{2}(VI)^2 = 10.03\frac{m^2}{s^2}, \qquad \omega = \frac{\sqrt{k}}{C_\mu^{\frac{1}{4}} L_t} = 481.8 s^{-1} \tag{2.6}$$

Where I is the turbulence intensity (assumed 0.01, low-Re), $C_\mu = 0.09$, and $L_t = 0.4\delta_{\max}$ (with $\delta_{\max}) = 3$ cm, the estimated maximum boundary-layer thickness). The energy equation was enabled, and the working fluid (air) was modeled as an ideal gas, with viscosity calculated according to Sutherland's law, ensuring an accurate representation of thermophysical properties across the considered Mach range.

Boundary conditions

- Inlet: pressure inlet, with total pressure and total temperature calculated from isentropic relations to account for compressibility effects at the selected Mach numbers.

$$\frac{P_0}{P} = \left(1 + \frac{\gamma - 1}{2} M^2\right)^{\frac{\gamma}{\gamma - 1}}, \qquad \frac{T_0}{T} = \left(\frac{a_0}{a}\right)^2 = 1 + \frac{\gamma - 1}{2} M^2 \tag{2.7}$$

where $P = 101325$ Pa and $T = 288.15$K

- Outlet: pressure outlet, set with a gauge pressure of 0 Pa.
- Lateral cylindrical surface: slip wall condition, to avoid artificial shear effects.
- Rocket surface: no-slip wall condition.

All simulations were performed at sea-level conditions to enable a direct comparison with RASAero plots, which are referenced at the same altitude. Accordingly, the operating pressure was fixed at $101325\ \mathrm{Pa}$. The simulations were run for Mach numbers ranging from 0.3 to 0.76, covering the entire expected flight envelope. For each case, the following outputs were extracted: pressure coefficient distribution along the rocket body, drag coefficient, and drag force. Since Mach 0.76 represents the highest velocity condition within the flight envelope, all figures and contour plots in this section refer to M = 0.76, unless otherwise stated. At this stage, the presented contour plots provide a qualitative overview of the aerodynamic behavior, highlighting how the flow evolves around the vehicle and where the main load concentrations occur. These visualizations are fundamental to identifying the most critical regions, such as the nosecone tip and the fin leading edges, which clearly emerge as the areas most exposed to aerodynamic stresses. Figure 2.13 shows the Mach number distribution, which clearly highlights the regions of local flow acceleration and deceleration, with pronounced effects at the nosecone tip and at the leading edges of the fins. These areas correspond to the points where the flow reaches its highest speeds relative to the freestream, indicating potential critical zones for aerodynamic loading.

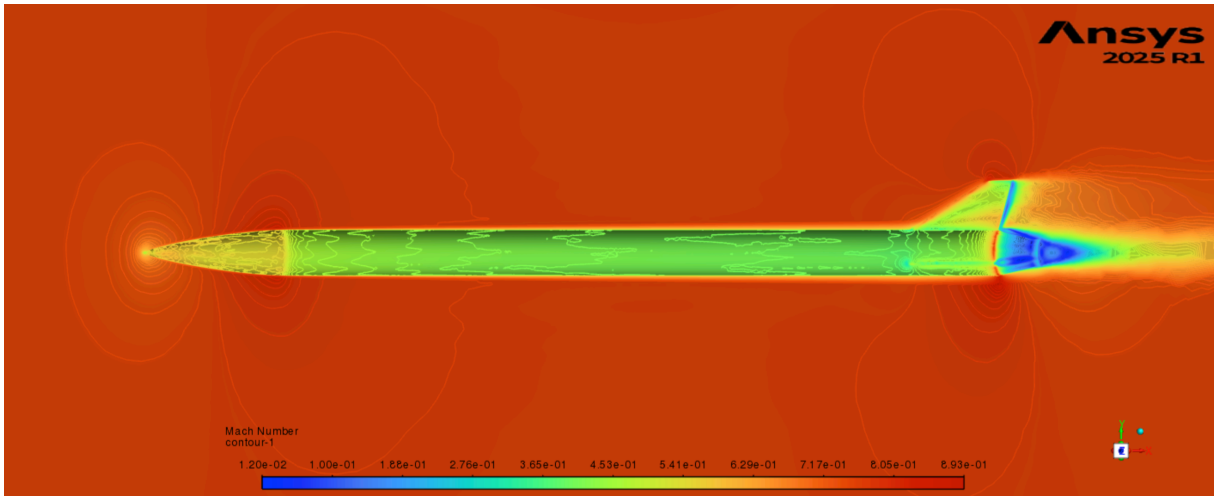

Fig. 2.13: Mach number distribution.

Figure 2.14 reports the pressure coefficient distribution along the vehicle. This representation emphasizes how pressure variations around the body generate aerodynamic forces, with marked low-pressure regions developing behind the fins due to wake formation.

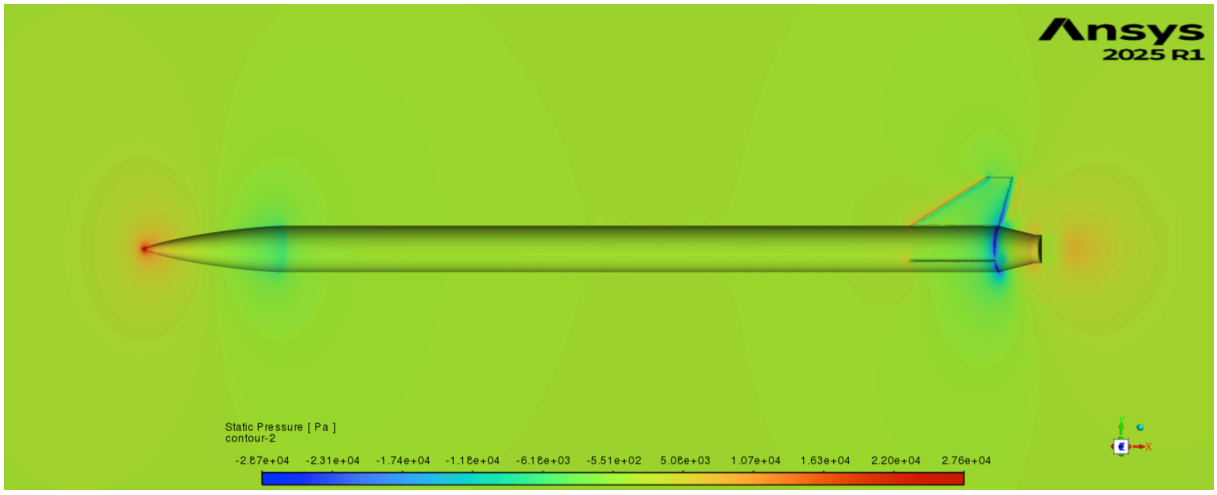

Fig. 2.14: Pressure coefficient distribution.

Finally, Figure 2.15 and Figure 2.16 show the absolute pressure contours around the rocket body. The visualizations clearly indicate the regions subject to the highest aerodynamic loads. In particular, the nosecone tip and the leading edges of the fins emerge as the most critical zones, where the flow stagnation and acceleration effects generate local peaks in pressure.

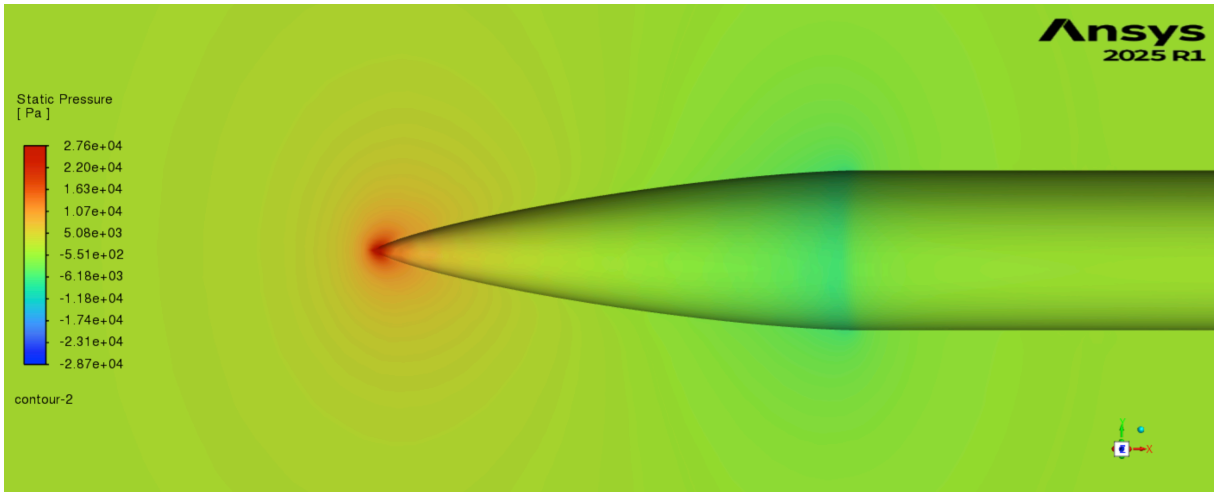

Fig. 2.15: Pressure coefficient distribution on the nose cone.

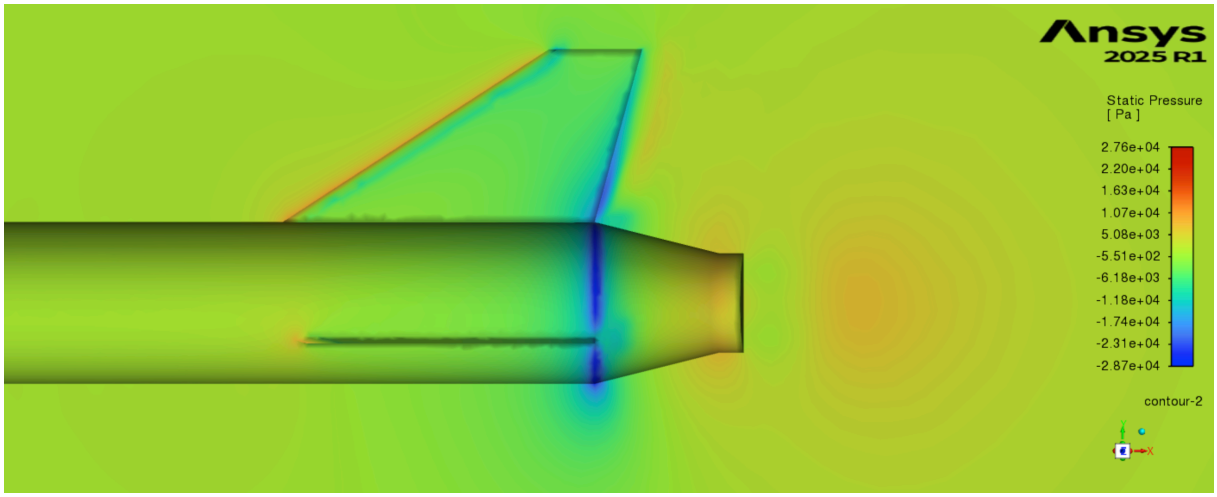

Fig. 2.16: Pressure coefficient distribution on the fins.

Figure 2.17 presents three C_D curves versus Mach at sea level: the CFD results obtained by our team without screws, rail guides, or surface roughness; RASAero predictions for the same clean configuration; and RASAero predictions including screws, surface roughness, and rail guides. Under identical geometric conditions the CFD results tend to slightly overestimate the drag coefficient compared with RASAero.

Because we currently lack the computational resources to run CFD cases that include roughness, screws, and rails, we relied on RASAero to assess the influence of these features: as shown, the inclusion of screws, roughness, and rails produces a substantial change in C_D, which supports using RASAero to explore those configurations.

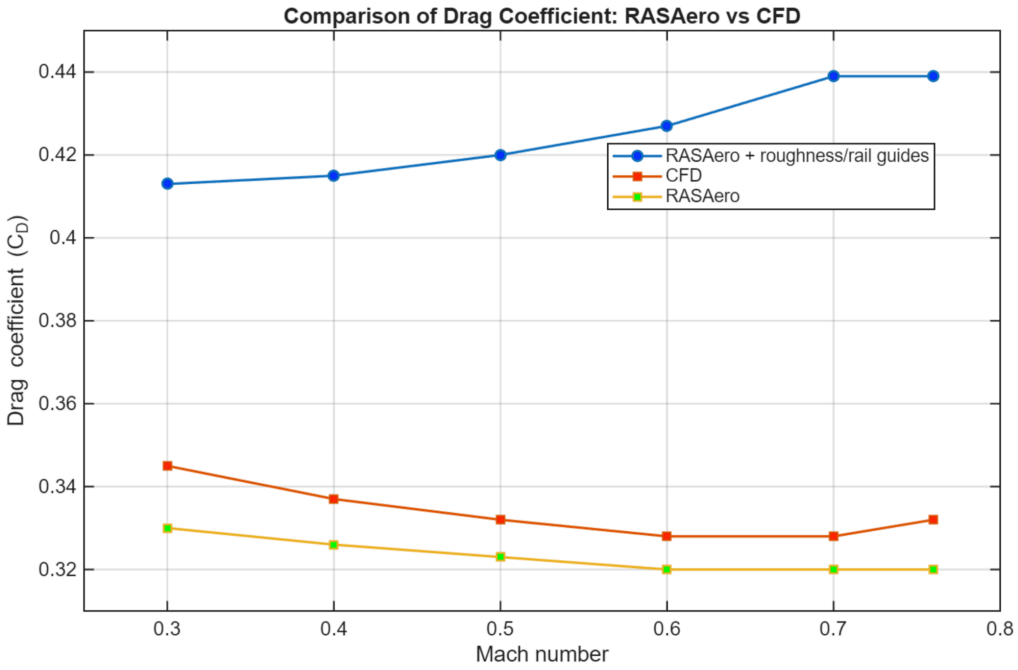

Fig. 2.17: Comparison of drag coefficient: RASAero vs CFD.

To better quantify the deviation between the two methods with the same clean configuration, the percentage difference in drag coefficient was calculated. Figure 2.18 reports the percentage difference as a function of Mach number. The comparison shows that the discrepancy remains relatively limited across the investigated range, with CFD systematically predicting slightly lower drag values at intermediate Mach numbers, with a maximum percentage difference of approximately 4.4%. This confirms the overall consistency of the two approaches.

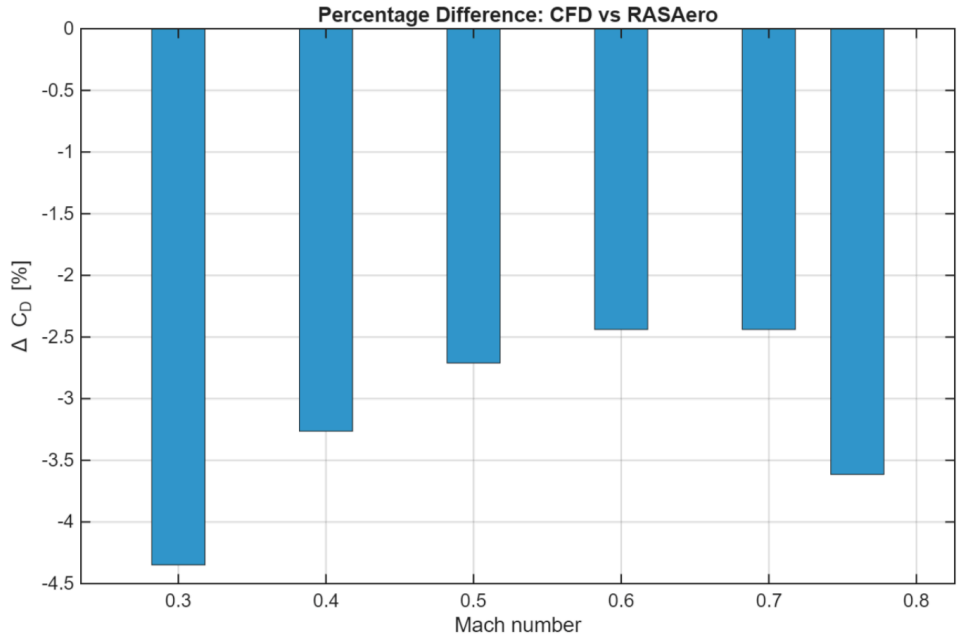

Fig. 2.18: Percentage difference: CFD vs RASAero.

6 Structural Analysis

The structural analysis targets the most critical parts under a conservative worst-case condition constructed to represent the upper bound of loads on the structure. Specifically, the following were considered simultaneously: maximum aerodynamic load (axial and lateral); maximum thrust delivered by the motor.

First, the peak aerodynamic loads are identified via CFD analysis in ANSYS Fluent, while the maximum thrust is obtained from the motor documentation. The analysis proceeds by building an equivalent beam model that preserves the total mass and its distribution, then applying the aerodynamic and propulsive loads to that model. Using ANSYS Static Structural, the distributions of internal actions along the beam as a function of length are obtained, namely axial force, shear force, bending moment, and torsional moment.

Finally, the real rocket components located at the beam-equivalent positions with the highest internal actions are identified, and those actions are applied to the corresponding components for structural verification. The required condition for each component is:

$$\mathrm{SF} > 1.5 \tag{2.8}$$

and the Table 2.2 lists the most stressed components with their corresponding safety factor (SF). The structural analysis is described in detail in Appendix I.

Table 2.2: Safety factor of most critical components.

Component	**SF**
Electronics Bay Rods	2.780
Third Flange	11.40
M4 Screw	15.00
Bulkhead	15.00
M8 Screw	15.00
Body Tube	4.716
Rail Buttons	1.544
Aether (Payload)	15.00

2.4 Recovery subsystem

Nemesis rocket adopts a dual-deployment configuration, involving two commercially available parachutes, a drogue and a main, manufactured by *Rocketman Enterprises*. Nemesis' two parachutes are deployed in two different events: the *initial deployment event* for the drogue and the *main deployment event* for the main.

The recovery system is in charge of bringing the rocket safely to the ground, within the competition's descent speed limits. The smaller drogue parachute deploys at apogee and its role is reducing any drifting that may be caused by the wind, thanks to a faster descent speed. Later during the rocket's descent, the main parachute deploys and slows the rocket for a safe touchdown.

Two kind of activation devices are adopted: the peregrine system, for the drogue parachute, and two wire-cutters, for the main. Both systems are activated by pyrotechnic charges within the recovery compartment. No other stored energy devices are present in this section, as they are all housed in the electronics compartment.

1 Initial deployment event

The initial deployment event consists of the ejection of the nose cone using the COTS Peregrine System (see Figure 2.20), which works thanks to two CO_2 cartridges that push an internal tube, where the recovery components are stored. When the avionic systems detect apogee, they activate the e-matches, which ignites the black powder, the CO_2 cartridge is propelled forward and breaches its seal against a stationary awl. This internal tube breaks the three shear pins that are located on the flange, shown in Figure 2.19, allowing the separation of the nosecone from the main body of the rocket.

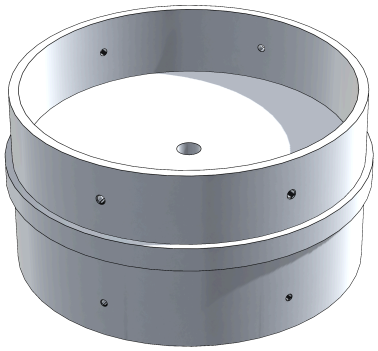

Fig. 2.19: The nose cone flange

Fig. 2.20: Tinder Rocketry Peregrine assembly

Simultaneously the nose cone is connected to the drogue which is also deployed. On the bottom of the internal tube and on top of the cartridges plate we insert a silicone seal to help maintain proper pressurization, sealing the gap (gap can be seen in the figure below) between the two cans to prevent any gas leakage. This way we are going to create an environment similar to a pressure vessel.

2 Main deployment event

Later on the descent, the main parachute is deployed using a three-ring release system which releases the drogue allowing it to extract the main parachute. The system uses a series of three rings of diameter each larger than the previous one, connected like illustrated in Figures 2.21 and 2.22.

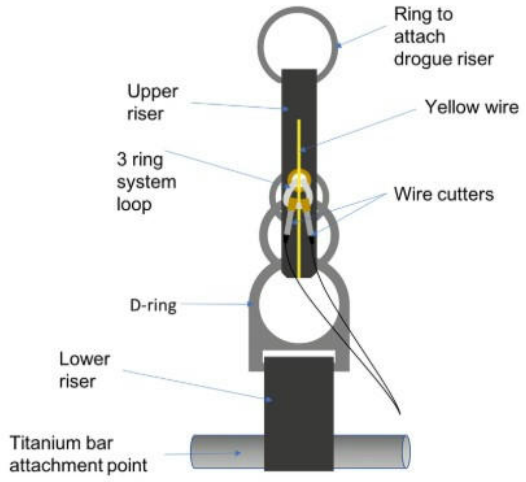

Fig. 2.21: Diagram of the main parachute release system.

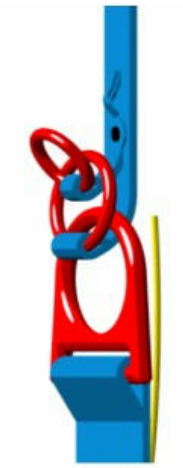

Fig. 2.22: 3D illustration of the main parachute release system.

The three rings are released,with an electrical signal which activates the wire cutters. As for the peregrine system, also the wire cutters work with e-matches that are connected directly to the electronic bay.

The safety critical wiring connecting the flight controller to the pyrotechnic parachute actuators is essential, as its malfunction could prevent parachutes from opening and compromise the safe landing of the rocket. The failure of the systems can be caused by a malfunction of the sensors as well as by issues in the connections between the e-matches and the electronics bay.

We use two wire cutters to ensure redundancy both in the recovery system and in the electronics. The wire-cutters (Piranha system) are COTS from Eurospace Technology.

3 Parachutes

Both the main and drogue parachutes are pf the hemispherical-type, made of high-tenacity nylon, with reinforced stitching and integrated suspension lines. See Figure 2.23 and 2.24.

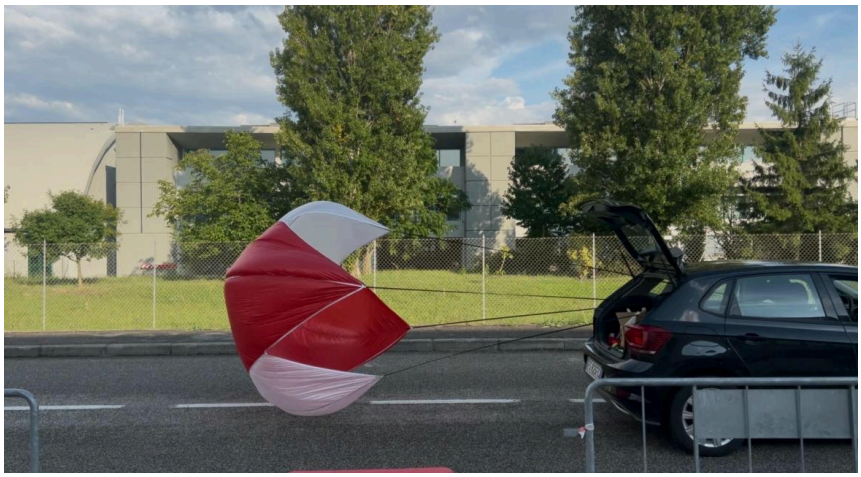

Fig. 2.23: Test of the Main Parachute.

Fig. 2.24: Test of the Drogue Parachute.

The parachutes characteristics are collected in Table 2.3.

Table 2.3: Characteristics of the parachutes.

Characteristic	Main Parachute	Drogue Parachute
Model	Rocketman Standard Main - 12 ft	Rocketman Standard Main - 3 ft
Geometry	Multi-panel hemispherical canopy	Reinforced hemispherical canopy with 4 panels
Material	High-strength nylon, tested for dynamic use in medium to large scale rockets	Lightweight ripstop nylon, tear-resistant
Shroud lines	Multiple suspension lines, fully sewn along the outer edge of the canopy for even load distribution	four nylon lines sewn $6''$ above the canopy base, improving stability and reducing tangling risk
Weight	0.63 kg	0.07 kg
Packed volume	≈ 2.27 l	$\approx 0.8 - 1.2$ l
Estimated descent rate	≈ 6 m/s	≈ 24.5 m/s
Load capability (datasheet)	33 lb (15 kg) $\Rightarrow$ 17 ft/s (5.2 m/s) 43 lb (19.5 kg) $\Rightarrow$ 20 ft/s (6.1 m/s)	
Function	Ensures a controlled and smooth landing near ground level, compliant with EuRoC descent rate limit	Stabilization during post-apogee descent, vertical energy dissipation, and minimization of horizontal drift
Additional Features	Good stability under gusty wind conditions. Central webbing loop for attachment to the shock cord	Reinforced borders. Includes an adjustable cord-lock allowing regulation of the effective line length. Use of materials with high load and dynamic stress resistance

The integration with a SRAD deployment bag for the main chute, shock cord channels, and the CO2-based ejection system ensures a smooth and progressive deployment, minimizing loads on the internal rocket. The eyebolts used are of the closed type and made of stainless steel.

4 Diagrams and interconnections

The Figure 2.25 depict the connection diagram of the recovery system. In the illustration, the connection lines and the layout of the recovery system can be observed. We used a series of quick links, eye bolts, shock cords and swivel links, which are used in order to avoid the effects of line torsion.

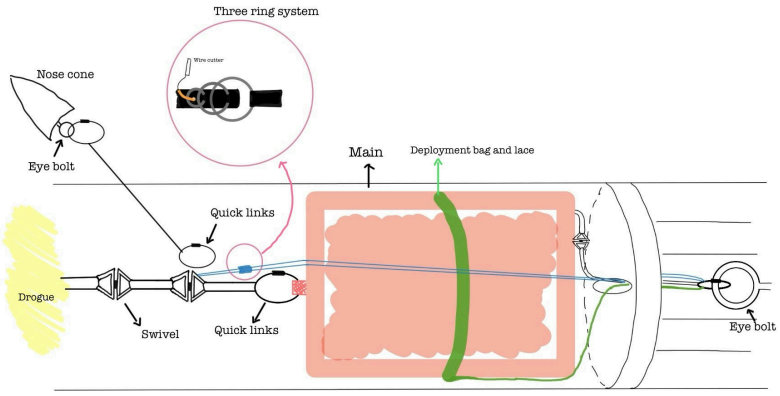

Fig. 2.25: Diagram of the parachutes lines.

The Figure 2.26 shows the recovery system during the first phase, once the Drogue has been deployed by the CO2 release mechanism.

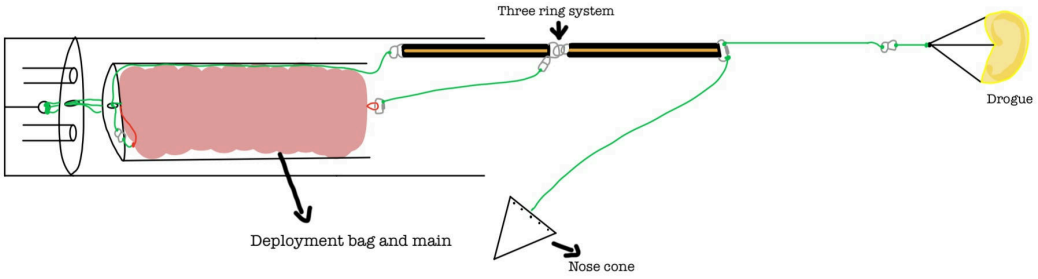

Fig. 2.26: Diagram of the first deployment phase.

Finally, Figure 2.27 shows the recovery system once the second phase is activated, when the Main is deployed.

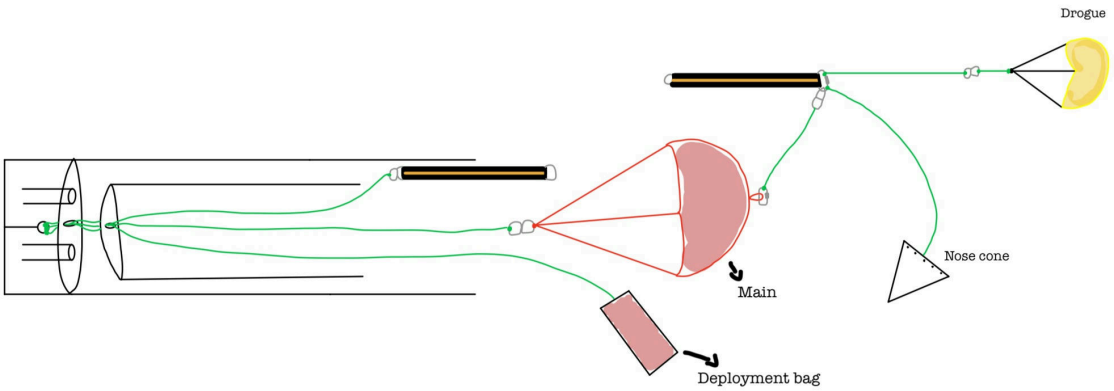

Fig. 2.27: Diagram of the second deployment phase.

5 Calculation for the shear pins

In order to determine the amount of CO_2 needed for separation, the force necessary to break the shear pins can be calculated with:

$$F = \tau A_s n \tag{2.9}$$

The friction between vehicle sections is assumed to be negligible in comparison to the force of the shear pins. The pressure necessary to break the shear pins can then be calculated from:

$$P = \frac{F}{A_b} \tag{2.10}$$

The sher pins implemented are M3 nylon screws. Let's assume that the pins are made from Nylon 6/6, characterized by a tensile strength of $\approx 72\ \mathrm{MPa}$ and a shear strength (τ) of $\approx 60\%$ of tensile $\approx 43\ \mathrm{Mpa}$. With a safety factor of 2, the shear strength becomes $21.5\ \mathrm{MPa}$.

For a M3 screw, we get:

$$A = \pi\left(\frac{d}{2}\right)^2 = \pi\left(\frac{2.4}{2}\right)^2\ \mathrm{mm} \approx 4.52\mathrm{mm}^2 \tag{2.11}$$

The shear force per number of pins n:

$$\frac{F}{n} = \tau \cdot A = 389\mathrm{N} \tag{2.12}$$

Force required to shear three M3 nylon shear pins:

$$F = 389N \cdot 3 = 1167\mathrm{N} \tag{2.13}$$

This pressure has to be compared with the pressure provided by the CO_2 cartridges. These cartridges release gas that expand to create pressure within the ejection compartment. The Peregrine system is designed to work with both $8\mathrm{g}$ and $12\mathrm{g}$ CO_2 cartridges. [1] According to the manufacturer's guidelines, the selection between $8\mathrm{g}$ and $12\mathrm{g}$ cartridges depends on the volume of the compartment and the required pressure. A standard CO_2 cartridge typically holds around $800\ \mathrm{PSI}\ (\approx 55\ \mathrm{bar})$ of pressure, with a conservative calculation. The area on which the gas acts is:

$$A_b = 2\pi\left(\frac{0.016\mathrm{m}}{2}\right)^2 = 4 \cdot 10^{-4}\mathrm{m}^2 \tag{2.14}$$

The force produced by this pressure, assuming it is instantly transmitted to the nosecone and so to the shear pin is:

$$F = PA_b = 5.5\ \mathrm{MPa} \cdot 0.0004\mathrm{m}^2 = 2211\mathrm{N} \tag{2.15}$$

The force produced by a single cartridge is more than the pressure required to shear three M3 nylon pins.

6 Overview of recovery system tests

- E-match and CO_2 Ejection System Failure: this failure could prevent the deployment of the nose cone and the parachutes. However, redundancy has been implemented in the ignition system, significantly reducing the probability of the e-matches failing simultaneously. Additionally, the system was tested several times, proving its reliability. As a COTS component, the CO_2 Ejection System's reliability is ensured by the supplier according to their quality standards.
- Shear Pins Not Breaking: if the shear pins do not break, the recovery compartments may fail to open. Calculations have been performed to select appropriate shear pin sizing and placement. These were validated through physical testing, making this failure mode unlikely. We have tested the breaking of the shear pins by placing parachutes and cords inside the internal tube and placing it on top of the peregrine system, then secured the flange and the nose cone with the shear pins and activated the system with an electrical signal. The force of the CO2 canisters has been verified as enough to break the shear pins. We also decided to add a silicone gasket to prevent gas leaks and create a sealed environment similar to a pressure vessel.

2.5 Payload subsystem

1 Introduction

In recent decades, satellite communications have become central in multiple domains, from weather forecasts and telecommunication to navigation and internet services. Launching a satellite into orbit has become cheaper throughout the years and many companies are shifting their infrastructure from terrestrial to orbital, as demonstrated by programs such as Starlink, Project Kuiper and IRIS2. The integration of satellite communications into aerospace systems opens new opportunities, allowing data exchange from aircraft and launchers even under critical operating conditions. Notable examples include the use of the Iridium NEXT constellation for civil aviation, operating in the L-Band range and Starlink for the video feed of Starship's reentry.

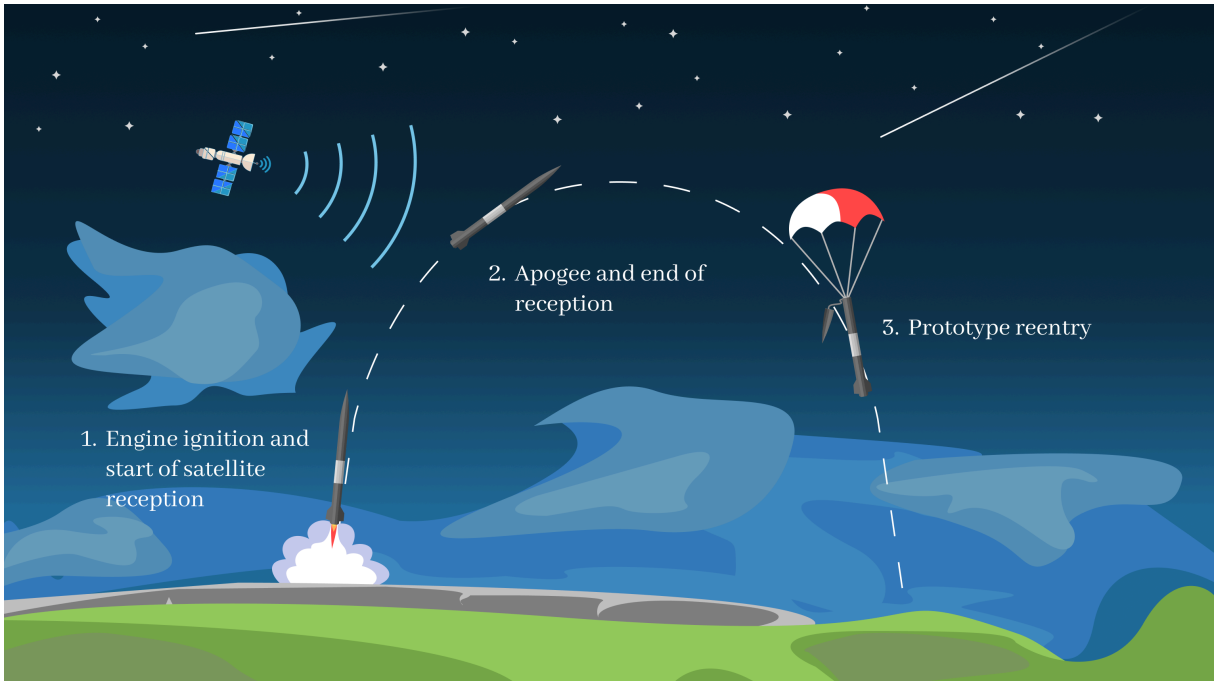

Fig. 2.28: The mission concept of Nemesis' scientific payload

Historically, receiving a satellite signal required specific demodulator that allows to decode the particular signal, therefore a receiving station could only decode the signals its demodulator was intended to. Today, with the introduction of a Software-Defined Radio, it's possible to digitalize the signal first and then use software based application to decode the signal present in the saved baseband.While this technology has been broadly used by amateur radio amateurs, its applicability into the aerospace sector is still being tested. Some of the possible applications of an SDR include calculating real-time measurement of a rocket's flight direction using the signal transmitted by multiple ground stations, which has already been tested by the Indonesian Space Agency (LAPAN) using GNU-radio for signal acquisition and MATLAB for processing the signals [4]. The same tracking system can also be applied to estimate the rocket's trajectory through the Doppler effect of the signals received from multiple satellites (i.e., the Iridium constellation), as described in the following conference by Orabi, Khalife, and Kassas (2021) [5].

Developing a system capable of doing such real-time signal analysis and calculations mid flight isn't simple; being a new team at EuRoC, we believe that delivering a system capable of the inflight signal processing, such as the one developed by LAPAN, as our first ever payload would be out of our capabilities. Instead, we developed Aether, a proof-of-concept CubeSat which includes all the satcom

required hardware. The main objective of the experiment is saving the received baseband of the geostationary satellites during the ascension phase of the rocket flight, to allow a post-flight analysis of the data collected to develop the next payload's iterations. The mission concept is illustrated in Figure 2.28. While the Iridium constellation would be more interesting for our experiment, the Inmarsat geostationary satellites have been chosen instead due for obvious reasons related to the reception windows and the possibility to legally decode their signals.

2 Form factor & structure

Aether is a non-deployable, 1U payload, capable of receiving and saving the baseband of L-band satellites, from the Inmarsat constellation of geostationary satellites, distant more than 35000 km from Earth's surface. The payload is located in the ogive, between two 3D printed supports, that have been topologically optimized to remove part of the unnecessary mass. The payload assembly is visible in Figure 2.29. The total weight of the CubeSat is little more than 1 Kg. The outer structure is made of ABS plastic while the inside is composed of different layers separated by brass spacers. The first layer host the batteries, the second one the PCB and the last the receiver equipment, connected to the patch antenna on the top.

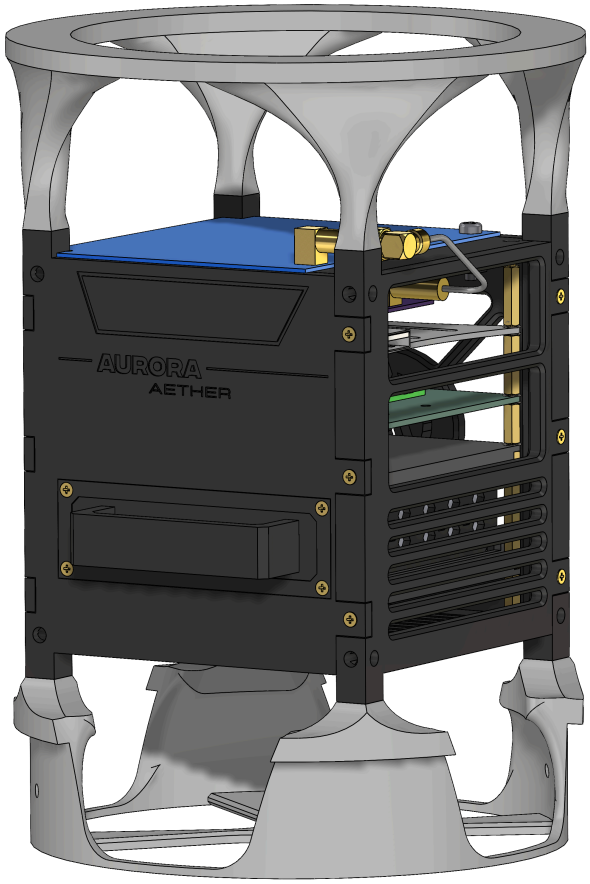

Fig. 2.29: The payload final assembly

The CubeSat can be easilily removed by unscrewing the nosecone to the flange, and removing the top support. The batteries are replaceable without a total disassembly, thanks to the handle on front, which locks the batteries inside their pack.

3 Functionality

The experiment main objective is a good reception of Inmarsat satellites' data during the ascension phase through the use of a SDR. The inmarsat constellation provides a vast range of services, including Aeronautinautical (Aero), involving packet data of ACARS and ADS, and Inmarsat-C (or STD-C or EGC messages), for global maritime distress and safety. With the help of softwares such as SatDump and Jaero, it is possible to decode the signals and get the packets. An example of a packet of the Inmarsat-C service, decoded with Aether, can be seen in Figure 2.30.

Fig. 2.30: EGC message decoded with SatDump

All these services are transmitted trough signals in the L-Band, around 1545.123 MHz for the Aero packets and 1537.10 MHz for STD-C packets. The exact frequencies varies depending on which of the four main geostationary satellites the signal is transmitted from. To work, Aether needs electronics devices that receive, digitalize and decode the satellite's signal. The signal processing chain is shown in Figure 2.31.

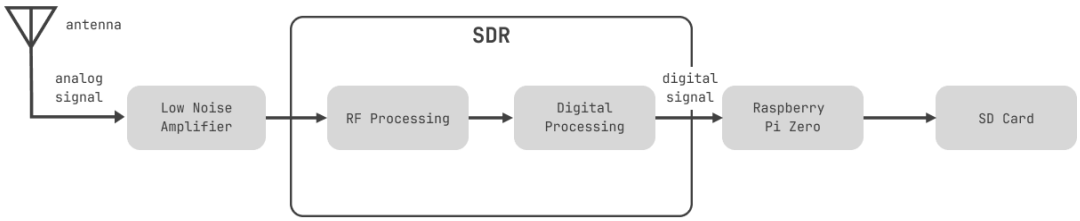

Fig. 2.31: Signal processing chain for satellite communication

Following is a description of each component of the chain:

A **Satcom Antenna** is needed for receiving the signal. The receiver dimensions are strictly correlated to the frequency of the signal, by the equation:

$$\lambda = \frac{c}{f} \tag{2.16}$$

It is clear how the dimension of the antenna increases the lower the frequency gets. Most of the antennas are designed to work with a fraction of the wavelength. In the case of a patch antenna, we have an effective length of the side equal to:

$$L \approx L_{\text{eff}} = \frac{\lambda_0}{2\sqrt{\varepsilon_{\text{eff}}}} \approx \frac{\lambda_0}{2\sqrt{\varepsilon_r}} \tag{2.17}$$

Where ε_{eff} is the relative permittivity of the material. Assuming FR4 Glass Epoxy as the material, with a dielectric constant of 4.36, and a height of the substrate of 1.5 mm, we get a length of approximately 4.65 mm, which is compatible with the dimensions constraints of the payload.

Instead of developing our own antenna, we decided to use a COTS one. The 1550 MHz Inmarsat antenna from Nooelec has been chosen due to its dimensions and low profile. The antenna is located on top of the payload and it's locked through one nylon screw.

A **Low Noise Amplifier** plays a fundamental role in SDR systems. This component amplifies the analog signal before it reaches the SDR's RF tuner and is subsequently digitized. Since input signals are often very weak, it is crucial that an LNA introduces as little noise as possible, maximizing the signal-to-noise ratio (SNR). The amplifier is placed very close to the antenna in order to avoid amplifying the noise introduced by the coaxial cable or other connections. The operating principle is shown in Figure 2.32.

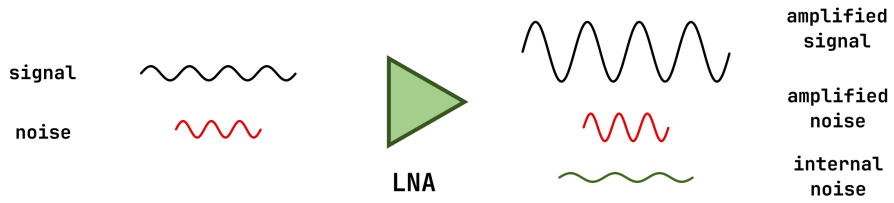

Fig. 2.32: Functionality of a Low Noise Amplifier

The LNA needs to be powered in order to work. The energy can be delivered through a dedicated system, using a micro usb cable for example, or by using the same RF cable connected to the SDR. This last method is called *bias-tee*, and is the one adopted in our configuration.

A *bias-tee* is a system consisting of a capacitor and an inductor, capable of supplying DC current over the coaxial cable to the amplifier. The capacitor is connected along the RF signal path and serves to block DC current, allowing only the high-frequency signal to pass through to the SDR. The inductor, on the other hand, is placed between the power source and the coaxial line: it allows the DC current needed to power the LNA to pass, while preventing the RF signal from flowing back to the power supply. In this way, the signal and the power travel over the same cable but remain electrically separated within the circuit.d

The manufacturer has not specified the power consumption of the amplifier integrated in the antenna; however, the consumption of a similar LNA (Nooelec SAWbird IR) can be used as a reference.

A **Software-Defined Radio** is a communication system that replaces many traditional hardware components with software. It operates through three main elements: the RF tuner, which isolates a specific frequency received by the antenna and shifts it to an intermediate frequency or baseband; the ADC, which converts the analog signal into a digital format suitable for computer processing; and the interface, typically USB, which transfers the digitized signal to the computer for demodulation and analysis.

When selecting an SDR, several factors must be considered. For our application, the most important ones are the supported frequency range, the availability of bias-tee, to power the amplifier through the RF cable, and the overall power consumption. A model that meets all these requirements is the Nooelec SMArTee v2 SDR. It operates with a DC supply of 4.5V at 250mA and supports bias-tee powering. Since the device uses a USB interface, an adapter will be required to connect it to the onboard computer. Finally, the supported frequency range is 25-1750 MHz, which covers the Inmarsat L-Band.

In our design, the LNA and the SDR are located in the third layer of the cubesat, as visible in Figure 2.33, inside a custom printed support.

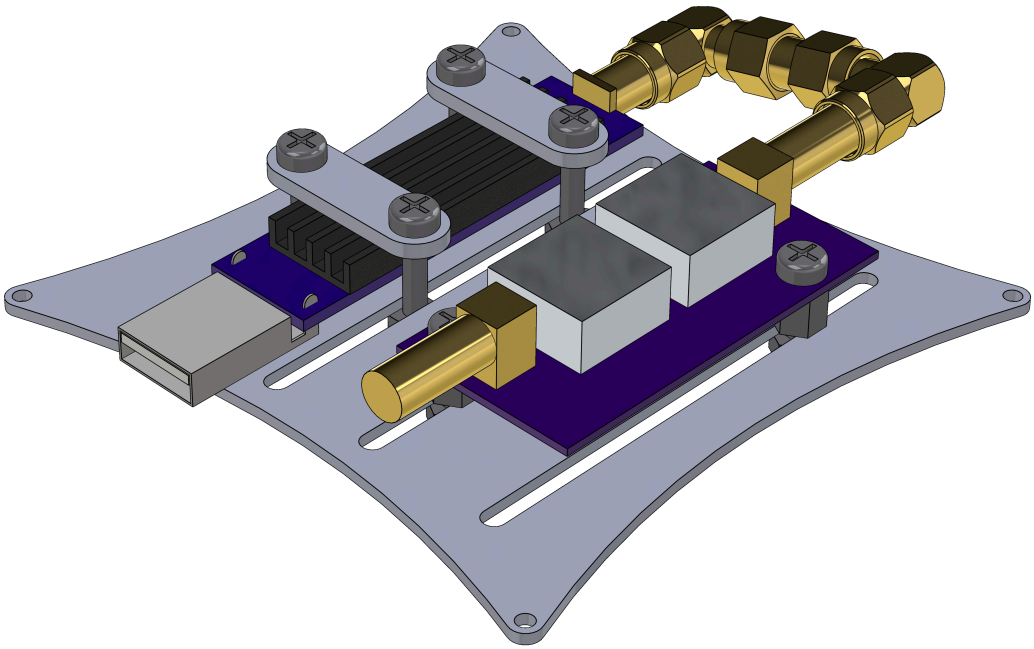

Fig. 2.33: Third layer of the Cubesat, with the SDR and LNA

For SDR data processing, a simple microcontroller is not sufficient. A Single Board Comouter is required to handle real-time data acquisition from the receiver and process it through software, often running on Linux. The **Raspberry Pi Zero 2 W** is a suitable choice. It is a compact board (65 mm × 30 mm) with a quad-core processor and wireless connectivity, allowing remote access even when installed on the launch vehicle through SSH. It supports Linux and a wide range of open-source SDR software, and its micro-USB port enables direct connection to receivers such as the Nooelec SMArTee via an adapter. Power consumption is very low, from about 120 mA in idle up to 450 mA peak at 5 V. At the end of the chain, the Raspberry Pi saves the baseband on a different Micro SD card.

4 Power & Energy

The various components of the telecommunication system and the onboard computer have been defined. It is therefore possible to proceed with sizing the electrical system. Table 2.4 shows the nominal power consumption of each component. For the Raspberry Pi Zero 2 W, the idle current consumption is considered, since it can be activated remotely before launch through the IMU sensor. The maximum consumption is reached only during ascent (about 20-30 seconds) and can be neglected compared to the hours spent on the launch pad.

Table 2.4: Required Power

Component	Power Consumption		
	Voltage [V]	Current [mA]	Power [W]
LNA	4.5	30	0.135
SDR	4.5	250	1.125
Raspberry Pi Zero 2 W	5	~ 120	0.6
Total			1.86W

A maximum required power consumption of 1.86 W is therefore obtained. Considering the mission requirement of 6 hours of autonomy, the necessary energy is

$$E_{\text{tot}} = Pt = 11.16 \text{ Wh} \tag{2.18}$$

It is therefore necessary to select a battery pack capable of powering our system. The student team already owns, from a previous project, LiFePo_4 batteries, which, as specified in the mission requirements, are allowed by the regulations and do not require particular precautions. These have a capacity of 1.5 Ah at 6.4 V, i.e., 9.6 Wh. Considering a transmission efficiency η equal to 90% and a depth of discharge DoD equal to 100%:

$$E_{\text{tot}} = \text{DoD } \eta \text{ N}C_b \tag{2.19}$$

$$\text{N} = \frac{E_{\text{tot}}}{\text{DoD } \eta C_b} \approx 1.3 \tag{2.20}$$

It is therefore possible to proceed with two batteries, ensuring a good safety margin for possible thermal losses and additional power draws from extra components, such as the buck step-down converter, necessary to step down from 6.4 V of the batteries to 5 V for the Raspberry Pi Zero 2 W. The SDR will then be powered via a USB cable connected to the Raspberry Pi.

5 Data output

The data expected to be received is a raw recording of the baseband at 1545.123 MHz through the use of the open-source software SatDump. Portugal is in the coverage of both Inmarsat-4 4F1 and Inmarsat-3 F5, so the baseband will contain both the signals. We opted for the Aero packets instead of STD-C due to a stronger reception during our testing. We aim to study the later received signals to develop a Matlab algorithm to calculate the rocket heading in real-time for next generations.

2.6 Avionics subsystem

The avionic subsystem is composed of two SRAD boards and a CATS Vega that acts as a redundant recovery system.

1 Sensor board

The sensor board, shown in Figure 2.34, hosts all the onboard sensors, the microcontroller and the power management system, along with LEDs and a buzzer to have visual and audible clues about what's going on. All components are SMD, except for the boards connectors, buzzer, buck converter and arduino which are THT.

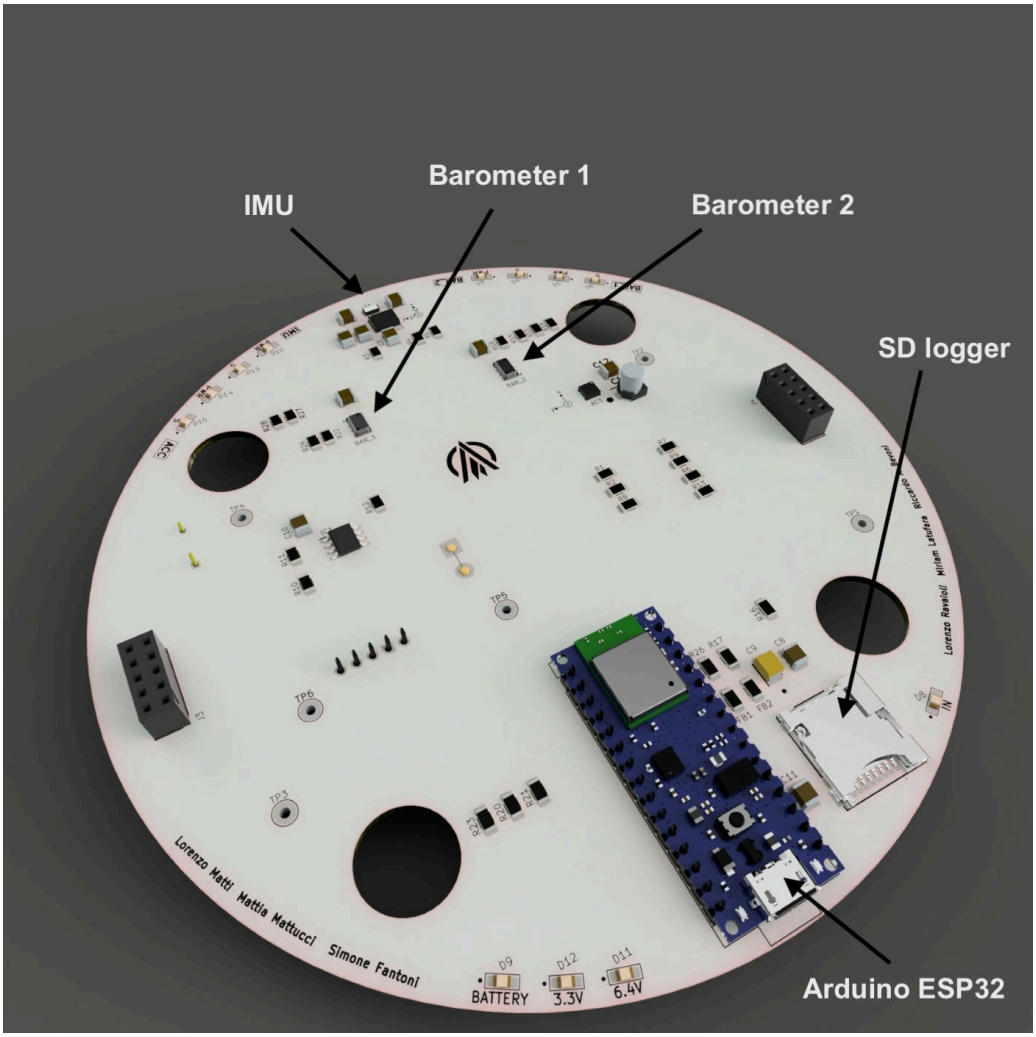

Fig. 2.34: Illustration of the sensor board

For the **onboard computer** we used a COTS solution, the Arduino nano esp-32. It is an arduino nano built around esp-32, a dual core microcontroller with a clock frequency of up to 240 MHz. Having lots of i/o pins and computational power was our priority. It communicates with the sensors via I2C and SPI. On the I2C bus we used ferrite filters to prevent potential EMI. We also implemented a micro-sd socket for data storage (come backup dei dati telemetrici mandati dall'antenna a terra).

The board stack is powered by two LiFePo4 **batteries** in parallel, with a total voltage of 6,4 V and a total capacity of 2600 mAh. With a board consumption of around 150mA this gives us a run time of around 17h . Part of the power available is directly fed to the actuators, and part of it is fed to a surge clamping e-fuse (TPS259620DDAR) which protects the sensors and the arduino. The arduino is powered

straight from the e-fuse, while the sensors are powered by a COTS buck converter (pololu D24V22F3) which brings down the 6.4 V to 3.3V. We choose a buck converter over a linear voltage regulator due to higher efficiency and lower heat dissipation. To help visualize potential problems and to help with troubleshooting we used smd leds (red coloured) labeled PWR for every sensor, which are connected to the 3.3 V trace that feeds the corresponding sensor. We also used 3 leds to check if the battery is giving power, the e-fuse and buck converter are working, the first one (blue) labeled BATTERY is connected between the battery connector and e-fuse, the second (orange) labeled 6.4V is connected between the e-fuse and buck converter and the third one (red) labeled 3.3V is connected after the buck converter. We also included a resistor divider composed of 15k and 10k resistors to know the battery voltage and a 10nF capacitor to stabilize the readings.

All the **sensors** are wired according to their datasheet, and each sensor has a blue led labelled S, which is connected to an arduino pin. This tells us if the arduino is receiving reasonable data from said sensor. Every sensor is powered by 3.3V and they all communicate via I2C. Decoupling capacitors are placed as near as possible to the Vin pads of each sensor. An important factor we kept in mind choosing each sensor is the maximum working temperature (every sensor is rated for 85 C°), and the error at higher than ambient temperature to guarantee correct readings at higher temperatures, which can develop inside the electronics bay. For the barometric pressure sensor we implemented the MS5611 by TE connectivity. It is an integrated digital pressure sensor with very high precision of up to 10 cm and very low power consumption, with a maximum current draw of 1.4 mA. For redundancy purposes we used two pressure sensors.

For the Inertial Measurement Unit (IMU), we selected Bosch Sensortec's BNO055 sensor. The need to ensure continuous and reliable acceleration data during high-g flight phases is one of the reasons why we included a dedicated accelerometer on the sensor board. This redundancy guarantees accurate measurements beyond the IMU's limitations, while the BNO055′s fusion algorithm still provides accurate orientation estimation during dynamic flight conditions. We also used a secondary 3-axis accelerometer for redundancy purposes and software aid, the LIS3DHTR by STMicroelectronics. It has a maximum acceleration of 16 g. It has some functions like freefall detection that helps with apogee detection.

We needed something sturdy that could keep the boards together,so we opted for a **shrouded board to board connector**, the IPT1-105-01-L-D by samtech. When mated the boards are around 11 mm apart. To avoid any mistake assembling the boards,the left and right connector lay on different diameters. When the boards aren't in the e-bay,the connectors are the only thing keeping the boards together mechanically speaking. However when the boards are inserted in the e-bay two bolts are used to keep everything in place. To avoid any bending of the antenna board and to isolate the boards from the mounting bars we use some tpu spacers.

2 Antenna board

The antenna board (see Figure 2.35) houses all the components needed to establish communication with the ground. The entire board is impedance-matched, aiming to achieve as close to 50 Ohms as possible on all tracks to maximize signal strength. The board includes a U-Blox GPS module, a Taoglass GPS ceramic patch antenna, an SMA connector, and a Samtech transceiver for radio communication with the ground. Additionally, the antenna board integrates the electronic system responsible for signaling the recovery bay to deploy the main and drogue parachutes. This signaling system is designed to be fail-safe, thanks to multiple layers of safety mechanisms.

As mentioned, the entire board is **impedance matched**. This was achieved through careful design choices and modifications during the development process. First, we calculated the appropriate thickness of the dielectric layer, concluding that the board needed to be very thin, specifically 0.6 mm. With this

thickness defined, all traces carrying signals were designed with precise widths to achieve proper impedance. To further improve matching, we filled the entire board with vias to ensure strong connections between the two ground planes, reducing signal loss. Wherever possible, traces were kept as straight as possible to minimize additional losses during signal transmission.

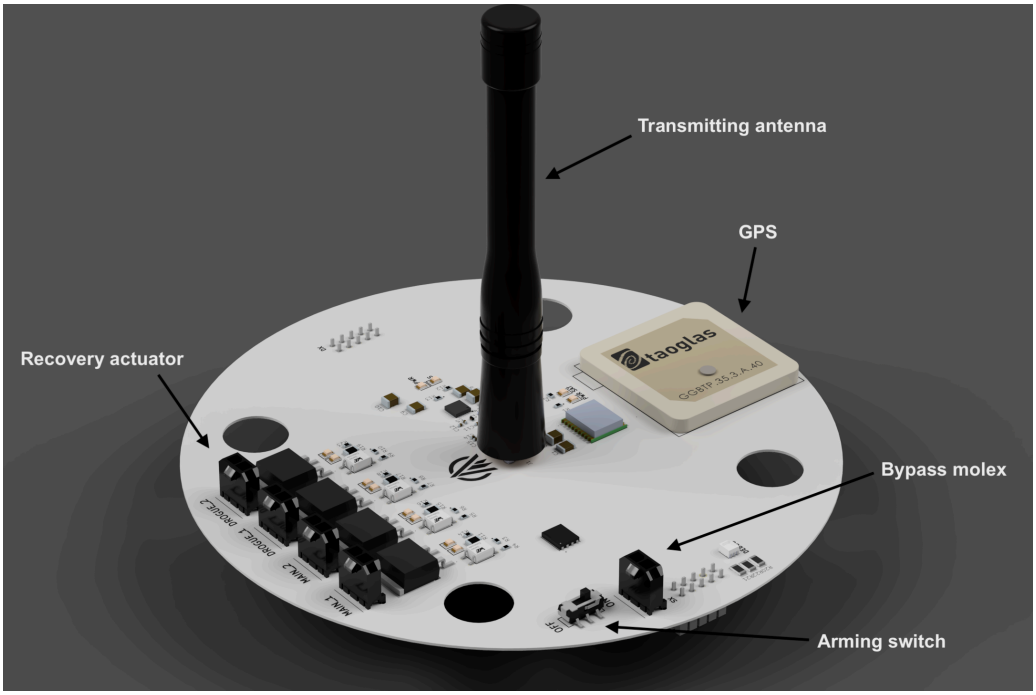

Fig. 2.35: Illustration of the antenna board

The **GPS system** consists of a U-Blox MAX-M10S GPS module, a dedicated Taoglass ceramic patch antenna, and two LEDs. The GPS is used to triangulate the rocket's horizontal position during flight and to locate it after landing. The two LEDs provide status information: a red LED indicates that the module is receiving power from the battery, while a blue LED, connected to the Arduino, indicates whether the module is locked onto enough satellites to provide an accurate position.

The **Radio** system consists of a Samtech 816 MHz radio transmitter and receiver, a male SMA connector for connecting the modular antenna, and a dedicated filter circuit designed to improve transmitter performance and eliminate noise generated by other parts of the rocket. Similar to the GPS system, two LEDs are included: a red LED for power status, and a blue LED to confirm communication with the ground station.

Two **different signals** are present on the board simultaneously: the 816 MHz radio frequency and the 1575.42 MHz GPS frequency, as well as the signal from the microcontroller that activates the parachute system. These signals must coexist without interfering with one another. To achieve this, we implemented a practical shielding solution by placing hundreds of vias to effectively divide the board into two isolated sections. This prevents cross-interference between the systems. Additionally, the main traces carrying the GPS and Radio signals were individually shielded with vias to further reduce interference.

The **parachute deployment system** provides reliable and fail-safe activation of the e-matches that release the parachute. Power is supplied by the onboard battery and routed through a high-side P-channel MOSFET, which acts as the master power switch. This MOSFET controls the supply rail for four independent low-side N-channel MOSFETs, each connected to a separate e-match. This arrangement ensures channel isolation and allows the flight computer to activate each e-match individually. The first safety layer is a physical two-position arm switch that controls the gate of the P-MOSFET. In the safe

position, power to the downstream stage is completely blocked. In the armed position, power is enabled but e-matches still cannot fire unless the microcontroller sends a digital command to the N-MOSFETs. As an additional safeguard, a bypass connector can be shorted to force the P-MOSFET into conduction. This guarantees that even if the arm switch is accidentally moved during flight due to vibration or mechanical shock, the e-match stage remains powered and the parachute can still be deployed. When the system is armed and the P-MOSFET is conducting, the microcontroller activates an e-match by driving the gate of the corresponding N-MOSFET high. This completes the circuit through the chosen e-match, heating it rapidly and triggering the parachute release. The combination of a manual arm switch, bypass override, and isolated firing channels ensures both a high level of safety against accidental activation and robust fail-safe performance in flight. To communicate with the SRAD avionics we have produced a SRAD ground station that always uses an 868MHz radio module based on LoRa modulation

3 Access

Access to the electronics and batteries can be rapidly obtained by removing the plexiglass fairings of the electronics bay: the cylindrical fairing is split into two symmetrical halves that allow their removal with the e-bay fully assembled. This step allows for the arming of the electronics before the launch event.

3 Mission concept of operations overview

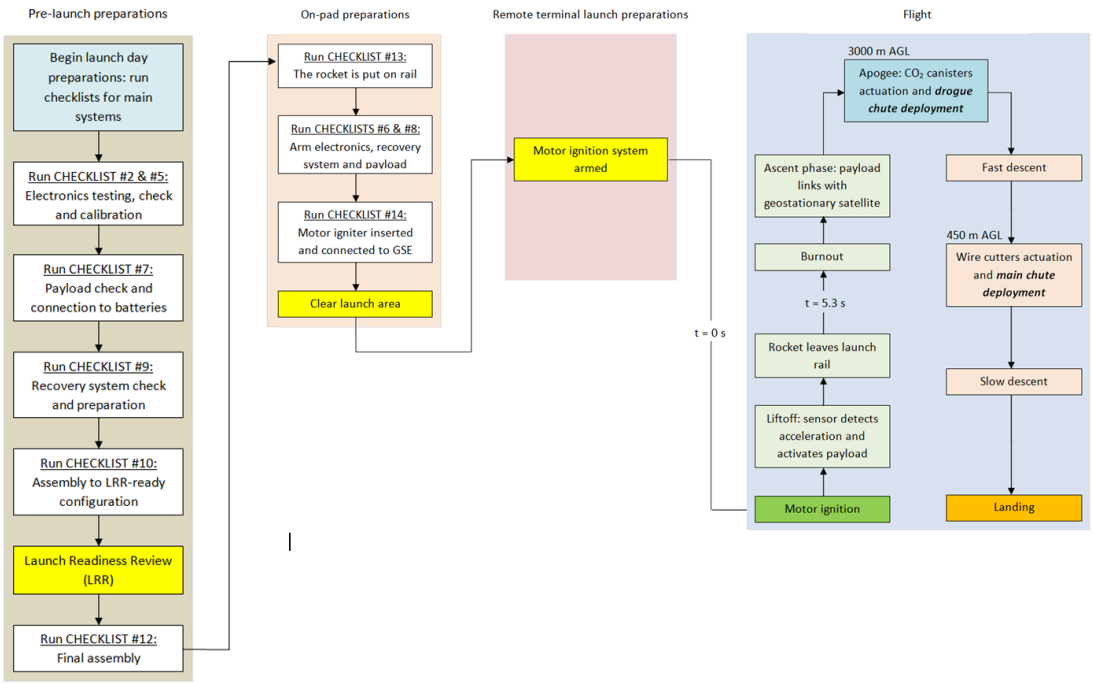

Fig. 3.1: CONOPS diagram.

3.1 Important notes

The rocket has been designed in a way that launch stability and out-of-rail velocity requirements are satisfied when using a *12 meters long launch rail*. Shorter launch rails might not be enough to grant sufficient out of rail velocity.

3.2 Operation phases

A. Pre-launch preparations

This phase begins after all FRR items have been resolved, and ends when the rocket is taken to the launch rail. Since this phase immediately precedes launch operations, all main systems are prepared for launch but stay safed. After all subsystems have been checked, the rocket is assembled;

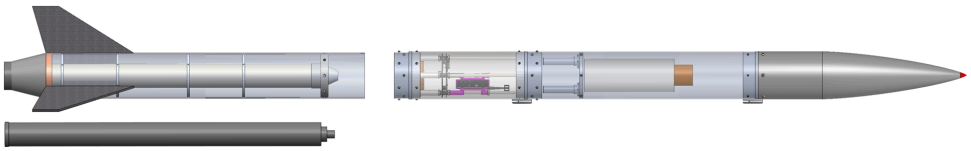

Fig. 3.2: LRR - ready rocket layout.

The rocket's motor section stays detached from the rest of the rocket (Fig. 3.2) in order to allow workers to anchor the motor to the motor bulkhead after the LRR. The motor casing stays outside of it, ready to be loaded with propellant after the LRR and before the final assembly.
After the LRR, the motor is assembled and inserted in the rocket, which is then taken to the launch pad.

B. On-pad preparations

This phase begins when the rocket is taken to the launch pad, and ends when the launch crew clears it. The rocket is mounted on the launch rail with the aftmost rail button kept in position by the bottom spacer, and the rail is inclined at 85 degrees; then, an operator reaches the electronics bay and arms the electronics.
After this step, the motor igniter is inserted and secured in the motor and the launch crew leaves the launch pad.

C. Remote terminal launch preparations

This phase begins when clearance for ignition arming is given and ends when the team is cleared to launch. When the launch pad is clear and upon receiving proper authorization, the mission control crew can arm the motor ignition system using the GSE provided by EuRoC and wait for launch clearance.

D. Flight

This phase begins when the ignition signal is given and ends when the rocket impacts the ground. It includes several steps:

1 Ignition

Ignition starts when the "fire" signal is received by the motor igniter and ends when the thrust generated is enough to overcome the weight of the rocket.

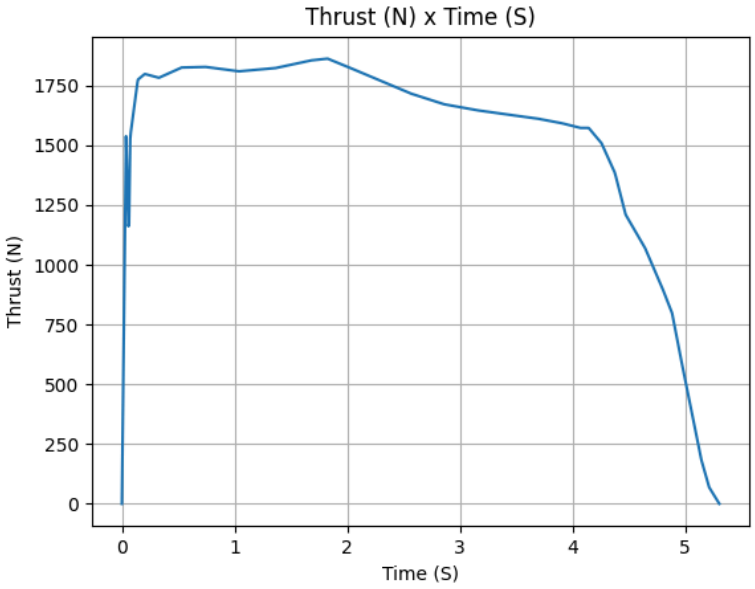

Fig. 3.3: Thrust Curve

2 Lift-off

Lift-off begins when the rocket starts moving and terminates when the last rail button leaves the rail. Velocity at rail departure is expected do be around 33 m/s.

3 Powered ascent

This phase begins after the rocket has left the launch rail and ends at motor burnout. In this phase the rocket is expected to oscillate while stabilizing its attitude, depending on the wind conditions; this oscillating motion is transient, as it is damped by the the rocket's fins according to the stability margin.

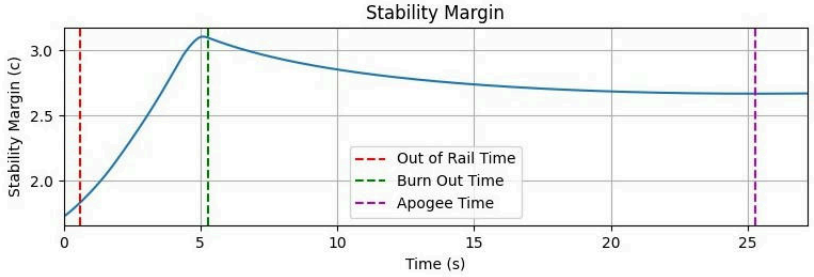

Fig. 3.4: Stability Margin.

At the end of this phase the rocket achieves maximum velocity.

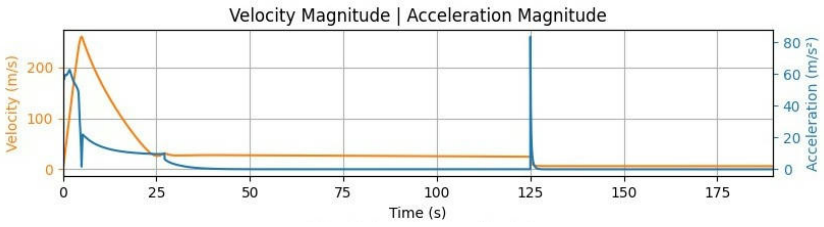

Fig. 3.5: Velocity & Acceleration Magnitude.

4 Un-powered ascent and payload operation

After motor burnout, the rocket continues on its trajectory until reaching apogee. The payload antenna establishes link with its target and begins downloading data, as the electronics on board monitor the sensors' readings and wait for apogee detection.

5 Apogee

This phase happens when the rocket's Kalman filter determines that the sensors have detected negative velocity continuously for a set amount of time (threshold), that also marks the duration of the phase. As soon as this criteria has been met, the electronics send an activation signal to the recovery actuators.

6 Drogue deployment and fast descent

Upon receiving the activation signal, the recovery system deploys the drogue parachute. The rocket then descends at a sustained speed of around 25 m/s (Figure 3.5), as the electronics on board monitor the sensors' readings and wait for it to detect an altitude of 450 m AGL.

7 Main deployment and slow descent

This phase begins when the rocket's Kalman filter determines that the sensors have detected an altitude below 450 m AGL (after having passed the apogee). When this happens, the electronics activate the wire-cutters and the main parachute is deployed, slowing the rocket's vertical velocity down to around 6 m/s.

8 Landing

Landing occurs when the rocket's main body touches the ground at an acceptable speed. The dispersion of the landing points strongly depends on rail inclination and weather features of the launch day.

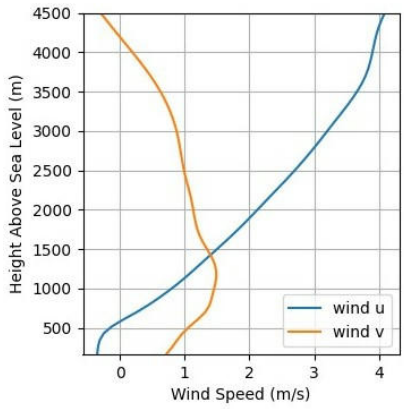

Fig. 3.6: Wind data for average weather conditions. (See Appendix H.2 for more info)

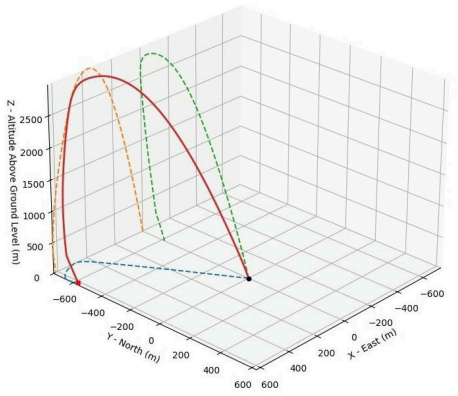

Fig. 3.7: Flight Trajectory for average weather conditions.

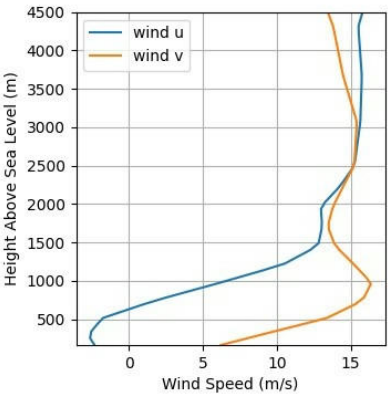

Fig. 3.8: Wind data for strong winds condition. (See Appendix H.2 for more info)

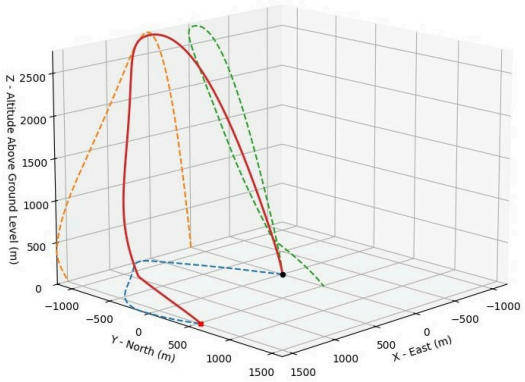

Fig. 3.9: Flight Trajectory for strong winds conditions.

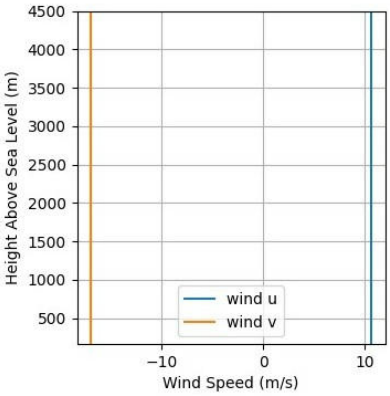

Fig. 3.10: Wind data for extreme weather conditions. (See Appendix H.2 for more info)

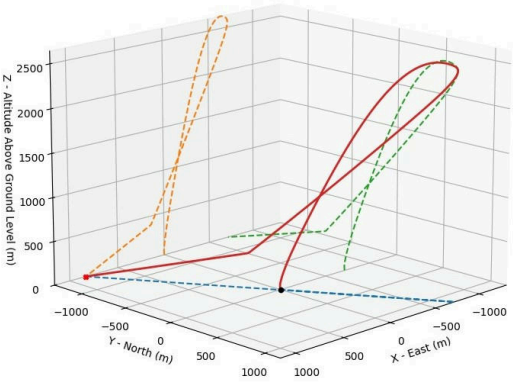

Fig. 3.11: Flight Trajectory for extreme weather conditions.

4 Conclusions and outlook

Based on our experience, it is clear that the impact on our academic path was significant. The workload was intense and required real sacrifices, both academic and personal, but it was one of the most formative and rewarding parts of the degree. It let us build something concrete that created value for all students in the association.

Beyond the engineering know-how (much more than in the early years of study), the project taught us something deeper: responsibility. We must recognize the risks we take (and that others take) when handling this kind of hardware. Public safety has absolute priority, even over flight performance. This awareness shaped our decisions, leading us to add redundancy and aim for high safety factors.

We started with a detailed analysis of motor retention and how loads move from the motor to the structure. The system proved adequate with a wide margin, and the centering rings add redundancy: they keep the motor aligned and also act as secondary load paths.

Then we carried out the aero-structural analysis: why and how we built the nosecone, fins, and boat tail; how we computed aerodynamic coefficients and validated them. We focused on structural integrity —especially the fins—showing that our flight regime is far from the flutter risk. We also checked the most stressed parts, meeting the required safety factor.

As required, the recovery subsystem uses a dual-deployment configuration and was tested many times. The first deployment happens at apogee, ejecting the nosecone and the drogue via a COTS Peregrine system; the main deploys near the ground to cut impact speed. Because a failure here could mean losing the vehicle and causing damage on the ground, we validated the system on several fronts: reliable link between avionics and the CO_2 ejection system (both in software and wiring), added redundancy, and tests on shear-pin break at drogue opening (since a missed break could damage the structure).

The avionics is split into two boards, sensors and antenna, fixed well and keyed so they can't be assembled backwards. Power is oversized and protected, with status LEDs for quick diagnostics. Data is not lost: two barometers, a standalone accelerometer alongside the IMU, and a micro-SD that logs even if the radio fails. Noisy functions are separated: GPS on one side, radio on the other, to avoid interference. Mechanically, spacers and screws keep everything rigid so connectors are not stressed. Recovery firing is handled by independent channels plus a backup path. Reliability and redundancy come first.

Operations are driven by checklists, from pre-launch to descent. Systems stay safed until a checklist step requires otherwise, and many simulations under required flight conditions give us control of the trajectory across different weather scenarios.

The work of these years produced concrete results, but the path is not finished. From an organizational and managerial point of view, there is still room for improvement, especially in inclusion and active participation. Operational urgencies often absorbed resources on the technical side, leaving the human side behind. On the technical side, however, the most feasible improvement given the experience gained over these years is the development of a hybrid rocket motor to be integrated into our prototypes.

The goal was to reach EuRoC, and we did. We would make the same choices again, now with a clearer idea of what to fix next time. In the end, what matters is looking honestly at our mistakes, so we can do better on the next attempt.

References

[1] “Cesaroni Technologies Inc. Pro38. A Better Way to Fly.” [Online]. Available: https://pro38.com/

[2] “System Requirements Document.” [Online]. Available: https://euroc.pt/wp-content/uploads/2025/03/PTS_EDU_EuRoC_ST_001928_SRD_v01-1.pdf

[3] L. Rebhi, M. Dinulovic, M. Dunjic, A. Grbovic, and B. Krstic, “Calculation of the effective shear modulus of composite sandwich panels,” *FME Transaction*, vol. 45, pp. 537–542, 2017, doi: 10.5937/fmet1704537R.

[4] R. Rustamaji, A. Prayogi, S. Kliwati, and W. Widada, “Study of real-time rocket direction using software defined radio,” 2021, p. 60016. doi: 10.1063/5.0060819.

[5] M. Orabi, J. Khalife, and Z. Kassas, “Opportunistic Navigation with Doppler Measurements from Iridium Next and Orbcomm LEO Satellites.” p. , 2021. doi: 10.1109/AERO50100.2021.9438454.

[6] I. d'Avila, “EuRoC System Requirements Document (SRD),” Mar. 2025. [Online]. Available: https://euroc.pt/wp-content/uploads/2025/03/PTS_EDU_EuRoC_ST_001928_SRD_v01-1.pdf

[7] “Cesaroni 8187M1545-P.” [Online]. Available: https://www.thrustcurve.org/motors/Cesaroni/8187M1545-P/

[8] “Calculation_of_the_effective_shear_modulus_of_composite_sandwich_panels.” [Online]. Available: https://www.researchgate.net/publication/323353536_Calculation_of_the_effective_shear_modulus_of_composite_sandwich_panels

Appendix A

System data

System Data (Lengths and Weights)			
Section Name	Section Length	Part	Weight
Nosecone	650 mm	Nosecone shell (α-01)	0.8 kg
		Payload and its support	1.3 kg
		Nosecone flange (α-02)	0.8 kg
Recovery Bay	730 mm	Recovery section tube (β-01)	2.6 kg
		Recovery system	2.2 kg
Electronics Bay	350 mm	Plexiglass tube (γ-02)	0.6 kg
		E-Bay flanges (γ-01+γ-03)	1.6 kg
		Steel rods (γ-05)	0.8 kg
		Avionics	0.6 kg
Motor Bay	1200 mm	Dry motor	3.1 kg
		Solid propellant	4.8 kg
		Motor section tube (δ-01)	3.8 kg
		Bulkhead (S-PRP-01)	1.1 kg
		Centering rings-phenolic tube assembly (S-PRP-02)	1.2 kg
		Boat tail (δ-04)	0.2 kg
		Fin set	0.4 kg
Screws and other hardware			1.0 kg
TOTAL LENGTH:	**2930 mm**	**TOTAL MASS:**	**26.9 kg**

Electronics System Data - Telemetry System	
Frequency	868 MHz
Bandwith	125 kHz
Modulation	LoRa (Chirp Spread Spectrum)
Comunication protocol	SPI
Power	25/31 mW (14/15 dBm)
Range	5 km

Main Expected Performance Parameters	
Expected apogee	2960 m AGL
Expected stability margin during flight	1.65 – 2.55 calibers
Expected acceleration	65 m/s^2
Expected off-the-rail speed	33.45 m/s
Expected max velocity	255 m/s

Appendix B

Detailed test reports

B.1 Recovery System Testing

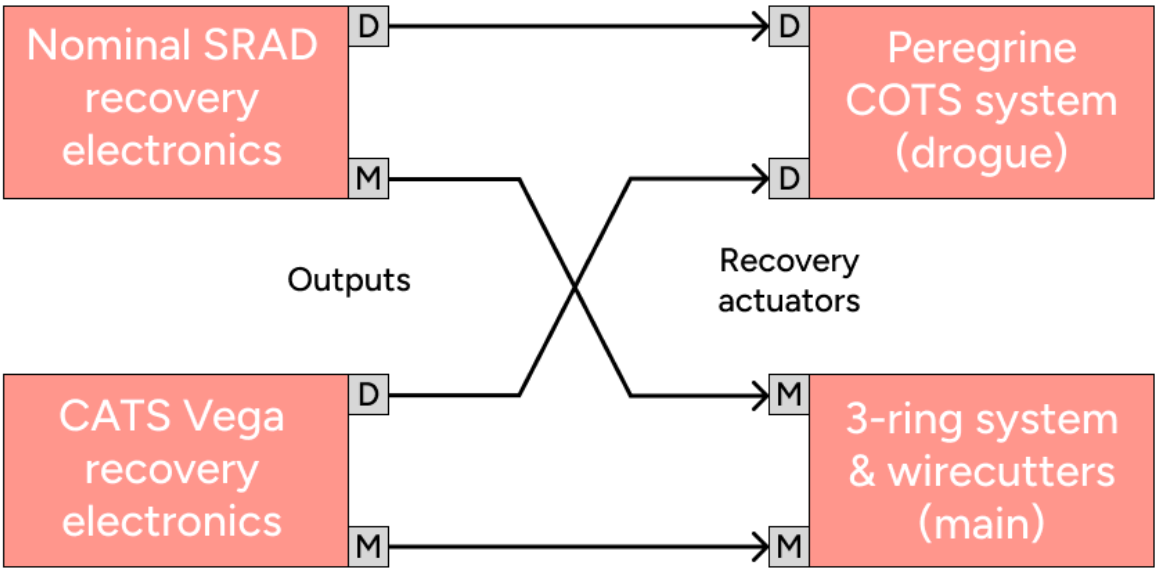

Fig. 4.1: Schematics of recovery system redundancy.

The redundancy of the recovery system in Figure 4.1 satisfy the requirements imposed by EuRoC documentation [6]: the SRAD electronics is paired with a CATS Vega board that can activate the recovery system independently from our in-house produced board. Redundancy is also applied to the actuators, since two E-matches (that can be fired from both COTS and SRAD boards) are used for both CO2 cartridges, and each of them is singularly capable of detaching the nosecone during the first deployment event.

Test Report: Shear Pins, E-match and CO2 Ejection System Test		
Team: Aurora Rocketry	**Team ID:** 06	**Date:** 12/09/2025

Test Motivation:

The aim of this test was to verify whether the E-match would work and fire the CO2 ejection system successfully, and then verify that the shear pins of the nose cone flange would break and allow the flange to be separated from the main body. Testing shear pins, E-matches and the CO2 ejection system is very important because any malfunction to this subsystem would jeopardize the whole recovery system, rendering it unable to function correctly and deploy the parachutes.

Nominal Test Description:

First, the test needs to be set up. This involves the preparation of the recovery system according to its checklist, which roughly translates to this sequence of elementary steps:

- The parachutes and the various wires and swivel-links have to be connected and put inside the inner tube, which should then be placed inside the main tube;
- The aft arresting plate needs to be put in position, making sure all cables go through its central cavity;
- E-matches have to be prepared and the CO2 ejection system has to be assembled and placed correctly inside the main tube;
- The flange has to be attached to the nose cone using six shear pins, with a payload consisting of four 500ml water bottles on it to account for the real load;
- After the initial setup, the whole assembly has to be taken to a safe location and placed almost vertically, to account for adverse gravity effects;
- From this position, the E-matches should be connected to the test battery to activate the recovery mechanism.

It was expected that the pressurized gas released by the canisters in the expansion chamber would cause the inner tube to move forward and break the shear pins, which would then allow the nose cone to be detached and deploy the drogue parachute.

Actual Test Description:

The test was performed in the early afternoon in sunny conditions, and all operations were conducted following the nominal sequence. It has to be noted that, compared to the system that was described in the technical report, two silicone pads were added to each end of the cylindrical chamber in which the CO2 cartridges eject their gases, to minimize dispersion and maximize pressure in that chamber, allowing the internal tube to thrust forward with maximum force to break the shear pins and eject the nosecone. In addition, all six shear-pins slots were used instead of three.

Final Results and Interpretation:

The CO2 canisters released enough force to be able to push the internal tube and break the shear pins, ejecting the nosecone despite the added weight, the almost vertical position and the inevitable pressure leakage, due to the cables going through both the aft arresting plate ahead of the expansion chamber and the CO2-cartridges-holding plate behind it.

This result was obtained consistently in multiple tests, without appreciable degradations of performance or system integrity. This was considered satisfactory, and the test was declared successful.

Components and test set-up pictures:




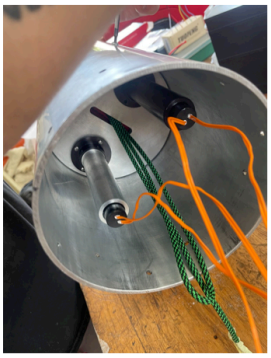


Pictures of the components after the test:




Responsibles:

Names	Signatures
Giorgia Capozucca	
Amira Benelkaid	
Caterina Laghi	

Test Report: Drogue Chute Deployment Test		
Team: Aurora Rocketry	**Team ID:** 06	**Date:** 21/08/2025

Test Motivation:

In this test we checked whether the drogue parachute opened correctly under the action of aerodynamic forces. It was very important to test the correct opening of this parachute because in case of a malfunction, the main parachute would not be able to open afterwards. We tried to test it by placing it against the wind and observing how the parachute material behaved, always trying to simulate a fall at approximately the speed with which the rocket will fall.

Nominal Test Description:

The test has to be performed by simulating the rocket's descent speed. To do this, it was decided to use a car and deploy the drogue parachute from its trunk, leaving it exposed to the relative wind and free to open completely.

The parachute is expected to open correctly and maintain a certain air resistance in order to create a certain deceleration.

Actual Test Description:

The test was prepared and executed without significant variations to the previous description.

Final Results and Interpretation:

The test went as expected, the drogue parachute opened successfully, allowing the implemented system to function correctly. This test strengthens our belief that the drogue will open correctly and that it will be able to provide the required deceleration for the rocket.

Responsibles:

Names	Signatures
Giorgia Capozucca	
Amira Benelkaid	
Caterina Laghi	

Test Report: 3-Ring Release System Test		
Team: Aurora Rocketry	**Team ID:** 06	**Date:** 14/08/2025

Test Motivation:

This test was carried out to check the correct functioning of the 3-ring release system, as well as to test the connection with the drogue and consequently the effective expulsion of the main chute. This test (as you can also see from the attached photos) was carried out using a 27 kg mass. Consequently, not only the functioning of the cable cutter system that holds the three rings together was tested, but also the force that the ropes can withstand. The cable cutter system (Piranha system) is composed of an e-match that triggers an exothermic reaction that cuts the cable with which the 3-ring release system remains connected. This was a relevant part to be tested, because a malfunction of this system could lead to the main parachute failing to deploy.

Nominal Test Description:

First, the e-matches have to be prepared and the Piranha system needs to be assembled and placed on the wire that is going to be cut by the system during the deployment of the main parachute. Then the top of the three-ring system cord has to be secured to a fixed element, and a mass of 27 Kg that simulates the weight of the rocket has to be attached to it to check whether the cords and the system could withstand the applied load.

Actual Test Description:

The test was successfully conducted without significant variations to the nominal description.

Final Results and Interpretation:

The 3-ring-system was correctly released, ensuring that the cords could withstand the applied load. The results of this test underline the reliability of the 3-ring release system and also of the cable cutting system connected to it.

Components and test set-up pictures:

- Left figure: Testing of the three ring system with a basket simulating the weight of the rocket.
- Right Figure: Elements of the three ring system being assembled.

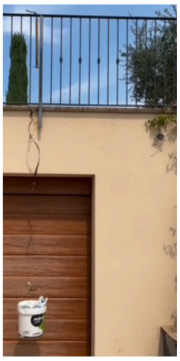

Responsibles:

Names	Signatures
Giorgia Capozucca	
Sara Ferrari	
Caterina Laghi	

Test Report: Main Parachute Deployment Test		
Team: Aurora Rocketry	**Team ID:** 06	**Date:** 14/08/2025

Test Motivation:

The correct opening of the main parachute had to be tested, attaching to it a weight that could simulate the rocket, thus checking that it could support such a load. This test was relevant for the recovery system, because without the correct opening of this parachute, the rocket would fall to the ground at around 25 m/s, compromising structural integrity after impact.

Nominal Test Description:

The parachute is expected to deploy without significant resistance by having the simulated rocket weight attached. The deployment bag and its behavior also have to be tested by applying that specific weight. It was expected for the main chute to exit the deployment bag practically instantaneously.

Actual Test Description:

The main parachute opened as expected and the deployment bag did not offer significant resistance to the parachute release, so it can be concluded that it does not create particular friction or obstacle to the main chute.

Final Results and Interpretation:

The test gave the expected results, which strengthens our expectations for the correct opening of the main chute. Furthermore, these results can be considered solid thanks to the use of swivels to prevent the tangling of cables and a well-assembled deployment sequence.

Responsibles:

Names	Signatures
Giorgia Capozucca	
Sara Ferrari	
Caterina Laghi	

B.2 Electronics Thermal Testing

Test Report: Electronics Thermal Testing		
Team: Aurora Rocketry	**Team ID:** 06	**Date:** 27/08/2025

Test Motivation:

The following test, in addition to being expressly required by regulation, is fundamental for understanding the behavior of the rocket's avionics in environments with stressful temperatures such as those inside the rocket's fuselage. It is therefore used to ensure that even if the rocket remains on the launch pad for prolonged periods at high temperatures, the reliability of the avionics is not compromised.

Minimum Objects and Expected Results:

System	Minimum Required Value	Expected Target Value	Expected Safety Factor
Battery Life	6h	16h	2.67

Tools and Equipment:

Tools	Protective Equipment	Vehicle Part Involved
Oven	/	SRAD Avionics
Multimeter	/	Batteries
Thermoresistence	/	/

Nominal Test Description:

The purpose of the test was to evaluate the avionics and the connected batteries over an extended period (6 hours, in accordance with the regulations proposed by the competition) at a temperature comparable to those likely to occur on the launch pad.
For this purpose, we determined that a temperature of 55 °C would be more than sufficient to assess the reliability of the boards.
Once the test conditions were defined, a program was loaded onto the boards to simulate the operation of all components simultaneously, while saving all the resulting data to a microSD card.
The goal was to leave the boards in the oven for 6 hours and log the following data:

- Accelerometer magnitude;
- Acceleration x, y, z (IMU);
- Angular velocity x, y, z (IMU);
- Barometer pressure 1 and 2;
- Temperature (measured by the barometer);
- Battery temperature and charge;

In addition to the data from the SRAD avionics, we also logged the battery temperature using an external resistance thermometer to check for possible overheating.
The test is considered passed if:

- There are no interruptions or errors in data reading for the entire 6 hours;
- The batteries continuously power the cards;

- The reduction in battery life must not be such that it prevents us from achieving the target 6 hours of battery life.

Actual Test Description:

The test performed as expected, with two discrepancies from the nominal values:

- At 2:40 PM, the board was removed from the oven for about two minutes to download the data stored on the microSD card up to that point and to verify that everything was proceeding as expected. As a result, some values may have varied while the board was being moved.
- Due to a software issue, the GPS and transmitting antenna did not function during the test. This resulted in lower battery consumption; according to the datasheet, this reduced the consumption by 30 mAh. Therefore, instead of the board's nominal consumption of 150 mAh, the load ultimately consumed 120 mAh.

Expected and Actual Results Comparison:

System	Minimum Required Value	Actual Value	Actual Safety Factor
Battery Life	6h	6h	1

Note: The actual value could potentially have been much higher, but since this is not a stress test we decided to limit ourselves to verifying that the autonomy required by the competition was achieved even under adverse conditions. Therefore, at the end of the 6 hours the batteries were removed from the oven, leading to this result.

Color Coding
Actual S.F. exceeds Expected S.F.
Actual S.F. between 1.0 and Expected S.F.
Actual S.F below 1.0.

Final Results and Interpretation:

The tests were successful because all three pass conditions were met:

- There were no interruptions or abnormal behavior of the board during the entire 6 hours, and temperature did not affect the accuracy of the collected data.
- The batteries maintained power for the entire 6 hours without overheating or excessive discharge.
- The battery discharge followed a curve similar to that observed under normal conditions; no degradation was observed. After 6 hours, 760 mAh was consumed, which is consistent with the board's consumption of 120 mA (excluding the 30 mA mentioned above). This leads us to conclude that, under nominal conditions, approximately 40 mA more than normal was consumed due to the stressful conditions in the oven. In percentage terms, this corresponds to a 5.5% increase in consumption.

Graphs:

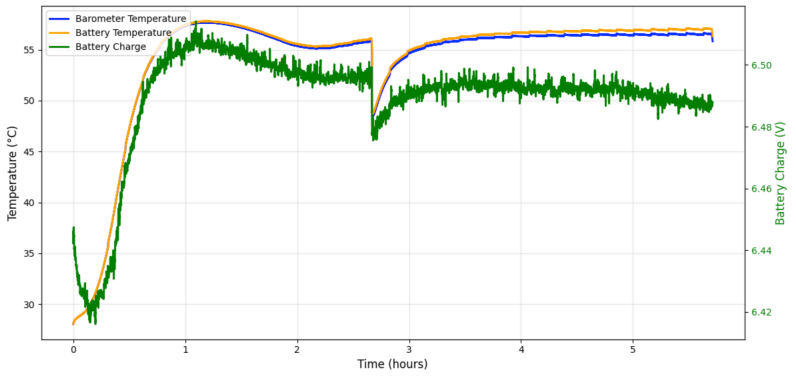

Fig. 4.18: Temperature and battery charge over time.

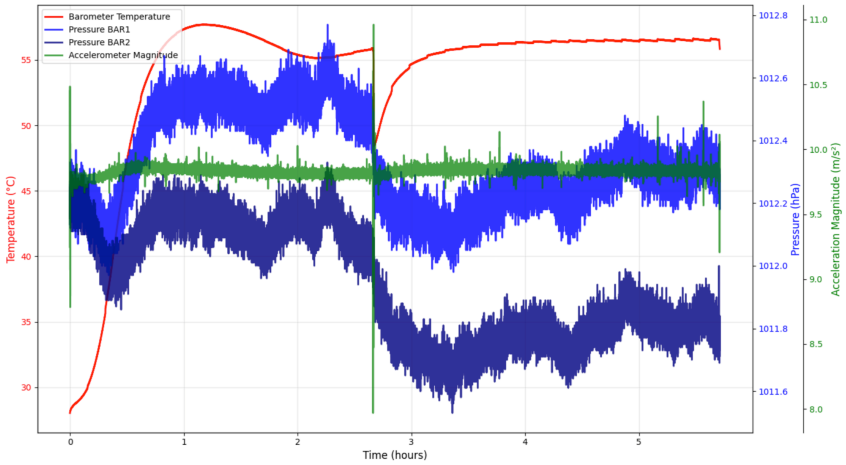

Fig. 4.19: Barometer temperature, pressure and accelerometer data over time.

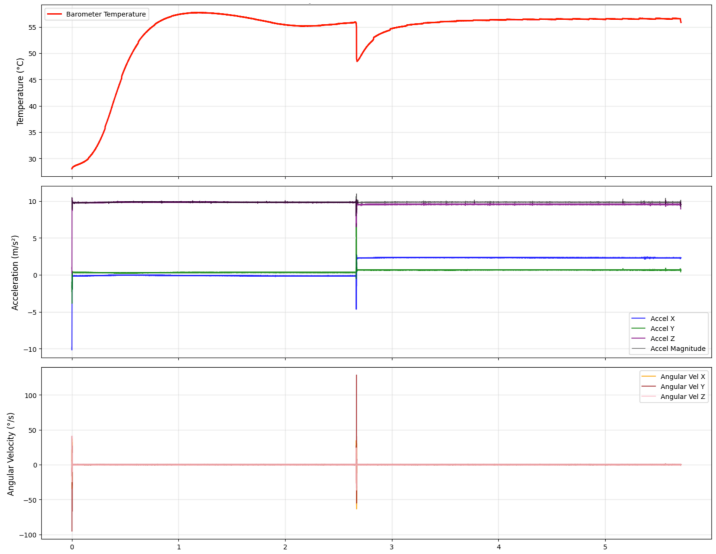

Fig. 4.20: Barometer temperature and IMU sensor data over time (hours).

Execution Images:

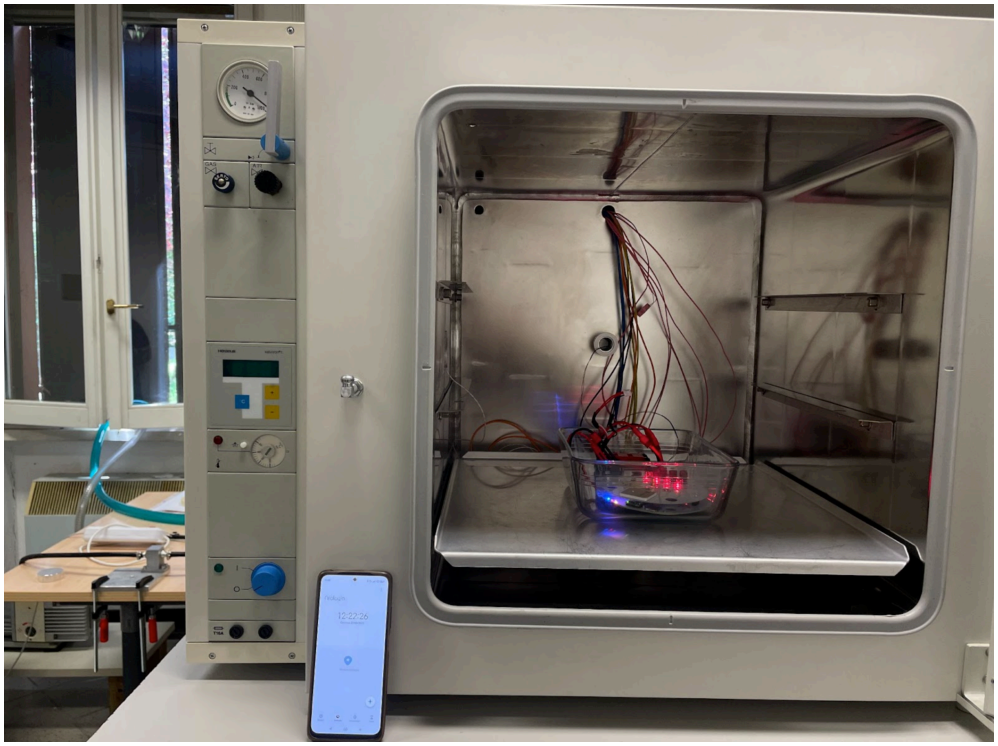

Fig. 4.21: Time 12:23 AM.

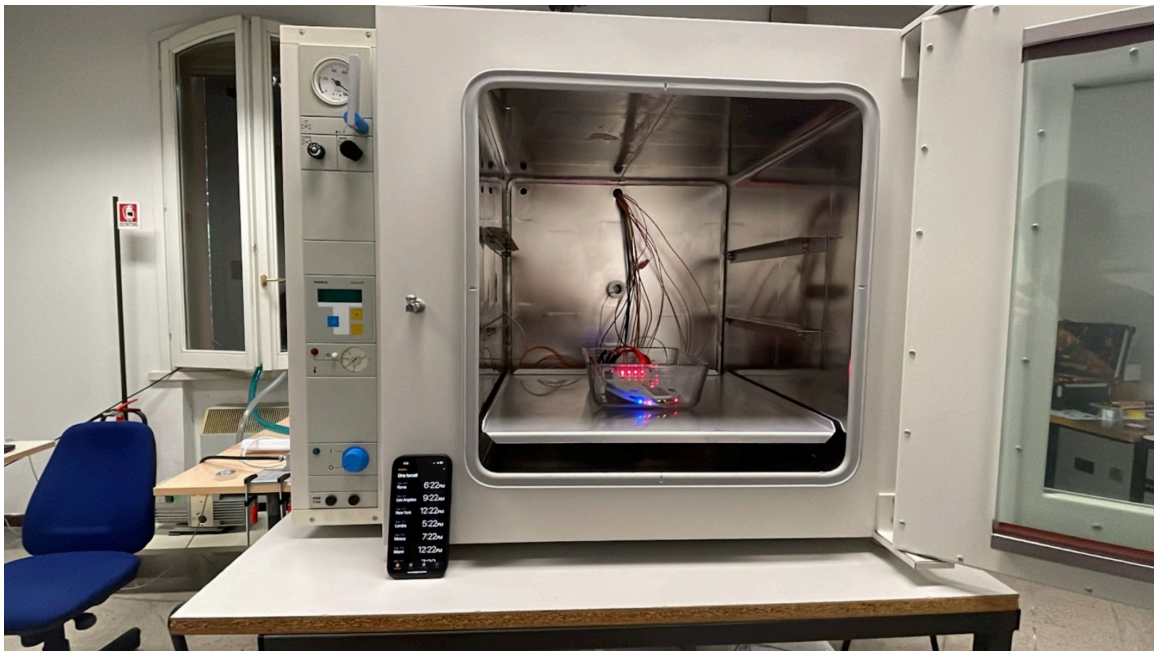

Fig. 4.22: Time 6:22 PM.

Responsibles:

Names	Signatures
Lorenzo Matti	
Giacomo Antonelli	
Lorenzo Ravaioli	
Simone Fantoni	

B.3 SRAD Propulsion System Testing

THIS PAGE IS INTENTIONALLY LEFT BLANK

B.4 SRAD Pressure Vessel Testing

THIS PAGE IS INTENTIONALLY LEFT BLANK

B.5 SRAD Electronics Apogee Detection Test

Test Report: SRAD Electronics Apogee Detection Test		
Team: Aurora Rocketry	**Team ID:** 06	**Date:** 05/09/2025

Test Motivation:

The objective of this test was to evaluate the functionality of the apogee detection algorithm and both parachute deployment routines implemented on the SRAD Avionics system.

Tools and Equipment:

Tools	Protective Equipment	Vehicle Part Involved
USB-C Cable	/	SRAD Avionics
Digital Multimeter	/	/
SD Card	/	/

Nominal Test Description:

The test uses a dataset generated through RocketPy simulations developed by our team. This dataset was processed using our Extended Kalman Filter (EKF) implementation, incorporating mathematically modelled sensor noise and errors to obtain a close approximation of actual flight data.

The processed dataset was saved onto an SD card mounted on the SRAD Avionics system, and subsequently fed into the Apogee Detection and Parachute Deployment algorithm.

To verify the correct operation of the deployment routines:

A digital multimeter was connected to the Drogue actuators to confirm activation at the correct time.

After the Drogue deployment was confirmed, the multimeter was connected to the Main actuators to verify their functionality.

Actual Test Description:

The test setup involved the following components:

- The Avionics Board, which includes the SD card reader and onboard sensors.
- The Antenna Board, which houses the actuators and telecommunication modules (LoRa and GPS).

The two boards were connected using the designated connectors. The MCU was connected to a PC via a USB-C cable for serial communication and logging.

A digital multimeter was attached to the Drogue actuator output to monitor voltage when deployment conditions were met during dataset playback. Actuator activation was confirmed when the multimeter measured a voltage of 5V across the actuator terminals, indicating that the deployment condition had been correctly evaluated and executed by the system.

The test program was developed to:

- Check SD card connection and health.
- Open and parse the CSV-formatted dataset.

- Run the data through the Apogee Detection algorithm with a fixed delay of 30 ms per loop iteration, simulating real-time operation.

Note: Although this test did not use live sensor readings, it relied on our EKF implementation with simulated data that closely resemble real flight data.

Expected and Actual Results Comparison:

System	Minimum Required Value	Actual Value	Actual Safety Factor
Drogue Actuators Vertical Velocity activation	0 m/s	−3.08 m/s	96.92%
Main Actuators Altitude threshold	450 m	446.0 m	99%
Drogue Actuators Safety Delay	300 ms	300 ms	100%
Main Actuators Safety Delay	100 ms	100 ms	100%
Drogue Actuators voltage	5 V	5 V	100%
Main Actuators voltage	5 V	5 V	100%

Color Coding
Actual S.F. over 95%
Actual S.F. between 80% and 95%
Actual S.F below 80%

Final Results and Interpretation:

The test confirmed that:

- The apogee detection algorithm performs as intended, correctly evaluating conditions based on altitude thresholds and timing constraints.
- The parachute deployment routines were executed promptly, with actuators triggered within milliseconds of the corresponding simulation events.

While the exact timing of actuator activation did not perfectly match the simulated flight profile, the deviations remained well within acceptable margins. It is important to note that the goal of this test was to validate the algorithm's logic and condition evaluation, not to test exact adherence to simulation timing.

The test was successful. The system behaved as expected, demonstrating that the apogee detection and parachute deployment logic is correctly implemented and operational under realistic conditions.

Graphs:

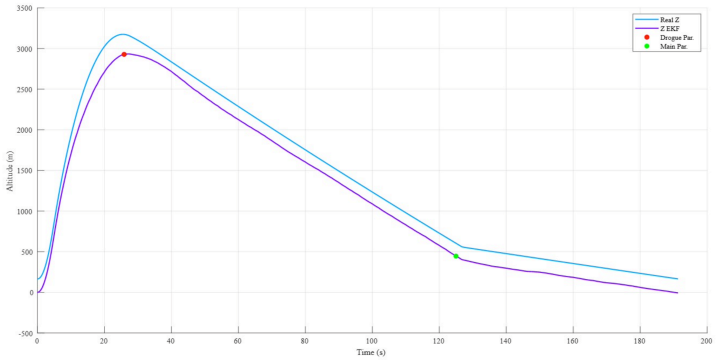

Fig. 4.27: Actuators activation on altitude vs time graph.

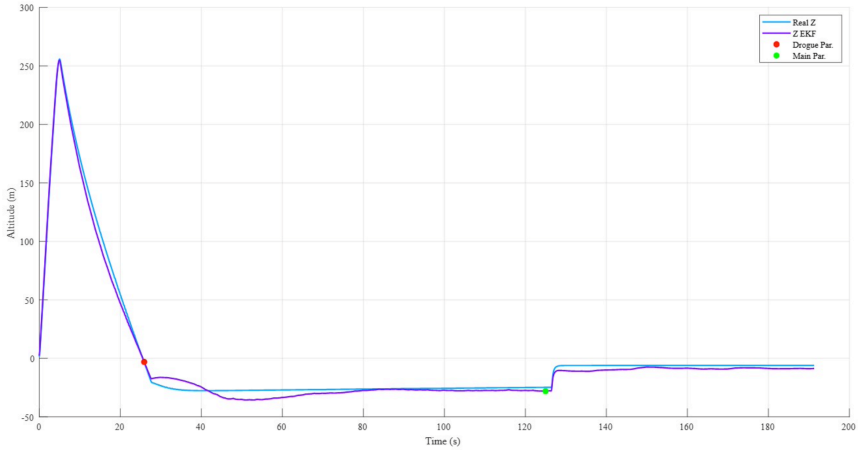

Fig. 4.28: Actuators activation on vertical velocity vs time graph.

Responsibles:

Names	Signatures
Alessandro Monticelli	
Giacomo Antonelli	
Lorenzo Matti	

B.6 Other tests

Test Report: Mechanical Stress Test on Connectors		
Team: Aurora Rocketry	**Team ID:** 06	**Date:** 14/09/2025

Test Motivation:

The aim of this test is to verify that the connections between the recovery section and the electronics bay are robust in order to avoid unwanted disconnections.

Minimum Objects and Expected Results:

System	Minimum Required Value	Expected Target Value	Expected Safety Factor
Connection strength	1 kg	1.5 kg	1.5

Tools and Equipment:

Tools	Protective Equipment	Vehicle Part Involved
Electrician’s cable ties	/	E-bay
20 AWG cables	/	/

Nominal Test Description:

The test will be performed as follows:

- The avionics board will be inserted and fixed into the e-bay.
- Cables will be prepared with a 2-pin MOLEX connector on one end to be inserted into the avionics board, and an indicator LED on the other end.
- The cable will be wrapped around the e-bay bars and secured with two cable ties to keep it secure.
- The male MOLEX connector on the cable will be inserted one by one into the various female connectors on the avionics board (these connectors are the ones that send the parachute opening signal to the recovery system).
- For each connector, the cable will be subjected to a pull of 1.5 kg for approximately 5 seconds.
- The test will be considered passed if the LED remains lit during these 5 seconds (indicating that electrical continuity has been maintained) and if this is successful for all 4 connectors on the avionics board.

Actual Test Description:

The test was carried out as described in the nominal test procedure and performed as expected. Once we observed that the cables could sustain more than the target load,we intentionally exceeded the target value on one actuator. This allowed us to successfully lift our setup, which weighs around 2.4 kg.

Expected and Actual Results Comparison:

System	Minimum Required Value	Actual Value	Actual Safety Factor
Connection strength	1 kg	1.7 kg	1.7

Color Coding
Actual S.F. exceeds Expected S.F.
Actual S.F. between 1.0 and Expected S.F.
Actual S.F below 1.0

Final Results and Interpretation:

The test results exceeded our expectations. All actuators were able to sustain approximately 1.7 kg for 5 seconds, with no continuity issues, as demonstrated by the yellow LED which remained lit. Below some pictures of the test.

Main Test Images:

Fig. 4.32: Connector 1 test (main).

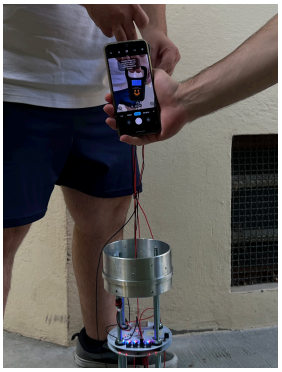

Fig. 4.33: Connector 2 test (main).

Drogue Test Images:

Fig. 4.34: Connector 3 test (drogue).

Fig. 4.35: Connector 4 test (drogue).

Responsibles:

Names	Signatures
Lorenzo Matti	
Mattia Mattucci	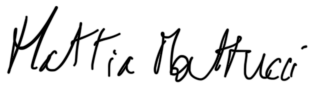
Riccardo Alessandro Bevoni	

Appendix C

Hazard Analysis Report

Hazard Analysis						
Hazardous Material	Storage	Handling	Transportation	Risk of Mishap	Mitigation	Risk after Mitigation
Black Powder	Stored in a safe container in a cupboard	Handled with gloves while wearing a faceshield	Transported in a small airtight plastic container	Medium, the risk is mainly linked to fire and heat sources	Low quantity of powder are used and the lid of the container is removed for a short peridot of time	Low

Appendix D

Risk Assessment

Risk Assessment					
Failure Mode	Phase	Failure Probability	Mishap Severity	Criticality Ranking	Team's Comments and Mitigation strategies
Fin Rupture due to Flutter	Powered ascent	1	3	3	See chapter 2.3.2 and Appendix B
Shear Pins not Breaking	Drogue deployment	1	3	3	See chapter 2.5.5 and Appendix B
Drogue Opening Failure	Drogue deployment	1	3	3	See chapter 2.5.3 and Appendix B
3-Rings Release System Failure	Main deployment	1	3	3	3-Rings release systems are highly common for their reliability; See chapter 2.5.4 and Appendix B
Main Opening Failure	Main deployment	1	3	3	See chapter 2.5.3 and Appendix B
Apogee not detected due to EKF failure, sensor bug, saturation or FSM hang	Apogee	1	3	3	A watchdog is implemented to force deployment if altitude falls below safe threshold or max time exceeded; will be tested
FSM state transition failure	Any phase	1	3	3	Watchdog monitoring, manual override logic; FSM unit will be tested
Ground launch detected as apogee (false apogee)	Liftoff	1	3	3	Required sustained descent rate and minimum time after launch before valid apogee detection
Accidental de-arming of the recovery detection system	Any phase	1	3	3	We reduced the chance of this issue by using a bypass system for the recovery switch. This is done with a connector: when it is plugged in, the system is disarmed; when it is removed, the system is armed. The only way the system could disarm by mistake is if a piece of conductive material touches both pins and closes the circuit. This is very unlikely. Even if it happens, the high current would probably burn the material quickly, reopening the circuit and letting the system work correctly
Connector detachment due to mechanical stress during separation of rocket stages and drogue parachute deployment	Drogue deployment	1	3	3	Mechanical Stress Tests will help us check if the connectors can resist the forces during separation (See Appendix B). This way, we make sure the system stays safe and reliable

Risk Assessment					
Battery malfunction due to high temperatures	Any phase	1	3	3	See Appendix B
Barometer drift or failure mid-flight	Any phase	1	2	2	Two barometers are used; cross-check and discard outliers via filter logic
Acceleration saturation or clipping during launch	Any phase	1	2	2	Sensor saturation detection and avoiding using clipped values in EKF; dynamic weighting
Bad IMU calibration	Any phase	1	2	2	Calibration to be performed only when system is stable; sanity check IMU data before launch
Telemetry not working	Any phase	2	1	2	Pre-launch telemetry health check, retry logic on send failure
EEPROM/Flash write error (e.g., flight log corrupted)	Any phase	1	1	1	Add retry logic, verify writes; critical data sent over telemetry
Bulkhead failure	Powered ascent	1	3	3	See chapter 2.4 and Appendix I
Upper electronics bay flange failure	Main deployment	1	3	3	See chapter 2.4 and Appendix I
Loss of bulkhead screws	Any phase	1	2	2	If a single screw pops off, redundancy is guaranteed by the screws that are still intact (8)
Loss of electronics bay screws	Any phase	1	1	1	If a single screw pops off, redundancy is guaranteed by the screws that are still intact (12 per bay)
Loss of centering ring screws	Any phase	1	1	1	If a single screw pops off, redundancy is guaranteed by the screws that are still intact (3 per ring)
Loss of Peregrine plate screws	Any phase	1	1	1	If a single screw pops off, redundancy is guaranteed by the screws that are still intact (6)
Aftmost rail button screw failure	On-pad preparations	1	3	3	See chapter 2.4 and Appendix I

Appendix E

Compliance matrix

Verification Methods Legend:

By Review of Design:	By Inspection:	By Analysis:	By Test:
- S = Simple confirmation (Basic) - A = Reasoned argumentation (Thorough)	- SC = Simple check (Basic) - I = Inspection (Thorough)	- C = Calculation (Basic) - IDT = In-depth proofing (theoretical) (Thorough)	- T = Previous testing (Basic) - IDE = In-depth proofing (experimental) (Thorough)

Propulsion System					
CODE	**TITLE**	**STATUS**	**VERIFICATION METHOD**	**REFERENCE**	**REMARKS**
LV-RQT-0010	Non-toxic propellants	Compliant	S	Chapter 2.2.1	Cots motor with non toxic compliant propellent
LV-RQT-0020	Air-start ignition circuit electronics	N.A.	S,I	-	-
LV-RQT-0030	Ground-start ignition circuit arming distance	Compliant	SC	Chapter 2.2.1	Ignition system directly provided by EUROC
LV-RQT-0040	Clustered vehicle release system	N.A.	I, IDT	-	The rocket uses a single motor
LV-RQT-0050	Clustered vehicle stability proof	N.A.	C	-	-
LV-RQT-0060	Clustered vehicle arming	N.A.	I, A	-	-
LV-RQT-0070	Air-start ignition circuit arming	N.A.	I, A	-	-
LV-RQT-0080	COTS solid motors	Compliant	S	Chapter 2.2	Engine selected from EUROC's approved engine list
LV-RQT-0090	Ignition systems for solid motors	Compliant	S	Chapter 2.2.1	Ignition system directly provided by EUROC

Recovery System and Avionics					
CODE	**TITLE**	**STATUS**	**VERIFICATION METHOD**	**REFERENCE**	**REMARKS**
LV-RQT-0240	Redundant recovery system electronics	Compliant	S	Chapter 2.6	CATS Vega implemented for redundancy

LV-RQT-0250	Redundant COTS recovery electronics	Compliant	S	Chapter 2.6	CATS Vega implemented for redundancy
LV-RQT-0260	Recovery electronics access panel	Compliant	SC	Appendix G E-BAY	Plexiglass tube will be divided in two halves to provide easy access
LV-RQT-0270	Recovery electronics location	Compliant	SC	Chapter 2.3 Fig. 2.4	It is accessible without a ladder
LV-RQT-0280	Recovery electronics access	Compliant	SC	Chapter 2.3 Fig. 2.4	Switches are easily accessible without interference from other components
LV-RQT-0290	Recovery system energetic devices	Compliant	S	Chapter 2.4	The recovery system is using a COTS E-matches System
LV-RQT-0300	Onboard power systems	Compliant	S, I	Chapter 2.6	LiFePo4 batteries are used
LV-RQT-0310	Onboard power systems access	Compliant	SC	Chapter 2.6.3	The electronics bay fairing is split and can be removed for easy access
LV-RQT-0320	Launch rail standby time	Compliant	S	Chapter 2.6	Standby time is estimated to be up to 17 hrs
LV-RQT-0330	Non-parachute/parafoil recovery systems	N.A.	S, I, A, IDT	-	-
LV-RQT-0340	Dual deployment recovery	Compliant	A, C	Chapter 2.4.3	Dual deployment is implemented
LV-RQT-0350	Initial deployment event altitude	Compliant	A, C	Chapter 2.4.1	Drogue parachute deployment triggered by apogee detection
LV-RQT-0360	Initial deployment event descent velocity	Compliant	A, C	Chapter 2.4, Table 2.3, Appendix H	The COTS parachute manufacturer guarantees

					compliant speeds for the mass of nemesis
LV-RQT-0370	Main deployment event altitude	Compliant	A, C	Chapter 2.4.2	On board electronics follow a compliant barometric criterion for deployment
LV-RQT-0380	Main deployment event descent velocity	Compliant	A, C	Chapter 2.4, Table 2.3, Appendix H	The COTS parachute manufacturer guarantees compliant speeds for the mass of nemesis
LV-RQT-0390	Ejection gas protection	N.A.	S, I	-	-
LV-RQT-0400	Parachute swivel links	Compliant	S, I	Chapter 2.4.4	A series of quick links, eye bolts, shock cords and swivel links is implemented in order to avoid the effects of line torsion
LV-RQT-0410	Dual deployment parachute coloration	Compliant	S	Chapter 2.4.3, Figures 2.23, 2.24	-
LV-RQT-0420	Parachute coloration	Compliant	S	Chapter 2.4.3, Figures 2.23, 2.24	-
LV-RQT-0430	Mandatory system	Compliant	S	Chapter 2.6	CATS vega board present into the electronics bay
LV-RQT-0440	CATS transmitter call-sign	Compliant	S	-	-
LV-RQT-0450	CATS Vega firmware update	Compliant	S	-	-
LV-RQT-0460	CATS receiver	Compliant	S	-	-
LV-RQT-0470	CATS electronics	Compliant	S	-	-
LV-RQT-0480	Cable management	Compliant	S, I	Chapter 2.6	The use of cables is minimal since self contained PCBs are used.

					All cables are properly secured and managed
LV-RQT-0490	Secure connections	Compliant	I	Chapter 2.6	All cables are properly secured and managed
LV-RQT-0500	Cryo-compatible wire insulation	N.A.	I	-	-
LV-RQT-0510	Electronics thermal testing	Partially compliant	T	-	Tests have been completed with success, but reports are yet to be finalized and delivered. All test reports will be sent together before the new deadline (14th of September)
LV-RQT-0520	Recovery system ground test demonstration	Partially compliant	T	-	Tests have been completed with success, but reports are yet to be finalized and delivered. All test reports will be sent together before the new deadline (14th of September)

Stored-Energy Devices					
CODE	**TITLE**	**STATUS**	**VERIFICATION METHOD**	**REFERENCE**	**REMARKS**
LV-RQT-0530	Energetic device safing and arming	Compliant	SC	Chapter 3 Fig. 3.1	Subsystems are only armed when the rocket is on the rail
LV-RQT-0540	Arming device access	Compliant	SC	Chapter 2.3 Fig. 2.4	Switches are easily accessible
LV-RQT-0550	Arming device location	Compliant	S	Chapter 2.3 Fig. 2.4	-

LV-RQT-0560	Burst discs	N.A.	A, I	-	The rocket does not use SRAD pressure vessels
LV-RQT-0570	Burst disc pressure	N.A.	A, I, C	-	-
LV-RQT-0580	Burst disc marking	N.A.	I	-	-
LV-RQT-0590	Burst discs material	N.A.	S	-	-
LV-RQT-0600	Relief device	N.A.	A, T	-	-
LV-RQT-0610	Designed burst pressure for metallic pressure vessels	N.A.	A, IDT	-	-
LV-RQT-0620	Designed burst pressure for composite pressure vessels	N.A.	A, IDT	-	-
LV-RQT-0630	Burst discs testing	N.A.	T	-	-
LV-RQT-0640	Proof pressure testing	N.A.	T	-	-

Active Flight Control System					
CODE	**TITLE**	**STATUS**	**VERIFICATION METHOD**	**REFERENCE**	**REMARKS**
LV-RQT-0650	Restricted control functionality	N.A.	S	-	The rocket does not implement active flight control systems
LV-RQT-0660	Unnecessary for stable flight	N.A.	A, C	-	-
LV-RQT-0670	Designed to fail safe	N.A.	A, IDT	-	-
LV-RQT-0680	Boost phase dormancy	N.A.	A, I	-	-
LV-RQT-0690	Active flight control system electronics	N.A.	SC	-	-
LV-RQT-0700	Active flight control system energetics	N.A.	S	-	-

Airframe Structures					
CODE	**TITLE**	**STATUS**	**VERIFICATION METHOD**	**REFERENCE**	**REMARKS**
LV-RQT-0710	Venting	Compliant	S, SC, C	-	3 mm holes will be made on the airframe for venting purposes.

LV-RQT-0720	Material selection	Compliant	S	Chapter 2.3	-
LV-RQT-0730	Load bearing eyebolts type	Compliant	SC	Chapter 2.4.3	-
LV-RQT-0740	Load bearing eyebolts and U-bolts material	Compliant	SC	Chapter 2.4.3	-
LV-RQT-0750	Coupling tubes	N.A.	A, SC	-	Coupling flanges are used to link the different sections of the rocket
LV-RQT-0760	Launch lugs mechanical attachment	Compliant	SC	Appendix I Rail Buttons Section	-
LV-RQT-0770	Aft launch lug support	Partially compliant	I, T	Appendix I	Simulations have been performed but a real test still has to be done
LV-RQT-0780	RF transparency	Compliant	S	Appendix G E-BAY Appendix G α-01	E-BAY window and Nose cone for the payload are both RF transparent
LV-RQT-0790	RF windows dimensioning	Compliant	S	Appendix G γ-02	-
LV-RQT-0800	RF windows material	Compliant	S	Appendix G E-BAY Appendix G α-01	E-BAY window is made of plexiglass Nose cone made of fiber glass
LV-RQT-0810	RF antennas' location	Compliant	S	Appendix G E-BAY	-
LV-RQT-0820	Internal RF antennas' location	Compliant	S	Appendix G E-BAY	-
LV-RQT-0830	Identifying markings	Compliant	S	-	Team numbers are on both sides of each fin

Payloads					
CODE	**TITLE**	**STATUS**	**VERIFICATION METHOD**	**REFERENCE**	**REMARKS**
LV-RQT-0840	Payloads	Compliant	S	Chapter 2.5	-
LV-RQT-0850	Payload form factor	Compliant	S	Chapter 2.5.2	-
LV-RQT-0860	Payload minimum mass	Compliant	I	Chapter 2.5.2	-
LV-RQT-0870	Payload mass factor	Compliant	S	Chapter 2.5.2	-
LV-RQT-0880	Independent payload functionality	Compliant	S	Chapter 2.5.3	-
LV-RQT-0890	Payload removal for weigh-in	Compliant	I	Chapter 2.5.2	-
LV-RQT-0900	Payload materials	Compliant	S	Chapter 2.5.2	-
LV-RQT-0910	Payload energetic devices	Compliant	S	Chapter 2.5.3	LiFePo4 batteries adopted
LV-RQT-0920	Recovery system	N.A.	S	-	The payload does not have a separate recovery system
LV-RQT-0930	Unique recovery system	N.A.	A, IDT	-	-
LV-RQT-0940	Descent velocity	N.A.	A, C	-	-
LV-RQT-0950	Recovery system electronics	N.A.	I	-	-
LV-RQT-0960	Payload safety critical wiring	N.A.	I	-	-
LV-RQT-0970	Recovery system testing	N.A.	T	-	-
LV-RQT-0980	Payload tracking	N.A.	S	-	-
LV-RQT-0990	Payload tracking call-sign	N.A.	S	-	-

Trajectory and Stability					
CODE	**TITLE**	**STATUS**	**VERIFICATION METHOD**	**REFERENCE**	**REMARKS**
LV-RQT-1000	Launch azimuth and elevation	Compliant	S	Chapter 3 and Appendix H	-
LV-RQT-1010	Rail take-off velocity	Compliant	C	Appendix H Fig 9	Since it is not significantly higher than 30 m/s, shorter rail guides will compromise this requirement

LV-RQT-1020	Hold-down system	N.A.	I, C, T	-	-
LV-RQT-1030	Stability margin	Compliant	C	Appendix H Fig 17	Stability calculations have been performed using OpenRocket and RocketPy

Launch Support Equipment					
CODE	**TITLE**	**STATUS**	**VERIFICATION METHOD**	**REFERENCE**	**REMARKS**
SE-RQT-0010	Operational range	N.A.	S	-	EuRoC-provided LSE and rails will be used for this launch
SE-RQT-0020	Fault tolerance and arming	N.A.	S	-	-
SE-RQT-0030	Safety critical switches	N.A.	S	-	-
SE-RQT-0040	Launch rail fit check	Partially compliant	I	-	It will be performed during the competition
SE-RQT-0050	Launch rail bottom spacer	Partially compliant	S	-	It is yet to be produced
SE-RQT-0060	Launch rail nominal elevation	N.A.	S	-	-
SE-RQT-0070	Launch rail elevation range	N.A.	S	-	-

Appendix F
Checklists

CHECKLIST #1: Preliminary operations

Team name:	Aurora Rocketry				
Team ID:	06	**Time to launch:**	On the first work day of the event	**Location:**	Paddock
Responsible/s:	Giorgia Capozucca		Giammarco Perugini		Davide Braglia
	Andrea Paoletti		Leonardo Cappetti		
Approved By:	Nicolò Basso				
Required time for completeness:			50 min		
Summary description:	The goal is to complete all preparation steps that will facilitate the work on the subsystems on the launch day; this includes assembling parts that were disassembled for transport.				

Equipment required:					
	Type:	**Quantity:**		**Type:**	**Quantity:**
Tools:	Spanner set	1	**Protective Equipment:**		
	Screwdriver set	1			

	Description	**Part ID**
Vehicle parts:	Thrust bulkhead	S-PRP-01
	Upper eye bolt	C-REC-EB
	Deployment bag	S-REC-04
	Disassembled AETHER payload & payload lower support	S-PLD-AET
	Nosecone flange	α-02
	200g ballast	-

	Main and drogue parachute lines	-
	Disassembled, inert parts of the 3-ring system	-

Steps:

Step:	Task description:	Comments:	Time required:	STATUS:	APPROVAL:
#1	Gather all necessary parts for this checklist	-	5 min	☐	☐
#2	Prepare the rocket stands to work on	Using the stands limits the risk of damage to the fins of the rocket.	3 min	☐	☐
#3	Build the Aurora AETHER cubesat using the parts in its box	-	20 min	☐	☐
#4	Run checklist #7 to test payload functionality	Remember to detach the batteries after the test	25 min	☐	☐
#5	Insert eye bolt in the nosecone flange from the bottom	-	0.5 min	☐	☐
#6	Place the lower payload support on the nosecone flange	Make sure that the threaded end of the eye bolt goes through the central hole in the payload support	2 min	☐	☐
#7	Fasten the eye bolt and the lower payload support to the nosecone flange using its nut and washer; add any necessary ballast to the eye bolt assembly	Ensure that two side holes of the support are lined up with two of the upper nosecone flange holes; check alignment with upper payload support; add any ballast to the eye bolt so as to secure it with its bolts (200 g)	2 min	☐	☐
#8	Insert the main parachute into its deployment bag	-	3 min	☐	☐
#9	Connect main and drogue parachute cords to swivels and to the 3-ring system	Verify knot security and swivel function	5 min	☐	☐
#10	Insert the thrust bulkhead into the motor bay and fasten it with its M8 screws	Gradually screw in the bolts and tighten them in a criss-cross pattern to evenly distribute the torque	4 min	☐	☐

#11	Glue the fins in position using the 3M dual-component glue; let the glue cure keeping the motor tube in an upright position	Verify the fit beofre applying the glue, and spread it evenly on all contact surfaces between the fins and the phenolic-centering ring assembly	15 min	☐	☐

We hereby confirm that all tasks of this checklist were completed.

Signature of Giorgia Capozucca

Signature of Giammarco Perugini

Signature of Davide Braglia

Signature of Andrea Paoletti

Signature of Leonardo Cappetti

Signature of Nicolò Basso - Responsible of Approval

CHECKLIST #2: Functional test of the electronic boards

Team name:	Aurora Rocketry				
Team ID:	06	**Time to launch:**	Day before and LRR - 90 min	**Location:**	Paddock + Tent/ Assembly area
Responsible/s:	Alessandro Monticelli		Lorenzo Matti		Mattia Mattucci
Approved By:	Alessandro Monticelli				
Required time for completeness:			15 min		
Summary description:	The goal is to test the boards taken to EUROC to ensure none of them were damaged during the transport, and the algorithm works consistently. This procedure tests the sensors, the actuators, the SD card memory and the data transmission. The software used for the test is designed to automatically follow the procedure, based on routines, and they can be repeated if an error shows up.				

Equipment required:					
	Type:	**Quantity:**		**Type:**	**Quantity:**
Tools:	PC	1	**Protective Equipment:**	LiFePo4 safety pack	2
	USB-C cable (data only)	1			
	Error Diagnostic Table	1			
	6.4V test battery	2			
	Generic electric wire	1m			

	Description	**Part ID**
Vehicle parts:	Sensor board(s)	S-ELC-01
	Antenna board(s)	S-ELC-02
	Wi-Fi board	-

	Omni-directional antenna	C-ELC-ODA

Steps:					
Step:	**Task description:**	**Comments:**	**Time required:**	**STATUS:**	**APPROVAL:**
#1	Check boards for damage	Inspect the boards for damages or missing parts.	1 min	☐	☐
#2	Join together the Sensor and Antenna boards	Fix together the Sensor board to the Antenna board by connecting the pins.	1 min	☐	☐
#3	Insert the SD card inside the Sensor board	-	-	☐	☐
#4	Power ON the board with the test battery pack	Use the 6.4V batteries to power on the boards.	1 min	☐	☐
#5	Connect the PC via USB-C (data only)	-	-	☐	☐
#6	Check if system status is “PRE_FLIGHT”	The system status is shown on the serial monitor.	-	☐	☐
#7	Ensure that the Power Supply LEDs are ON	• Battery • 6.4V • 3.3V • PWR (x4) • S (x4) • IN (flashing)	-	☐	☐
#8	Ensure that the SD LED is ON	Check if the IN LED is flashing	-	☐	☐
#9	Ensure that the Actuators LEDs are ON	-	-	☐	☐
#10	Type “PASSED” to continue	If one of the previous test failed, type “FAILED” to repeat the tests.	-	☐	☐
#11	Start the Sensor Test routine	-	-	☐	☐
#12	Check if output on serial monitor are positive	Make sure the data are correct by manually checking them, to ensure that the outputs are realistic.	2 min	☐	☐

#13	Type “PASSED” to continue	If one of the previous test failed, type “FAILED” to repeat the tests.	-	☐	☐
#14	Start the Actuator Test routine	-	-	☐	☐
#15	Power ON the actuators one by one and check LEDs	Ensure that the LED lights up with its corresponding actuator.	2 min	☐	☐
#16	Type “PASSED” to continue	If one of the previous test failed, type “FAILED” to repeat the tests.	-	☐	☐
#17	Start the SD Card Test routine	-	-	☐	☐
#18	Check if data can be read and written on the SD	-	-	☐	☐
#19	Type “PASSED” to continue	If one of the previous test failed, type “FAILED” to repeat the tests.	-	☐	☐
#20	Install the Omni-directional antenna	Install the antenna by screwing it in to the Antenna board	5 min	☐	☐
#21	Check transmission between the Antenna board and the Ground Station	-	2 min	☐	☐
#22	Type “PASSED” to continue	If one of the previous test failed, type “FAILED” to repeat the tests.	-	☐	☐
#23	Power OFF both boards	Power OFF the boards by disconnecting the power cable from the batteries.	1 min	☐	☐

We hereby confirm that all tasks of this checklist were completed.

Signature of Alessandro Monticelli

Signature of Lorenzo Matti

Signature of Mattia Mattucci

Signature of Alessandro Monticelli - Responsible of Approval

CHECKLIST #3: Ground station final assembly

Team name:	Aurora Rocketry				
Team ID:	06	**Time to launch:**	On the first work day of the event	**Location:**	Paddock
Responsible/s:	Mattia Mattucci		Lorenzo Matti		Simone Fantoni
Approved By:	Mattia Mattucci				
Required time for completeness:			15 min		
Summary description:	The goal for this procedure is to assemble the SRAD Ground Station, making sure the board, the screen and the antenna are ready for the flight.				

Equipment required:					
	Type:	**Quantity:**		**Type:**	**Quantity:**
Tools:	PC	1	**Protective Equipment:**		
	USB-C cable (data only)	1			
	Multimeter	1			
	Generic electric wire	1m			

	Description	**Part ID**
Vehicle parts:	Ground station	S-ELC-01
	Spare ground station boards	-
	Spare antennas	-

Steps:					
Step:	**Task description:**	**Comments:**	**Time required:**	**STATUS:**	**APPROVAL:**
#1	Check assembly for completeness	Inspect the Ground Station for damages or missing parts	1 min	☐	☐
#2	Check power inside the 12V battery pack using the Multimeter	Make sure that the battery pack reads a voltage $\geq$ 12.8V. If the reading is lower, charge the battery.	2 min	☐	☐
#3	Remove top panel	Remove top screws and lift the upper panel	1 min	☐	☐
#4	Connect the PC via USB-C (data only) to the Arduino	Make sure that the cable passes through the hole.	-	☐	☐
#5	Connect the battery cable to the board	Connect the battery cables to the screw terminal on the board. Make sure that the cable passes through the hole.	1 min	☐	☐
#6	Ensure the RED LED lights up	If the LED does not light up: Check voltage with the multimeter between +5 volt and GND: • if readback is = 5 V proceed, the LED is broken; • If readback is negative, check voltage between the screw terminal; • If readback is = 12 V, the board needs to be changed (voltage regulator failure);	2 min	☐	☐
#7	Make sure that the OLED and LED connectors are all connected to the board	-	1 min	☐	☐
#8	Assemble top panel	Make sure to tight all the top screws	2 min	☐	☐
#9	Test avionics-to-ground communication	Make sure that the ground station receives the signal from the electronics of the rocket	2 min	☐	☐

#10	Check if the OLED screen lights up	If the OLED screen does not light up, check if its a software issue. If not, change the OLED screen.	1 min	☐	☐
#11	Ensure the transmission LED is blinking	If the LED is not blinking, check for issues regarding the electronics of the rocket. If no issues are found, change the antenna module or the board.	2 min	☐	☐

We hereby confirm that all tasks of this checklist were completed.

Signature of Mattia Mattucci

Signature of Lorenzo Matti

Signature of Simone Fantoni

Signature of Mattia Mattucci - Responsible of Approval

CHECKLIST #4: Electronics Bay assembly

Team name:	Aurora Rocketry				
Team ID:	06	**Time to launch:**	On the first work day of the event	**Location:**	Paddock
Responsible/s:	Giammarco Perugini		Lorenzo Matti		Simone Fantoni
	Andrea Cecchini				
Approved By:	Giammarco Perugini				
Required time for completeness:			70 min		
Summary description:	This checklist describes the assembly procedure for the structure of the Electronics Bay and for the installation of all the components (boards, batteries and antenna) inside of it, ensuring a fixed and stable position during flight.				

Equipment required:					
	Type:	**Quantity:**		**Type:**	**Quantity:**
Tools:	Spanner set	1	**Protective Equipment:**	Gloves	4 pairs
	Allen wrench kit	1			
	Hot glue gun	1			
	Tweezers	1			
	Zip ties	-			
	Multimeter	1			
	Generic electric cable	1m			

	Description	**Part ID**
Vehicle parts:	E-Bay FWD flange	γ-01
	E-Bay AFT flange	γ-03

	Steel bars	γ-05
	E-Bay plexiglas cover (2 halves)	γ-02
	Sensor board	S-ELC-02
	Antenna board	S-ELC-03
	2 x 6.4V batteries	C-ELC-BAT1
	12.8V battery pack (2 x 6.4V)	C-ELC-BAT2
	4 x Rubber dampers assembly	S-ELC-04
	Omni-directional antenna	C-ELC-ODA
	12 x M10 nuts	NUT-M10
	CATS Vega board	C-ELC-VEGA
	CATS Vega support	γ-04
	Lower eye bolt	C-REC-EB
	Wi-Fi assembly	C-ELC-WIFI
	Wi-Fi support	-

Steps:					
Step:	**Task description:**	**Comments:**	**Time required:**	**STATUS:**	**APPROVAL:**
#1	Check assembly for completeness	Make sure to have all necessary components	1 min	☐	☐
#2	Place the four steel beams in their place in the lower E-bay flange and secure them with their nuts and washers	Do not over-tighten the external nuts		☐	☐
#3	Check power inside the 6.4V batteries using the Multimeter	Make sure that the batteries all read a voltage $\geq$ 6.4V	2 min	☐	☐
#4	Check power inside the 12.8V battery pack using the Multimeter	Make sure that the battery pack reads a voltage $\geq$ 12.8V	2 min	☐	☐
#5	Install and fix the batteries	Fix both the 12.8V and the 6.4V batteries to the e-bay. Ensure a stable installation	5 min	☐	☐

#6	Join together the Sensor and Antenna boards	Fix together the Sensor board to the Antenna board by connecting the pins. Make sure to install the rubber dampers inside of the 4 holes around both boards	5 min	☐	☐
#7	Install the boards inside the Electronics Bay	Make sure that the retention nuts are installed and fixed on the E-Bay struts, if not present install them too (make sure they are all on the same level from the bottom of the E-Bay). Slide the boards in (the antenna board has to stay on top) until they touch the bottom retention nuts.	2 min	☐	☐
#8	Screw on the top retention nuts	Do not tighten for now, just install them	1 min	☐	☐
#9	Install the Omni-directional antenna	Install the antenna by screwing it in to the Antenna board	5 min	☐	☐
#10	Tight both top and bottom retention nuts	Make sure not to offset the bottom retention nuts. If that happens follow step 9	1 min	☐	☐
#11	Assemble the Cats-Vega board on the support	Install the Cats-Vega on its support and insert the dampers	2 min	☐	☐
#12	Install the Cats-Vega assembly	Slide the Cats-Vega support and board to the bottom	2 min	☐	☐
#13	Screw on the top retention nuts and torque them	Use the spanner set	2 min	☐	☐
#14	Assemble the Wi-Fi antenna on its support	-	2 min	☐	☐
#15	Install the Wi-Fi antenna assembly	-	2 min	☐	☐
#16	Screw on the top retention nuts and torque them	Use the spanner set	2 min	☐	☐

#17	Screw the four internal upper M10 nuts so as to be approximately in position to hold the upper flange at the correct distance from the lower one	-	2 min	☐	☐
#18	Insert the upper flange and place both halves of the plexiglas cover	Adjust the internal nuts of the upper flange so that it slightly compresses the plexiglas	1 min	☐	☐
#19	Use the nut-bearing rings to screw in one half of the plexiglas cover on both flanges, and remove the other half cover of the plexiglas	-	5 min	☐	☐
#20	Verify leveling of the upper flange using a bubble level	-	2 min	☐	☐
#21	Screw in the internal upper M10 nuts below the upper flange until they are flush with the upper flange	-	1 min	☐	☐
#22	Insert the E-Bay eye bolt on the upper flange of the E-Bay from above, and secure it with its nut and washer	-	0.5 min	☐	☐
#23	Screw in the second half of the plexiglas cover on both flanges	-	5 min	☐	☐
#24	Carefully tighten the external M10 nuts on both flanges using the spanner set	-	5 min	☐	☐
#25	Verify leveling of the upper flange using a bubble level	-	2 min	☐	☐
#26	Tighten the external M10 nuts on both flanges using the spanner set slightly further	-	1 min	☐	☐
#27	Verify leveling of the upper flange using a bubble level	-	2 min	☐	☐
#28	Unscrew one half of the plexiglas cover	-	1 min	☐	☐
#29	Final tightening of the nuts using the spanner	-	2 min	☐	☐
#30	Verify that the removed plexiglas cover can be reinstalled and removed smoothly	-	5 min	☐	☐

#31	Verify leveling using a bubble level	-	2 min	☐	☐

We hereby confirm that all tasks of this checklist were completed.

Signature of Giammarco Perugini

Signature of Lorenzo Matti

Signature of Simone Fantoni

Signature of Andrea Cecchini

Signature of Giammarco Perugini - Responsible of Approval

CHECKLIST #5: Electronics check and calibration

Team name:	Aurora Rocketry				
Team ID:	06	**Time to launch:**	LRR – 75 min	**Location:**	Tent / Assembly area
Responsible/s:	Lorenzo Matti		Simone Fantoni		Alessandro Monticelli
Approved By:	Lorenzo Matti		Mattia Mattucci		Simone Fantoni
Required time for completeness:			35 min		
Summary description:	The goal is to check and calibrate all electronic components, performing pre-flight tests for both the boards and the antenna.				

Equipment required:					
	Type:	**Quantity:**		**Type:**	**Quantity:**
Tools:	Tweezers	1	**Protective Equipment:**	Gloves	3 pairs
	Spanner set	1			
	Wire cutters	1			
	6.4V test batteries	2			
	PC	1			
	USB-C Cable (data only)	1			
	Multimeter	1			
	Generic electric wire	1m			

	Description	Part ID
Vehicle parts:	Assembled electronics bay	-
	Ground station (running)	S-ELC-01
	Bypass Molex	C-ELC-BpMx
	Ground antenna	C-ELC-YAGI

Steps:					
Step:	**Task description:**	**Comments:**	**Time required:**	**STATUS:**	**APPROVAL:**
#1	Ensure previous checklist was successful		-	☐	☐
#2	Check assembly for completeness	Inspect the Electronics Bay and the Ground Station for damages or missing parts	2 min	☐	☐
#3	Remove one half of the plexiglas cover from the Electronics Bay	-	3 min	☐	☐
#4	Insert the SD card inside the Sensor board			☐	☐
#5	Switch the Power to OFF on the Antenna board and install the Bypass Molex	-	3 min	☐	☐
#6	Power ON both the boards	By connecting the Power cable from the batteries (6.4V), give power to both the boards. This step starts the boards' testing.	1 min	☐	☐

#7	Ensure that the following LED light up on the Sensor board	Battery 6.4V 3.3V PWR (x4) S (x4) IN (blinking) If one of the LED does not light up: -Check fasteners -Check batteries with the multimeter If the issue cannot be located change boards by following again step 6 to 9	2 min	☐	☐
#8	Ensure that the following LED light up on the Antenna board	PWR (x2) SAT S RGB diagnostic table	2 min	☐	☐
#9	Connect the PC via USB-C (data only)	-	-	☐	☐
#10	Access the gyroscopic data and align the board to the terrain	Start the routine by typing “CALIBRATE”.In order to align the gyroscope, put the E-Bay on a surface parallel to terrain and by screwing/ unscrewing the bottom retention nut align the boards.	8 min	☐	☐
#11	Check the Antenna signal from the Ground station	Ensure that the following sensor data are transmitted: IMU Barometers (both) Accelerometer GPS If the transmission is not working: -Unscrew and screw on again the antenna -Check the Ground Station antenna	5 min	☐	☐

#12	Power ON the Cats-Vega board	By connecting the Power cable from the batteries (12.8V), give power to the board. This step starts the Cats-Vega testing.	2 min	☐	☐
#13	Ensure that the following LED light up on the Cats-Vega board	POWER STATUS (blinking) GNSS LINK If one of the LED does not light up: -Check pins -Check batteries with the multimeter.	2 min	☐	☐
#14	Check the Cats-Vega signal from the COTS Ground station	Ensure that the following sensor data are transmitted: Barometer IMU GPS	2 min	☐	☐
#15	Renstall the Plexiglas fairings	-	1 min	☐	☐

We hereby confirm that all tasks of this checklist were completed.

Signature of Lorenzo Matti

Signature of Simone Fantoni

Signature of Alessandro Monticelli

Signature of Lorenzo Matti - Responsible of Approval

Signature of Mattia Mattucci - Responsible of Approval

Signature of Simone Fantoni - Responsible of Approval

CHECKLIST #6: Electronics arming

Team name:	Aurora Rocketry				
Team ID:	06	**Time to launch:**	T – 30 min	**Location:**	Launch pad
Responsible/s:	Lorenzo Matti		Mattia Mattucci		Simone Fantoni
Approved By:	Lorenzo Matti		Mattia Mattucci		Simone Fantoni
Required time for completeness:			20 min		
Summary description:	The goal is to connect all the fasteners from the Recovery System to the boards, power the Electronics Bay on and arm the system just before launch.				

Equipment required:					
	Type:	**Quantity:**		**Type:**	**Quantity:**
Tools:	Screwdriver	1	**Protective Equipment:**	Gloves	3 pairs
	Spanner set	1			
	Multimeter	1			

	Description	**Part ID**
Vehicle parts:	Fully assembled rocket	-
	Ground station	S-ELC-01
	CATS - Vega ground station	C-ELC-VEGAGS

Steps:					
Step:	**Task description:**	**Comments:**	**Time required:**	**STATUS:**	**APPROVAL:**
#1	Ensure that precedent checklist are completed	-	-	☐	☐
#2	Check assembly for completeness	Inspect both the E-Bay and the Recovery System for damages or missing parts	-	☐	☐
#3	Remove the Plexiglas fairings		2 min	☐	☐
#4	Coil the recovery cable to the struts inside the Electronics Bay.	Make sure all the fasteners are near their respective boards.	2 min	☐	☐
#5	Fix the cable to the struts using zip ties	-	1 min	☐	☐
#6	Ensure that the 4 red LEDs on the Mosfets are OFF	The red LEDs on the Mosfets signal that the system is armed.	-	☐	☐
#7	Ensure that the following LED light up on the Sensor board	Battery 6.4V 3.3V PWR (x4) S (x4) IN (blinking)	1 min	☐	☐
#8	Ensure that the following LED light up on the Antenna board	PWR (x2) SAT S RGB diagnostic table	1 min	☐	☐
#9	Ensure that the following LED light up on the Cats-Vega board	POWER STATUS (blinking) GNSS LINK If one of the LED does not light up: -Check pins -Check batteries with the multimeter. -Check connection with COTS Ground station	2 min	☐	☐

#10	Check the Antenna signal from the Ground station	Ensure that the following sensor data are transmitted: IMU Barometers (both) Accelerometer GPS	5 min	☐	☐
#11	Check the Cats-Vega signal from the COTS Ground station	Ensure that the following sensor data are transmitted: Barometer IMU GPS	5 min	☐	☐
#12	Connect the fasteners of the recovery cables on both SRAD and COTS boards	-	2 min	☐	☐
#13	Remove the Bypass Molex	-	-	☐	☐
#14	Ensure that the 4 red LEDs on the Mosfets are ON	-	-	☐	☐
#15	Flip the arming switch to ON	-	-	☐	☐
#16	Flip the arming switch to OFF	-	-	☐	☐
#17	Flip the arming switch to ON	-	-	☐	☐
#18	Ensure that the 4 red LEDs on the Mosfets are ON	-	-	☐	☐
#19	Install the Plexiglass fairings	-	2 min	☐	☐

We hereby confirm that all tasks of this checklist were completed.

Signature of Lorenzo Matti

Signature of Mattia Mattucci

Signature of Simone Fantoni

Signature of Lorenzo Matti - Responsible of Approval

Signature of Mattia Mattucci - Responsible of Approval

Signature of Simone Fantoni - Responsible of Approval

CHECKLIST #7: Payload check and connection to batteries

Team name:	Aurora Rocketry				
Team ID:	06	**Time to launch:**	LRR – 90 min	**Location:**	Tent / Assembly area
Responsible/s:	Nicolò Basso		Mattia Mattucci		Daniele Bandini
Approved By:	Nicolò Basso		Alessandro Monticelli		
Required time for completeness:			15 min		
Summary description:	The goal of this checklist is to check the payload structure and electrical connections for damage, as well as to check signal reception quality and successful anchorage of the payload on the rocket.				

Equipment required:					
	Type:	**Quantity:**		**Type:**	**Quantity:**
Tools:	Laptop	1	**Protective Equipment:**		
	Screwdriver set	1			

	Description	**Part ID**
Vehicle parts:	Non-powered payload	S-PLD-AET
	Payload batteries	C-PLD-BAT

Steps:					
Step:	**Task description:**	**Comments:**	**Time required:**	**STATUS:**	**APPROVAL:**
#1	Check correct attachment to upper and lower supports	-	1 min	☐	☐

#2	Connect batteries	Unscrew battery housing, insert batteries, attach cables, close the holders	5 min	☐	☐
#3	Check correct usb connection to software-defined radio	-	1 min	☐	☐
#4	Check correct reception chain connection with LNA and Antenna	-	1 min	☐	☐
#5	Access the payload via SSH and check reception	-	5 min	☐	☐

We hereby confirm that all tasks of this checklist were completed.

Signature of Nicolò Basso

Signature of Mattia Mattucci

Signature of Daniele Bandini

Signature of Nicolò Basso - Responsible of Approval

Signature of Alessandro Monticelli - Responsible of Approval

CHECKLIST #8: Payload arming

Team name:	Aurora Rocketry				
Team ID:	06	**Time to launch:**	T – 30 min	**Location:**	Launch pad
Responsible/s:	Nicolò Basso		Lorenzo Piccinini		Alessandro Monticelli
Approved By:	Nicolò Basso				
Required time for completeness:			5 min		
Summary description:	The goal of this checklist is to turn on the payload and start signal reception.				

Equipment required:					
	Type:	**Quantity:**		**Type:**	**Quantity:**
Tools:	Laptop	1	**Protective Equipment:**		
	Screwdriver set	1			
	Description		**Part ID**		
Vehicle parts:	Fully assembled payload		S-PLD-AET		

Steps:					
Step:	**Task description:**	**Comments:**	**Time required:**	**STATUS:**	**APPROVAL:**
#1	SSH into the Raspberry Pi via Wi-Fi	-	5 min	☐	☐
#2	Start the reception system	-	1 min	☐	☐

We hereby confirm that all tasks of this checklist were completed.

Signature of Nicolò Basso

Signature of Lorenzo Piccinini

Signature of Alessandro Monticelli

Signature of Nicolò Basso - Responsible of Approval

CHECKLIST #9: Recovery check and preparation

Team name:	Aurora Rocketry				
Team ID:	06	**Time to launch:**	LRR – 90 min	**Location:**	Tent / preparation area
Responsible/s:	Giorgia Capozucca		Andrea Paoletti	Leonardo Cappetti	
	Sara Iannì				
Approved By:	Giorgia Capozucca		Lorenzo Piccinini		
Required time for completeness:			45 min		
Summary description:	This checklist covers the integration of the main parachute and recovery system, including the 3-ring system, inner tube assembly, CO_2 cartridge plate, and attachment of drogue and nosecone. The process ensures correct positioning of cords, e-matches, and parachutes for safe deployment after launch.				

Equipment required:					
	Type:	**Quantity:**		**Type:**	**Quantity:**
Tools:	Screwdriver	1	**Protective Equipment:**	Gloves	4 pairs
	Spanner kit	1			
	Needle and thread	1			
	Scissors	1			
	Tape	2			
	Rubber bands	4			
	Super glue	1			
	Fabric hole punch	1			

	Description	Part ID
Vehicle parts:	Outer aluminum tube	β-01
	Inner PVC tube	S-REC-01
	CO_2 cartridges holding plate	S-REC-02
	Aft arresting plate	S-REC-03
	Deployment bag	S-REC-04
	Upper and lower eye bolts	C-REC-EB
	6 × green shock cords	C-REC-ShCo
	4 × swivels	C-REC-SWIV
	4 x quick links	C-REC-QLnk
	2 × black and yellow shock cords (for the 3-ring system)	C-REC-3RS
	Main parachute	C-REC-MaPC
	Drogue parachute	C-REC-DrPC
	1 × PEREGRINE System	C-REC-PRG
	2 × PIRANHA System (3RS)	C-REC-PRN

Steps:					
Step:	**Task description:**	**Comments:**	**Time required:**	**STATUS:**	**APPROVAL:**
#1	Make sure the previous checklist was successfully completed	In particular, make sure that the preliminary operations have been completed	-	☐	☐
#2	Check assembly for completeness	-	2 min	☐	☐
#3	Assemble the 3-ring system (PIRANHA System)	Ensure correct alignment and secure fasteners	7 min	☐	☐
#4	Assemble the CO_2 system (PEREGRINE System)	Pay close attention when handling black powder	10 min	☐	☐
#5	Insert cords (3-ring, main parachute lines) and parachutes into the inner tube, through the aft arresting plate and the plate holding the CO_2 cartridges	Keep cords untangled and in correct order	10 min	☐	☐

#6	Insert the inner tube inside the main body tube	Make sure to let the cords through the central hole in the aft arresting plate	3 min	☐	☐
#7	Pull 3-ring system cord and ematches towards the front end of the tube until they are positioned above the main parachute	Ensure cord tension	5 min	☐	☐
#8	Place drogue parachute on top of assembly	Fold and pack drogue properly	5 min	☐	☐
#9	Secure plate holding CO_2 cartridges	Tighten screws and check stability	3 min	☐	☐
#10	Connect eye bolt in the nosecone flange to the drogue parachute and secure it with shear pins	Check shear pin integrity	5 min	☐	☐
#11	Connect eye bolt in the forward electronics bay flange to the main parachute cord, the deployment bag and the 3-ring system	-	5 min	☐	☐
#12	Check and clear the working station	-	1 min	☐	☐

We hereby confirm that all tasks of this checklist were completed.

Signature of Giorgia Capozucca

Signature of Andrea Paoletti

Signature of Leonardo Cappetti

Signature of Sara Iannì

Signature of Giorgia Capozucca - Responsible of Approval

Signature of Lorenzo Piccinini - Responsible of Approval

CHECKLIST #10: Rocket assembly to LRR-ready state

Team name:	Aurora Rocketry				
Team ID:	06	**Time to launch:**	LRR – 55 min	**Location:**	Tent / Assembly area
Responsible/s:	Giammarco Perugini		Maurizio Romagnolo		Andrea Cecchini
	Leonardo Olmi		Davide Braglia		
Approved By:	Giammarco Perugini		Lorenzo Piccinini		
Required time for completeness:			40 min		
Summary description:	This checklist regulates the assembly of the rocket, from its pre-assembled subsystems to its LRR-ready configuration.				

Equipment required:					
	Type:	**Quantity:**		**Type:**	**Quantity:**
Tools:	Screwdriver	1	**Protective Equipment:**		
	Allen wrench kit	1			

	Description	**Part ID**
Vehicle parts:	30x M4 screws	SCW-M4
	3x M5 screws	SCW-M5
	7x M8 screws	SCW-M5
	Nosecone	α-01
	Fully assembled Aether Cubesat (Payload)	S-PLD-AET
	Payload lower support	S-PLD-02
	Fully assembled recovery subsystem	-

	Fully assembled electronics subsystem	-
	Motor bay	-
	3x Rail buttons	ω-01

Steps:					
Step:	**Task description:**	**Comments:**	**Time required:**	**STATUS:**	**APPROVAL:**
#1	Make sure the previous checklist was successfully completed	-	-	☐	☐
#2	Check assembly for completeness	-	5 min	☐	☐
#3	Orient the Aether cubesat so that the flat square antenna is pointing up	-	1 min	☐	☐
#4	Line up the four pins on the upper payload support with the 4 small holes present on the cubesat	-	1 min	☐	☐
#5	Carefully insert the upper support pins into the cubesat's respective holes	-	1 min	☐	☐
#6	Line up the four pins on the lower payload holder with the 4 small holes present on the cubesat	-	1 min	☐	☐
#7	Carefully insert the lower support pins into the cubesat's respective holes	-	1 min	☐	☐
#8	Line up the fiberglass nosecone with the nosecone flange	Hold the payload in position during the process	2 min	☐	☐
#9	Insert the nosecone onto the flange, lining up the respective holes	-	2 min	☐	☐
#10	Fasten the nosecone with its respective M4 screws	Be careful to not overly tighten the screws and follow a criss-cross pattern to evenly distribute the torque	3 min	☐	☐

#11	Connect the recovery electronics quick connectors you'll find coming out of the recovery subsystem and the electronic bay's upper flange	Pay attention to not intertwine the electronic connection's cables with the recovery ropes	5 min	☐	☐
#12	Insert the main body tube of the recovery section onto the E-bay's upper flange, lining up correctly the screw holes present on each one	Pay attention to tidy up the rope while coupling the two components	6 min	☐	☐
#13	Fasten the E-bay onto the recovery section main tube: 12 M4 bolts are used for this procedure	Gradually screw in the bolts and tighten them in a criss-cross pattern to evenly distribute the torque; make sure to line up the livery pattern	6 min	☐	☐
#14	Fasten the three rail buttons with their M5 screws	The three rail buttons are located on the forward and aft electronics bay flanges and on the thrust bulkhead	5 min	☐	☐

We hereby confirm that all tasks of this checklist were completed.

Signature of Giammarco Perugini

Signature of Maurizio Romagnolo

Signature of Andrea Cecchini

Signature of Leonardo Olmi

Signature of Davide Braglia

Signature of Giammarco Perugini - Responsible of Approval

Signature of Lorenzo Piccinini - Responsible of Approval

CHECKLIST #11: Propellant loading

Team name:	Aurora Rocketry				
Team ID:	06	**Time to launch:**	Preparation day	**Location:**	Tent / Assembly area
Responsible/s:	Lorenzo Piccinini		Federico Pedicini		Maurizio Romagnolo
	Daniele Bandini		Caio Scattolini		Giovanni Bacchini
	Alex Petrani				
Approved By:	Daniele Bandini		Lorenzo Piccinini		
Required time for completeness:			65 min		
Summary description:	This checklist regulates the propellant loading procedure according to the manufacturer's instructions, available at https://pro38.com, and the subsequent final assembly of the rocket.				

Equipment required:					
	Type:	**Quantity:**		**Type:**	**Quantity:**
Tools:	Screwdriver	1	**Protective Equipment:**	Gloves	3 pairs
	Spanner	1		FFP3 face masks	3
	Allen wrench kit	1		Protective goggles	3
	Rubber head hammer	1			
	Pro 75 wrench	1			
	Gorilla polyurethane glue	-			
	O-ring lubricant / grease	-			

	Description	Part ID
Vehicle parts:	Pro 75 6GXL Motor casing	C-PRP-P75
	Pro 75 Forward closure	C-PRP-P75FC
	Pro 75 Nozzle holder	C-PRP-P75NH
	Pro 75 Forward retaining ring	C-PRP-P75RR
	Pro 75 Thrust ring	C-PRP-P75TR
	Case liner	C-PRP-LINER
	Nozzle	C-PRP-NOZ
	Forward insulator disk	C-PRP-FID
	Pro75 O-ring kit	C-PRP-OR
	Tracking smoke assembly	C-PRP-TSA
	M1545 Propellant grains	C-PRP-M1545

Steps:					
Step:	**Task description:**	**Comments:**	**Time required:**	**STATUS:**	**APPROVAL:**
#1	Re-read all propellant loading instructions carefully	Be sure you fully understand each step before proceeding with motor assembly.	5 min	☐	☐
#2	Inspect the components of the reload kit carefully before starting assembly	DO NOT use any parts that appear damaged or faulty in any way.	2 min	☐	☐
#3	Check both ends of the phenolic case liner	Ensure that the inside ends have been chamfered or deburred. If not, use a hobby knife or coarse sandpaper to remove the sharp inner edge to allow components to be inserted easily.	2 min	☐	☐
#4	Insert the smoke tracking charge insulator in the forward closure	Apply a light coating of o-ring lubricant or grease to the inside of the cavity in the forward closure. Insert the smoke tracking charge insulator into this cavity and ensure it is seated fully	1 min	☐	☐

#5	Grease one end of the smoke tracking grain	Apply a liberal layer of grease or o-ring lubricant to one end of the smoke tracking grain. Be sure the entire face is coated.	1 min	☐	☐
#6	Insert the smoke tracking grain in the forward closure	Insert the smoke tracking grain into the smoke tracking charge insulator, coated end first. Push the grain in with sufficient force to fully seat it and spread the lubricant. The excess lubricant will help prevent gas leakage forward as well as protecting the forward closure from heat and combustion products from the smoke tracking charge.	1 min	☐	☐
#7	Make sure to work with the nozzle/case liner assembly and motor case horizontally on your work surface up to step #15	-	-	☐	☐
#8	Apply adhesive on the outside (paper liner) of the first grain and use a small brush to spread it evenly	Ensure no adhesive is applied on the grain faces or bore of the propellant.	3 min	☐	☐
#9	Push the grain in the liner from the nozzle end while twisting it	Twisting the grain while inserting it will properly distribute the adhesive. Push it about 1” into the liner.	2.5 min	☐	☐
#10	Fit one grain spacer o-ring to the top face of the grain	Ensure that it sits flat on the end of the grain.	0.5 min	☐	☐
#11	Insert the second grain, push it in a short ways, then add another grain spacer, and so on until you have loaded all propellant grains into the case liner	Excess adhesive might be scraped off around the end of the liner. This can simply be wiped off. Do NOT install a spacer o-ring after the last grain (between the bottom grain and the nozzle).	15 min	☐	☐

#12	Inspect the external o-ring grooves on the forward closure and nozzle holder, as well as the internal groove on the nozzle holder and the motor casing	Ensure that the inside of the motor case has been thoroughly cleaned.	2 min	☐	☐
#13	Fit the nozzle to one end of the paper/phenolic case liner tube and wipe off any excess adhesive	It may be a snug fit. Push it carefully but with sufficient force to seat the shoulder on the nozzle all the way into the insulator tube	1 min	☐	☐
#14	Fit the smaller o-ring to the internal groove of the nozzle holder	-	1 min	☐	☐
#15	Push the nozzle holder over the nozzle until fully seated	Apply additional lubricant to the nozzle exit section if necessary to facilitate assembly.	2 min	☐	☐
#16	Carefully install the two larger o-rings into the external grooves of the nozzle holder and forward closure	Handle these components with care from this point on so as not to damage or contaminate the o-rings.	2 min	☐	☐
#17	Place the case liner/nozzle assembly on the work surface with the nozzle end down, and push the top grain down gently through the hole in the forward insulator plate	-	2 min	☐	☐
#18	Let the liner/grain assembly cure in an upright position	-	5 min	☐	☐

We hereby confirm that all tasks of this checklist were completed.

Signature of Daniele Bandini

Signature of Caio Scattolini

Signature of Maurizio Romagnolo

Signature of Giovanni Bacchini

Signature of Lorenzo Piccinini

Signature of Federico Pedicini

Signature of Alex Petrani

Signature of Daniele Bandini - Responsible of Approval

Signature of Lorenzo Piccinini - Responsible of Approval

CHECKLIST #12: Final assembly

Team name:	Aurora Rocketry				
Team ID:	06	**Time to launch:**	Post LRR	**Location:**	Tent / Assembly area
Responsible/s:	Giammarco Perugini		Maurizio Romagnolo		Andrea Cecchini
	Daniele Bandini		Caio Scattolini		Leonardo Olmi
Approved By:	Daniele Bandini		Lorenzo Piccinini		
Required time for completeness:			20 min		
Summary description:	This checklist regulates the installation of the motor on the rocket, and the assembly of the motor section with the rest of the rocket after the LRR.				

Equipment required:					
	Type:	**Quantity:**		**Type:**	**Quantity:**
Tools:	Screwdriver	1	**Protective Equipment:**	Gloves	3 pairs
	Allen wrench kit	1		Protective goggles	3
	Pro75 wrench	1			
	Wet rag	1			

	Description	**Part ID**
Vehicle parts:	LRR-state rocket	-
	Assembled motor	-
	3/8″ screw	SCW-3/8“
	30x10x2 mm washer	C-PRP-WASH

Steps:					
Step:	**Task description:**	**Comments:**	**Time required:**	**STATUS:**	**APPROVAL:**
#1	Slide the motor case down rear end first over the top of the liner towards the nozzle	A light coat of grease on the liner exterior will aid assembly, disassembly and cleanup.	1 min	☐	☐
#2	Lay the motor case assembly down horizontally, and push on the nozzle ring until the assembly is far enough inside the case that the threads are partly exposed and the screw ring can be threaded into the rear of the case	Don't push on the nozzle itself as it will be pushed out of the nozzle holder.	1 min	☐	☐
#3	Screw in the nozzle retaining ring using the wrench	Push the nozzle/ nozzle ring/case liner assembly forward as you proceed. Screw it in only until the retaining ring is exactly even with the end of the motor case - do not thread it in as far as it will go. Then, back the retaining ring out one half of a turn.	1 min	☐	☐
#4	Fit the forward insulating disk to the top of the case liner	Check that the top grain spacer (if used) is still properly in place.	1 min	☐	☐
#5	Verify that the inside of the motor case is clean ahead of the liner assembly before proceeding	Wipe with a clean rag, tissue or wet-wipe if required	0.5 min	☐	☐
#6	Apply a light coat of silicone o-ring lubricant onto the inside of the motor case ahead of the liner assembly after cleaning.	-	2 min	☐	☐
#7	Insert the assembled forward closure into the top of the motor case	Push it down carefully with fingers until you can thread in the retaining ring.	0.5 min	☐	☐

#8	Thread in the forward retaining ring using the wrench, until you feel it take up a load against the top of the case liner	The ring should be approximately flush with the end of the motor case, or slightly submerged. If it extends out the case at this point by more than about one half a turn, check the nozzle end to make sure the ring is not screwed in too far forward. If so, unscrew the nozzle retaining ring another half turn and screw the forward closure retainer in further. It is best to have the forward closure retaining ring flush or slightly submerged and the nozzle retaining ring protruding by a half turn or so, than vice versa.	5 min	☐	☐
#9	Insert the loaded motor into the phenolic motor tube	-	2 min	☐	☐
#10	Secure the motor from the front with the 3/8″ screw and the washer on the motor bulkhead	-	1 min	☐	☐
#11	Screw in the Aeropack Motor Retainer	-	1 min	☐	☐
#12	Connect the Motor Bay with the lower flange of the Electronics Bay using the nut-holding rings	-	5 min	☐	☐

We hereby confirm that all tasks of this checklist were completed.

Signature of Daniele Bandini

Signature of Caio Scattolini

Signature of Giammarco Perugini

Signature of Maurizio Romagnolo

Signature of Andrea Cecchini

Signature of Leonardo Olmi

Signature of Daniele Bandini - Responsible of Approval

Signature of Lorenzo Piccinini - Responsible of Approval

CHECKLIST #13: Rocket positioning on launch rail

Team name:	Aurora Rocketry				
Team ID:	06	**Time to launch:**	T – 55 min	**Location:**	Launch pad
Responsible/s:	Lorenzo Piccinini		Giammarco Perugini		Davide Braglia
	Leonardo Olmi		Andrea Cecchini		Maurizio Romagnolo
Approved By:	Lorenzo Piccinini		Nicolò Basso		Daniele Bandini
Required time for completeness:			25 min		
Summary description:	The purpose of this checklist is to provide a guide to mount the rocket on the launch rail before launch.				

Equipment required:					
	Type:	**Quantity:**		**Type:**	**Quantity:**
Tools:	Screwdriver	1	**Protective Equipment:**	Helmet	6
	Spanner	1			
	Description		**Part ID**		
Vehicle parts:	Fully assembled rocket		-		

Steps:					
Step:	**Task description:**	**Comments:**	**Time required:**	**STATUS:**	**APPROVAL:**
#1	Tilt the vertical rail	Tilt the vertical rail with the maximum downward inclination	3 min	☐	☐

#2	Insert the spacer in the rail	Make sure it traveled all the way to the bottom of the rail	5 min	☐	☐
#3	Insert the rocket in the rail using the rail buttons	-	10 min	☐	☐
#4	Hoist the rail to the desired angle (Nominal: 85 degrees)	-	5 min	☐	☐

We hereby confirm that all tasks of this checklist were completed.

Signature of Lorenzo Piccinini

Signature of Giammarco Perugini

Signature of Maurizio Romagnolo

Signature of Davide Braglia

Signature of Leonardo Olmi

Signature of Andrea Cecchini

Signature of Lorenzo Piccinini - Responsible of Approval

Signature of Nicolò Basso - Responsible of Approval

Signature of Daniele Bandini - Responsible of Approval

CHECKLIST #14: Igniter insertion and pad clearance

Team name:	Aurora Rocketry				
Team ID:	06	**Time to launch:**	T – 10 min	**Location:**	Launch pad
Responsible/s:	Lorenzo Piccinini				
Approved By:	Lorenzo Piccinini				
Required time for completeness:			10 min		
Summary description:	The goal of the checklist is to regulate ignition arming operations: to arm the engine, putting the rocket into a launch-ready state, and then safely leave the launch area.				

Equipment required:					
	Type:	**Quantity:**		**Type:**	**Quantity:**
Tools:	Scissors	1	**Protective Equipment:**	Protective glasses	2
	Tape	1		Protective helmet	2
	Walkie-talkie	2		Gloves	2 pairs

	Description	**Part ID**
Vehicle parts:	Fully assembled rocket	-
	Igniter	C-PRP-IGN

Steps:					
Step:	**Task description:**	**Comments:**	**Time required:**	**STATUS:**	**APPROVAL:**
#1	Check functional test results	Make sure the previous checklist was successfully completed	-	☐	☐
#2	Check assembly for completeness	Inspect the Motor nozzle for damage	2 min	☐	☐
#3	Install the supplied igniter	Ensure that it travels forward until it is in contact with the forward closure.	3 min	☐	☐
#4	Securely retain the igniter to the motor nozzle with tape, or (if supplied) the plastic cap, routing the wires through one of the vent holes.	Ensure that whatever means is used provides a vent for igniter gases to prevent premature igniter ejection.	4 min	☐	☐
#5	Alert ground control that the igniter has been inserted using the walkie-talkie	Wait for “Roger” or “Affirmative” message from ground control	1 min	☐	☐
#5	Clear the pad and alert ground control	Check that there are no tools left in the launch area	1 min	☐	☐

We hereby confirm that all tasks of this checklist were completed.

Signature of Lorenzo Piccinini

Signature of Lorenzo Piccinini - Responsible of Approval

CHECKLIST #15: Rocket recovery

Team name:	Aurora Rocketry				
Team ID:	06	**Time to launch:**	-	**Location:**	Launch range
Responsible/s:	Daniele Bandini		Leonardo Neri	Alessio Mrass	
Approved By:	Daniele Bandini				
Required time for completeness:			-		
Summary description:	The purpose of this checklist is to list the procedures to be followed during the recovery of the rocket immediately after its landing on the ground.				

Equipment required:					
	Type:	**Quantity:**		**Type:**	**Quantity:**
Tools:	Containers for rocket fragments	Depends on expected rocket integrity (2-4)	**Protective Equipment:**	Protective glasses	3
	LiFePO4 batteries container	1		Protective helmet	3
	Allen wrench kit	1		Gloves	3 pairs
	Cords to facilitate carrying parts / boxes	-			
	Shovels	Depends on expected rocket integrity (1-3)			
	Walkie-talkies	2			

	Description	**Part ID**
Vehicle parts:	Rocket	-
	GPS tracker	-

Steps:					
Step:	**Task description:**	**Comments:**	**Time required:**	**STATUS:**	**APPROVAL:**
#1	Wait for clearance by RSO and instructions from the MCO	-	-	☐	☐
#2	The Aurora Recovery Team joins the EuRoC Recovery Team on the search for rocket	-	-	☐	☐
#3	Search the rocket using the GPS tracker and the instructions about the landing point received by the MCO; when the rocket is found, alert GC that "Nemesis has been found", state its general condition and wait for an answer that confirms the reception of the message	It's important to test the correct functioning of the GPS tracker before the launch day	-	☐	☐
#4	Account for all parts of the rocket and their contents. Check each square as you locate the corresponding part: ☐ α-01 ☐ α-02 ☐ β-01 ☐ γ-01 ☐ γ-02 ☐ γ-03 ☐ γ-04 ☐ γ-05 ☐ δ-01 ☐ δ-02 ☐ δ-03 ☐ δ-04 ☐ ω-01	Check the table below for the description of the vehicle parts. If there are any smaller fragments, check that they match the components on the list. Once you've identified all the pieces, place them back in the boxes. If the batteries are damaged, place them in the LiPo batteries container.	-	☐	☐

Vehicle parts legend		
	Description	**Part ID**
Vehicle Parts	Nosecone	α-01
	Nosecone flange	α-02
	Body tube - recovery section	β-01
	FWD E-Bay flange	γ-01
	Plexiglas fairings E-Bay	γ-02
	AFT E-Bay flange	γ-03
	CATS-Vega support	γ-04
	Steel bars	γ-05
	Body tube - motor section	δ-01
	Fins	δ-02
	Boat-tail support	δ-03
	Boat-tail	δ-04
	Rail buttons	ω-01

We hereby confirm that all tasks of this checklist were completed.

Signature of Daniele Bandini

Signature of Leonardo Neri

Signature of Alessio Mrass

Signature of Daniele Bandini - Responsible of Approval

EMERGENCY CHECKLIST #1: Catastrophic structural failure on the rail

Team name:	Aurora Rocketry				
Team ID:	06	**Time to launch:**	-	**Location:**	Launch pad
Responsible/s:	Giammarco Perugini		Maurizio Romagnolo		Lorenzo Piccinini
Approved By:	Lorenzo Piccinini				
Required time for completeness:			9 min		
Summary description:	This non-nominal checklist regulates the course of action in the event of catastrophic structural failures on the rail, such as aftmost rail button screw failure, in which case the launch must be canceled and the rocket removed from the launch pad.				

Equipment required:					
	Type:	**Quantity:**		**Type:**	**Quantity:**
Tools:	Screwdriver	1	**Protective Equipment:**		
	Spanner	1			

	Description	**Part ID**
Vehicle parts:	Fully assembled rocket	-
	Spare M5 screws	-
	Spare rail buttons	-

Steps:					
Step:	**Task description:**	**Comments:**	**Time required:**	**STATUS:**	**APPROVAL:**
#1	Detach the igniter	Necessary if failure happens after the igniter has been inserted	-	☐	☐
#2	Tilt the vertical rail	Tilt the vertical rail with the maximum downward inclination	3 min	☐	☐
#3	Remove the rocket from the vertical rail	-	4 min	☐	☐
#4	Remove the spacer	-	2 min	☐	☐

We hereby confirm that all tasks of this checklist were completed.

Signature of Giammarco Perugini

Signature of Maurizio Romagnolo

Signature of Lorenzo Piccinini

Signature of Lorenzo Piccinini - Responsible of Approval

EMERGENCY CHECKLIST #2: Accidental de-arming of the payload

Team name:	Aurora Rocketry				
Team ID:	06	**Time to launch:**	-	**Location:**	-
Responsible/s:	Nicolò Basso		Lorenzo Matti		
Approved By:	Nicolò Basso				
Required time for completeness:			14 min		
Summary description:	The goal of this checklist is to coordinate the correct response to an unexpected de-activation of the payload.				

Equipment required:					
	Type:	**Quantity:**		**Type:**	**Quantity:**
Tools:	Laptop	1	**Protective Equipment:**		
	Description		**Part ID**		
Vehicle parts:	Fully assembled payload		-		

Steps:					
Step:	**Task description:**	**Comments:**	**Time required:**	**STATUS:**	**APPROVAL:**
#1	Detach the igniter	Necessary if failure happens after the igniter has been inserted	3 min	☐	☐
#2	Check the cable connection	-	2 min	☐	☐

#3	Change the battery pack	-	6 min	☐	☐
#4	Re-arm the payload	-	2 min	☐	☐
#5	Check the led	-	1 min	☐	☐

We hereby confirm that all tasks of this checklist were completed.

Signature of Nicolò Basso

Signature of Lorenzo Matti

Signature of Nicolò Basso - Responsible of Approval

EMERGENCY CHECKLIST #3: Battery pack malfunction

Team name:	Aurora Rocketry				
Team ID:	06	**Time to launch:**	-	**Location:**	Launch pad
Responsible/s:	Lorenzo Matti		Mattia Mattucci		Simone Fantoni
	Lorenzo Piccinini				
Approved By:	Lorenzo Matti		Lorenzo Piccinini		
Required time for completeness:			10 min		
Summary description:	This procedure ensures a safe change of the battery pack in case a malfunction takes it out.				

Equipment required:					
	Type:	**Quantity:**		**Type:**	**Quantity:**
Tools:	Screwdriver	2	**Protective Equipment:**	Gloves	4 pairs
	Spanner set	1		Safety goggles	4
	Multimeter	1			

	Description	**Part ID**
Vehicle parts:	2 x 6.4V batteries	C-ELC-BAT1
	12.8V battery pack (2 x 6.4V)	C-ELC-BAT2
	Bypass Molex	C-ELC-BpMx

Steps:					
Step:	**Task description:**	**Comments:**	**Time required:**	**STATUS:**	**APPROVAL:**
#1	Check power inside the 6.4V replacement batteries using the Multimeter	Make sure that the batteries all read a voltage $\geq$ 6.7V. Do this step before approaching Nemesis	0.5 min	☐	☐
#2	Check power inside the 12.8V replacement battery pack using the Multimeter	Make sure that the battery pack reads a voltage $\geq$ 13V. Do this step before approaching Nemesis	0.5 min	☐	☐
#3	Detach the motor igniter	This step must be completed by the specific personnel.	5 min	☐	☐
#4	Remove the plexiglas fairings	-	2 min	☐	☐
#5	Remove the fasteners from both SRAD and COTS boards	-	1 min	☐	☐
#6	Disconnect the power cables from the battery pack	-	-	☐	☐
#7	Using the multimeter, check if the voltage inside the batteries is nominal	By using the multimeter, check if the voltage inside the batteries is nominal. If it's not, proceed with this checklist. If it's nominal, further inspection is needed	3 min	☐	☐
#8	Disconnect the damaged batteries and dispose of them in the LiFePO4 safety pack	In order to avoid further danger, once the batteries are removed take them away from the launchpad	2 min	☐	☐
#9	Install the bypass Molex	-	1 min	☐	☐
#10	Reinstall the igniter	-	5 min	☐	☐

We hereby confirm that all tasks of this checklist were completed.

Signature of Lorenzo Matti

Signature of Mattia Mattucci

Signature of Simone Fantoni

Signature of Lorenzo Piccinini

Signature of Lorenzo Matti - Responsible of Approval

Signature of Lorenzo Piccinini - Responsible of Approval

Appendix G

Engineering drawings

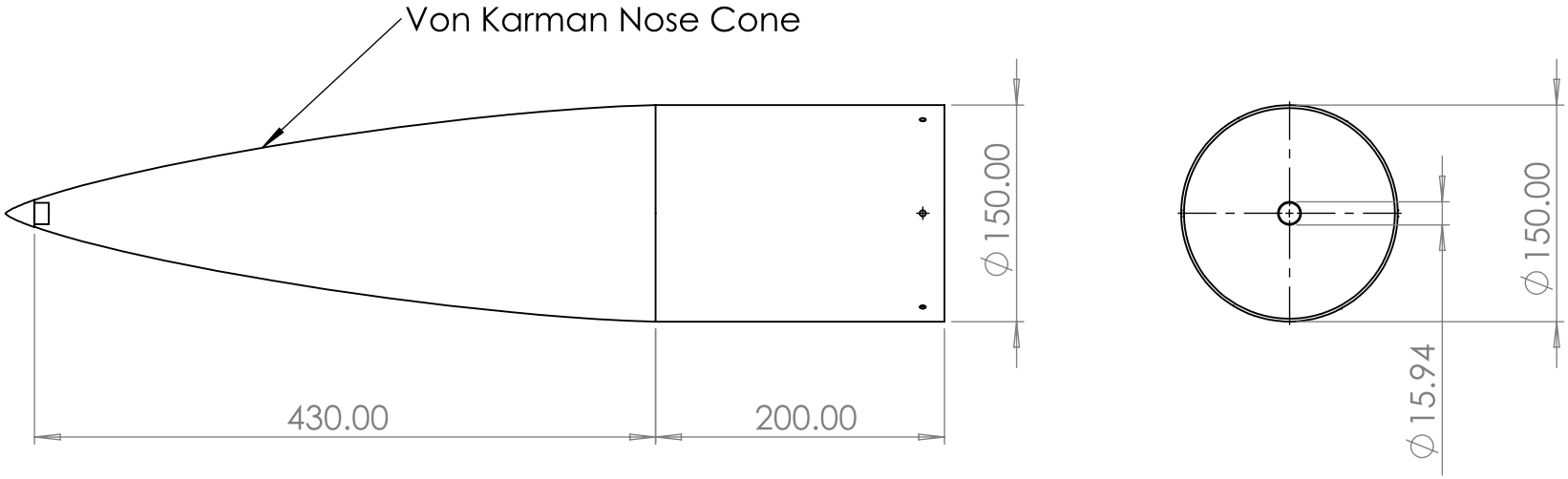

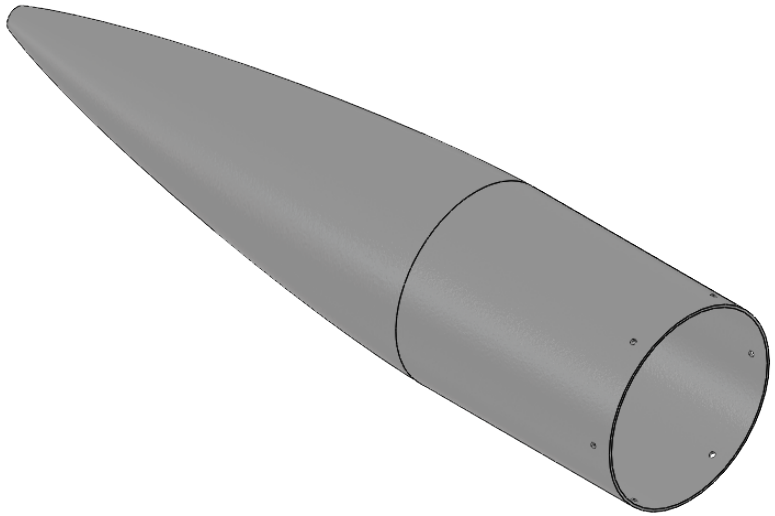

Project: Nemesis	Created by: Leonardo Olmi	Approved by: Lorenzo Piccinini
AURORA ROCKETRY	Document Type: Part	Status: APPROVED
	Title: a-01	Scale: A4 1:5
		Rev: 1 / Date of issue: XXXXXXX / Sheet: 1/1

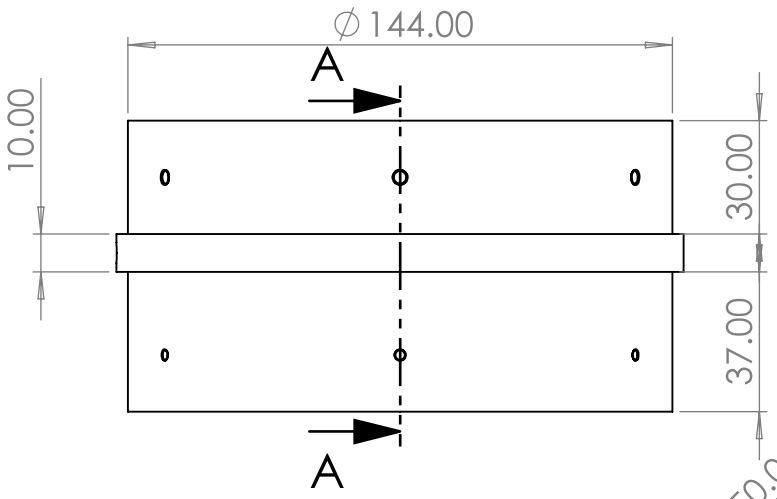

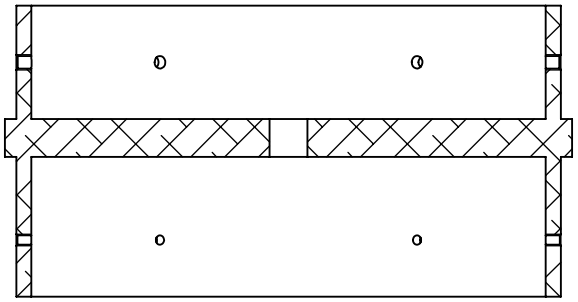

SECTION A-A

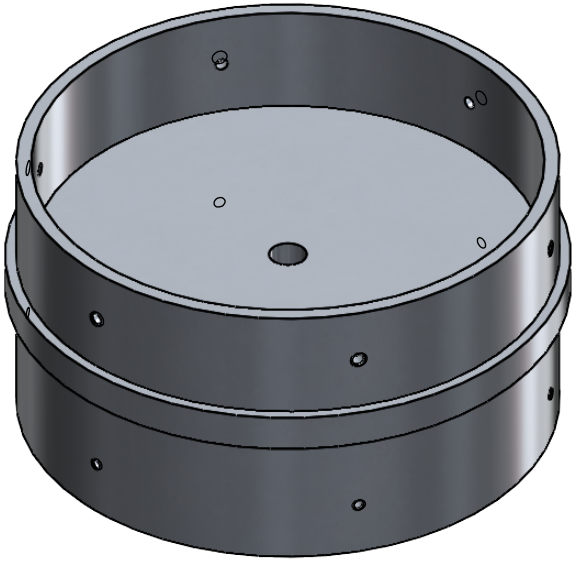

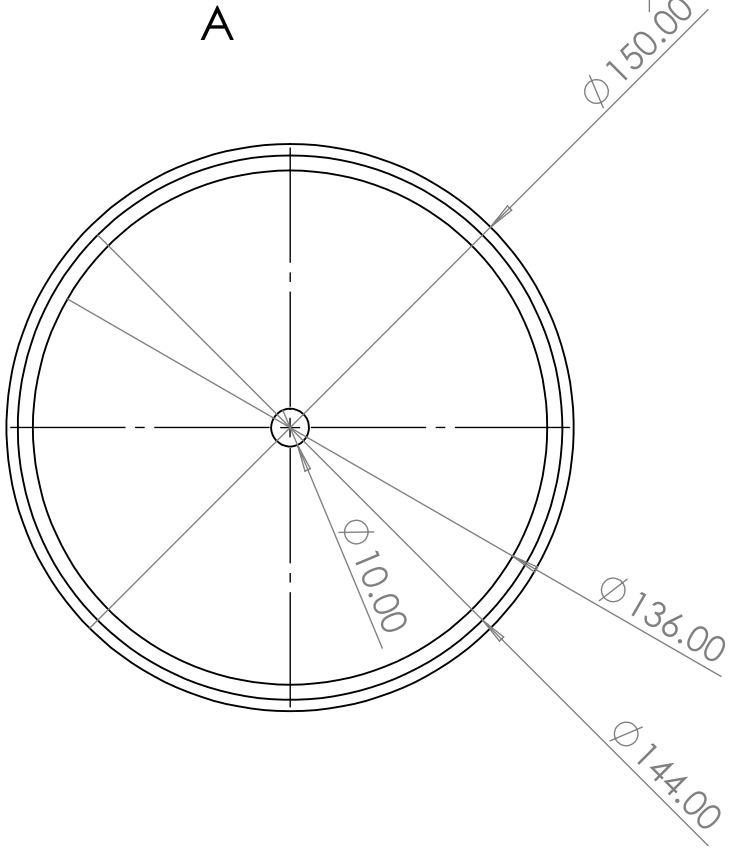

Project: Nemesis	Created by: Andrea Cecchini	Approved by: Nicolò Basso
AURORA ROCKETRY	Document Type: Part	Status: APPROVED
	Title: a-02	Scale: A4 1:2
	Rev: 1	Date of issue:
		Sheet: 1/1

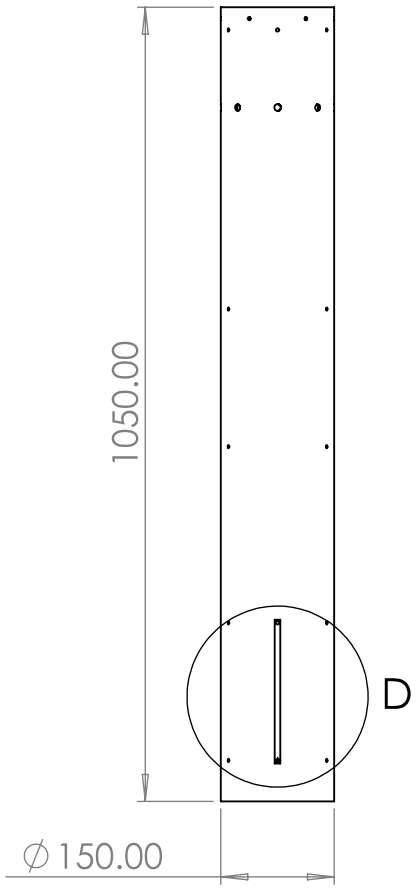

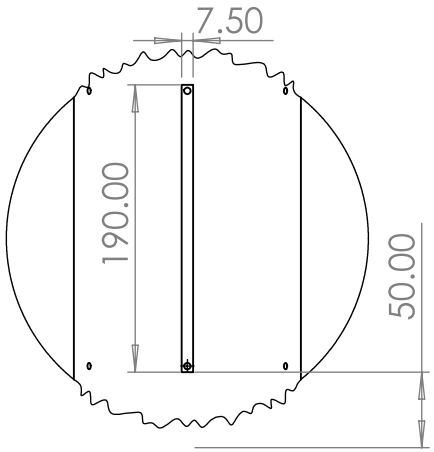

DETAIL D

SCALE 1 : 5

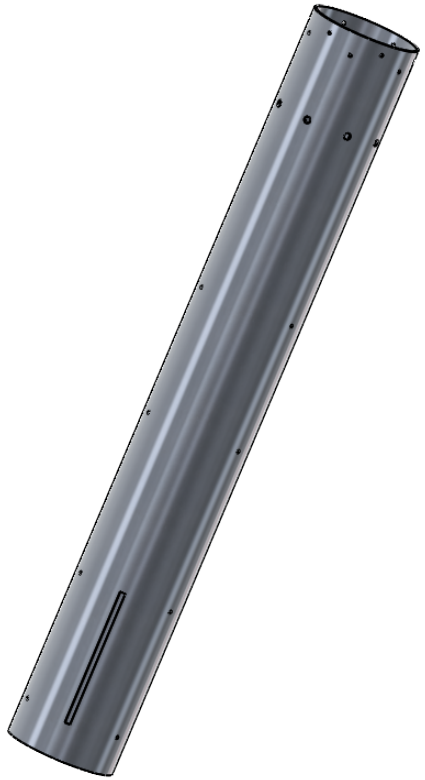

Project: Nemesis	Created by: Giammarco Perugini	Approved by: Lorenzo Piccinini
AURORA ROCKETRY	Document Type: Part	Status: APPROVED
	Title: δ-01	Scale: A4 1:10
	Rev: 1	Date of issue:
		Sheet: 1/1

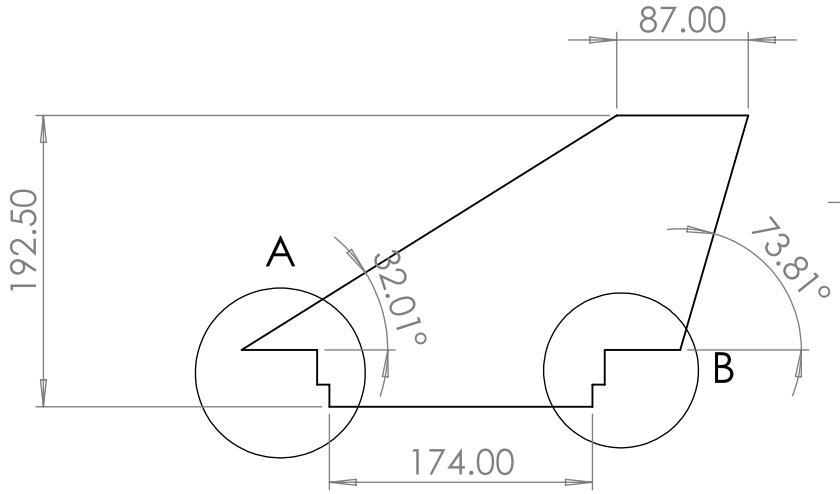

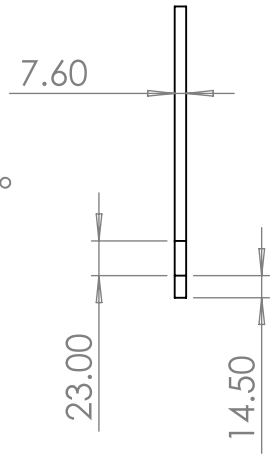

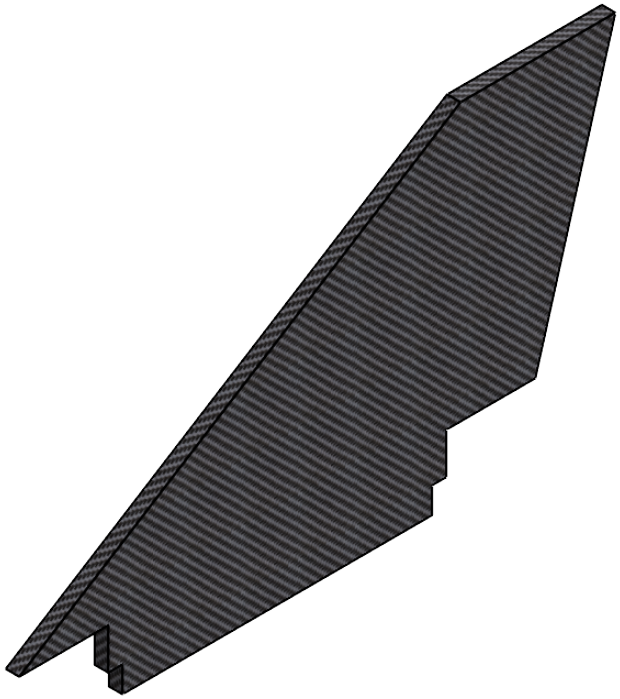

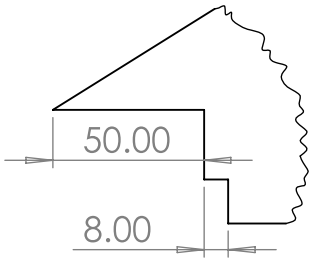

DETAIL A
SCALE 2 : 5

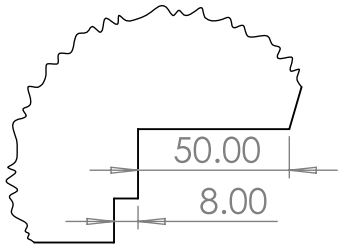

DETAIL B
SCALE 2 : 5

Project Nemesis	Created by Diego Dascola	Approved by Nicolò Basso
AURORA ROCKETRY	Document Type Part	Status APPROVED
	Title δ-02	Scale A4 1:5
	Rev 1	Date of issue
		Sheet 1/1

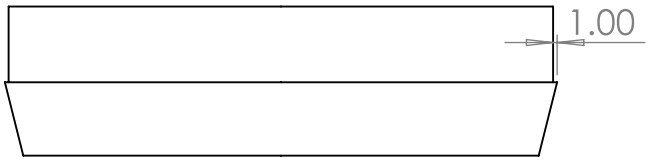

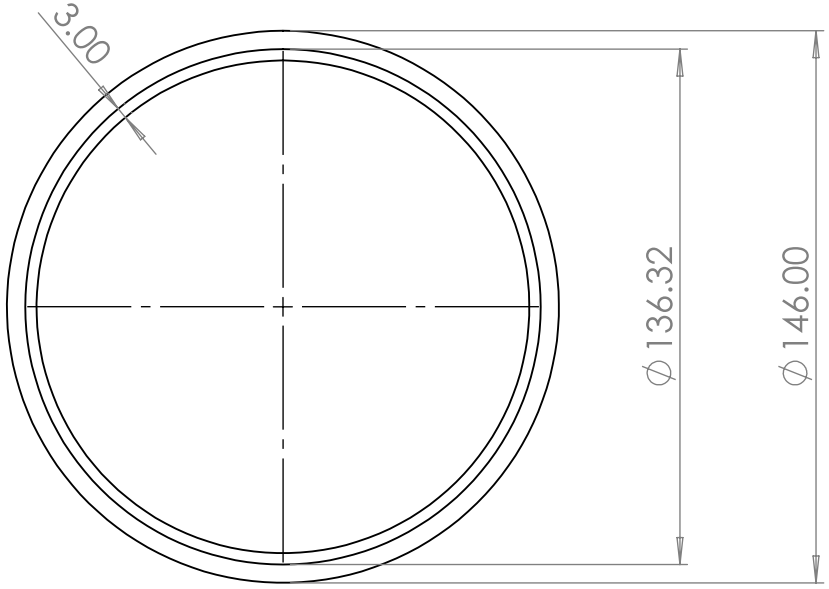

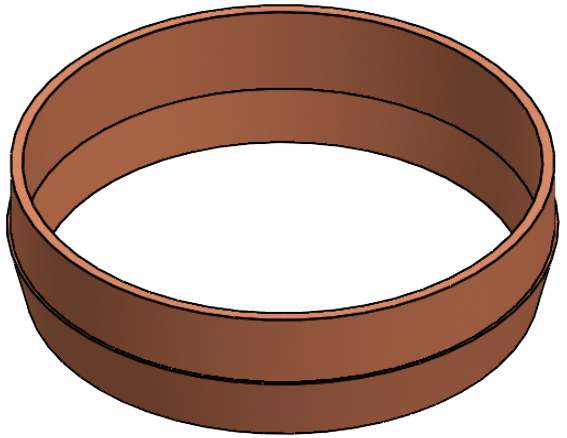

Project: Nemesis	Created by: Maurizio Romagnolo	Approved by: Lorenzo Piccinini
AURORA ROCKETRY	Document Type: Part	Status: APPROVED
	Title: δ-03	Scale: A4 1:2
	Rev: 1	Date of issue:
		Sheet: 1/1

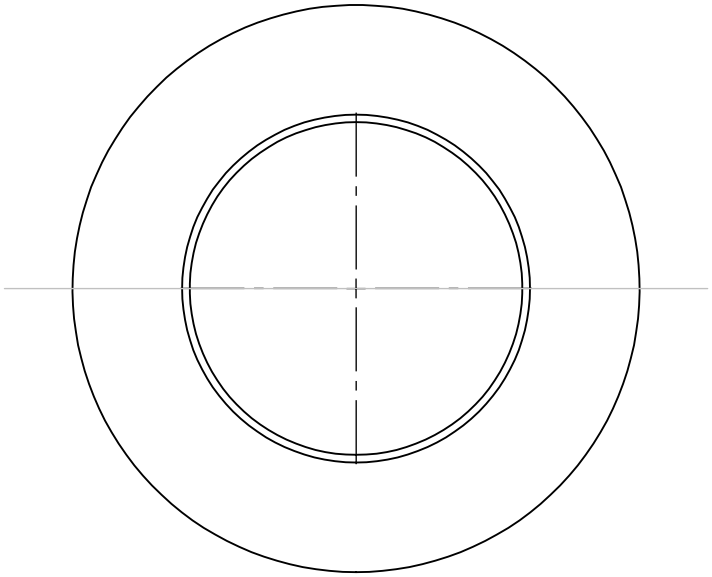

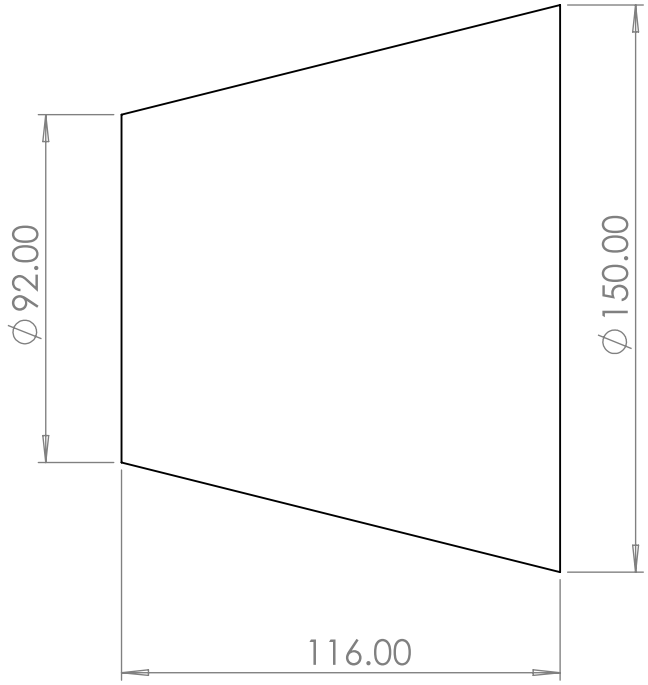

Project Nemesis	Created by Maurizio Romagnolo	Approved by Lorenzo Piccinini
AURORA ROCKETRY	Document Type Part	Status APPROVED
	Title δ-04	Scale A4 1:2
		Rev: 1 / Date of issue: / Sheet: 1/1

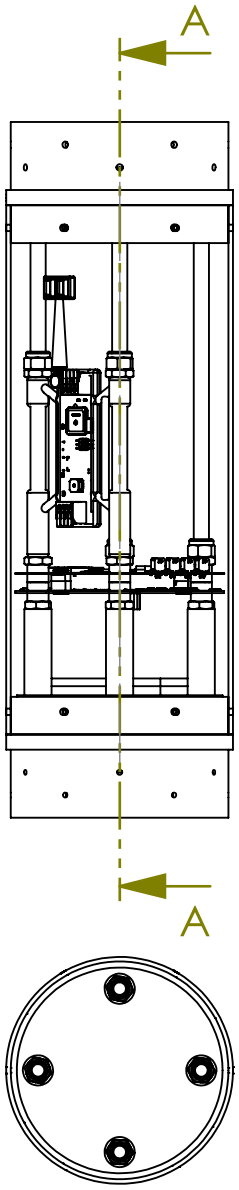

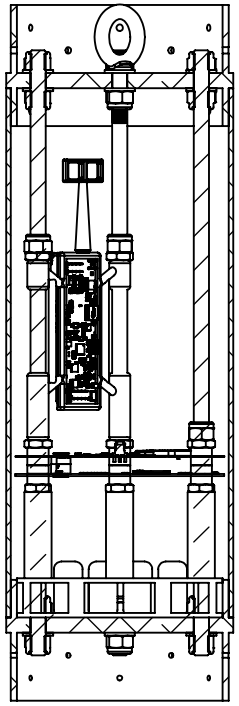

SECTION A-A

SCALE 1 : 5

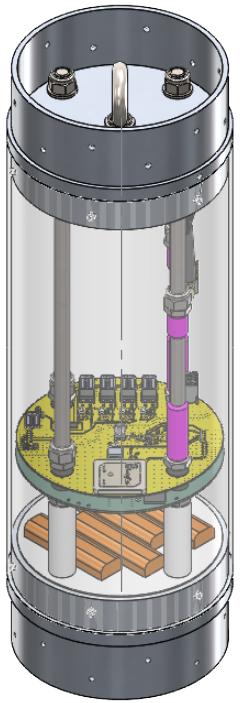

Project: Nemesis	Created by: Andrea Cecchini	Approved by: Lorenzo Piccinini
AURORA ROCKETRY	Document Type: Assembly	Status: APPROVED
	Title: E-BAY	Scale: A4 1:5
		Rev: 1 / Date of issue: / Sheet: 1/1

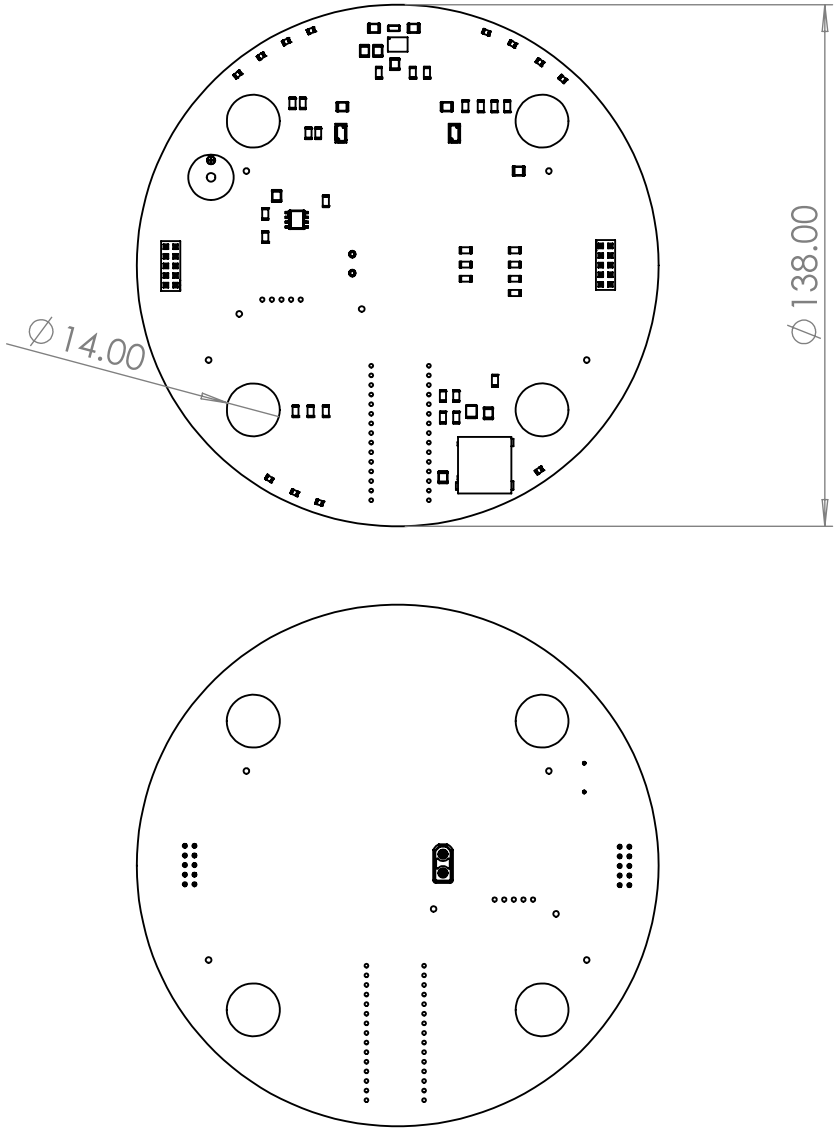

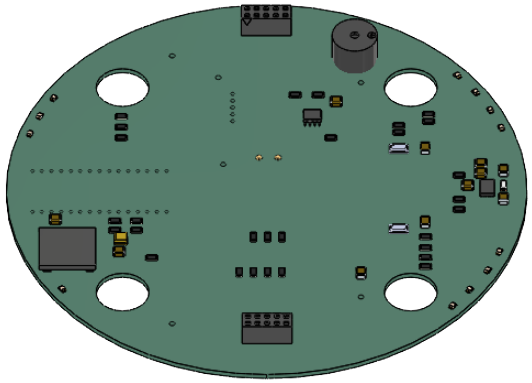

Project	Created by	Approved by
Nemesis	Lorenzo Matti	Nicolò Basso
AURORA ROCKETRY	Document Type: Part	Status: APPROVED
	Title: S-ELC-02	Scale: A4 1:2
	Rev: 1	Date of issue: A4 1:2 / Sheet: 1/1

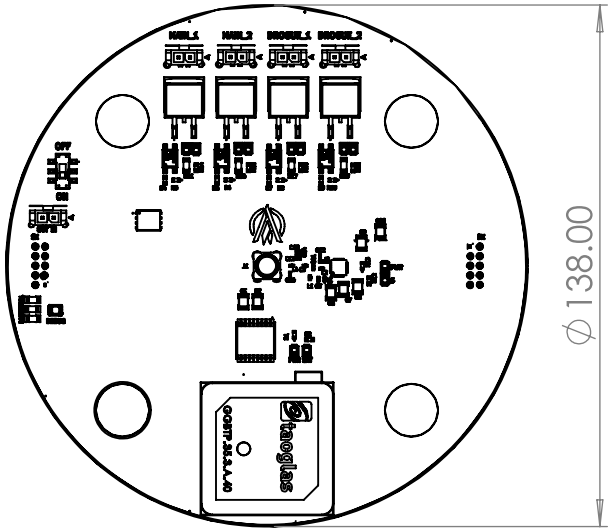

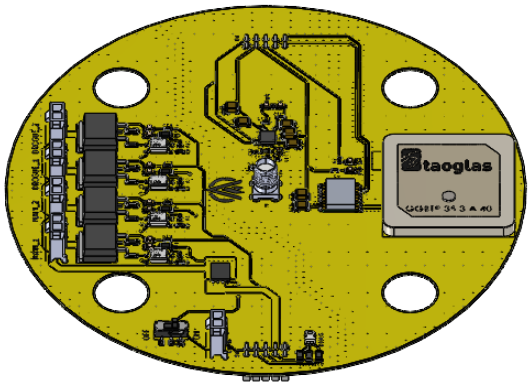

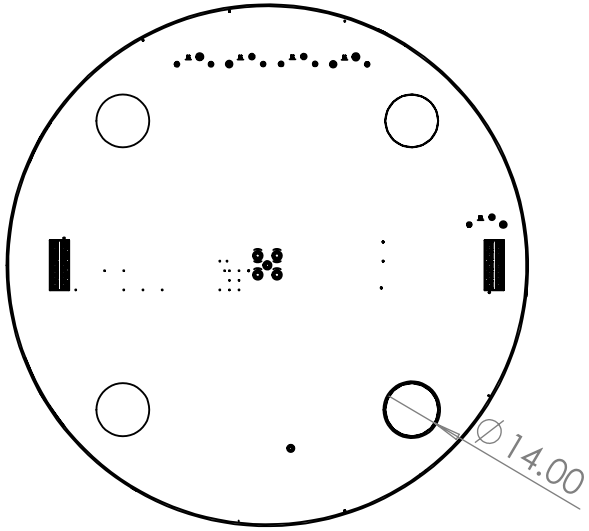

Project Nemesis	Created by Lorenzo Matti	Approved by Nicolò Basso
AURORA ROCKETRY	Document Type Part	Status APPROVED
	Title S-ELC-03	Scale A4 1:2
	Rev 1	Date of issue
		Sheet 1/1

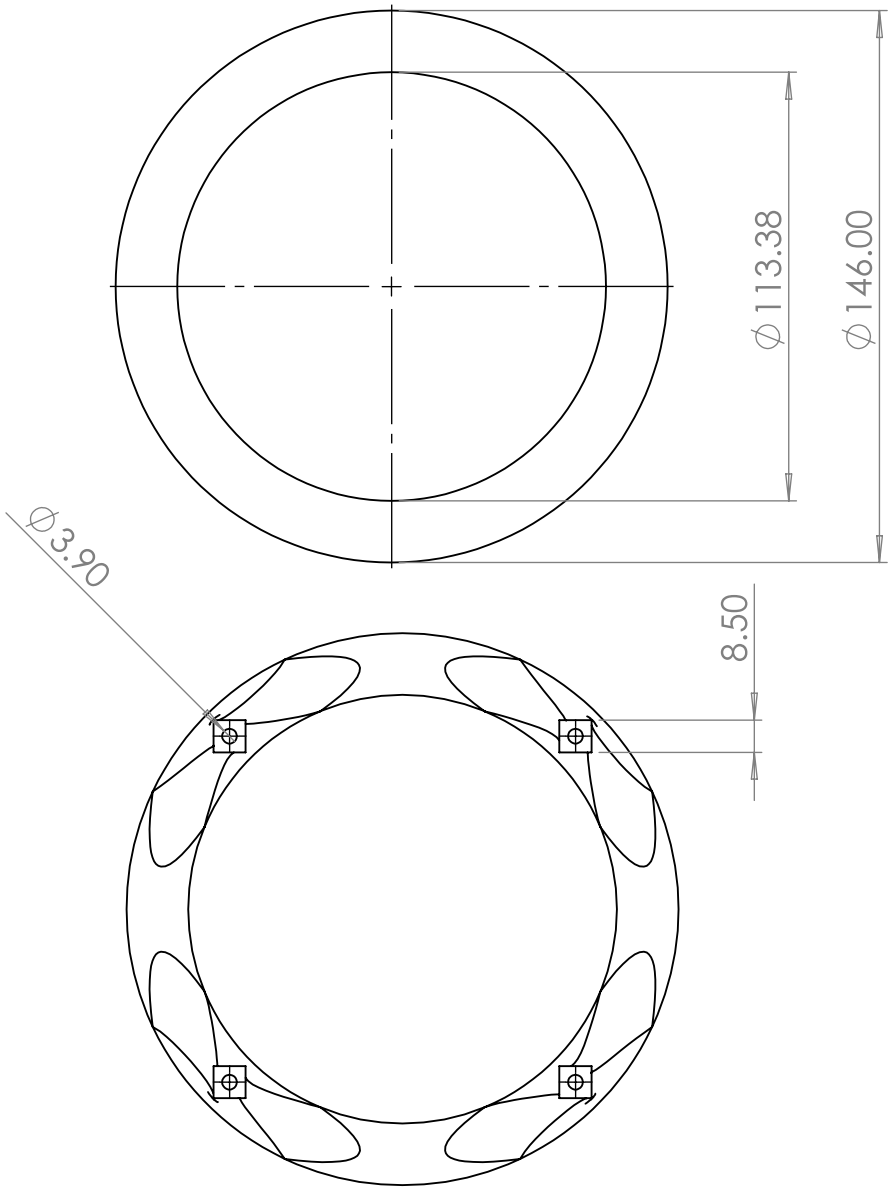

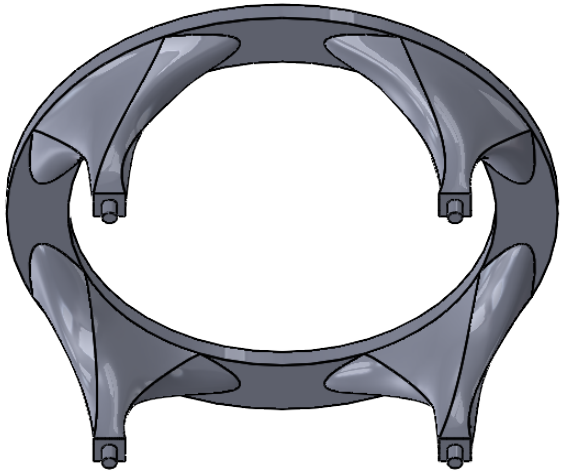

Project: Nemesis	Created by: Nicolò Basso	Approved by: Nicolò Basso
AURORA ROCKETRY	Document Type: Part	Status: APPROVED
	Title: S-PLD-01	Scale: A4 1:2
	Rev: 1	Date of issue:
		Sheet: 1/1

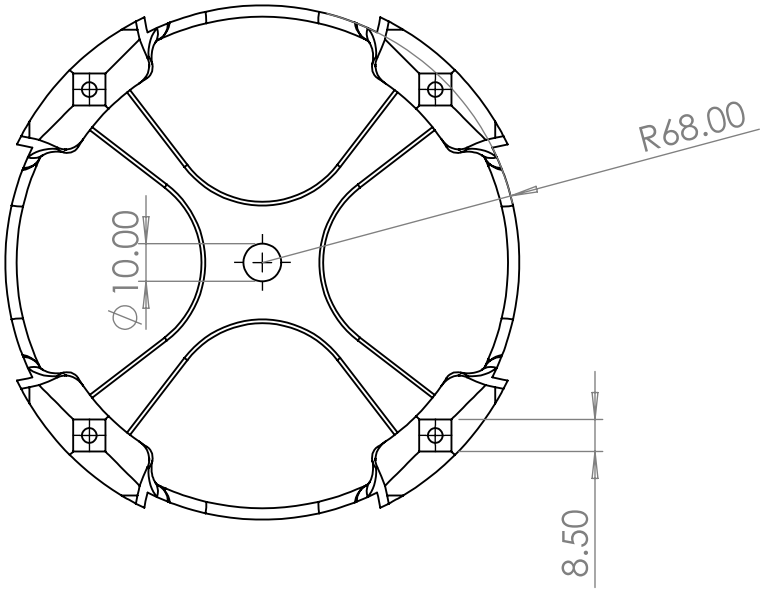

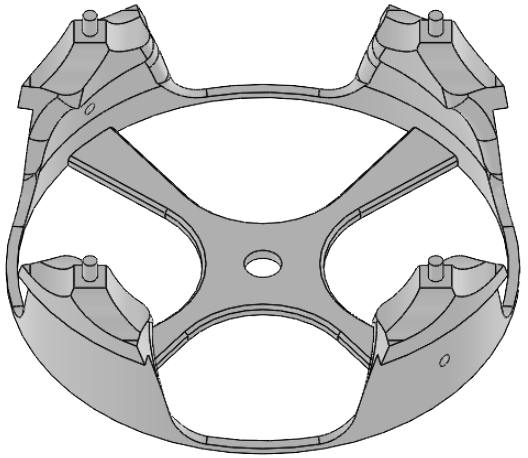

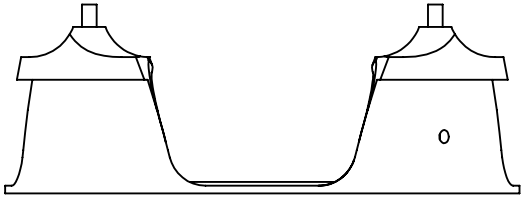

Project: Nemesis	Created by: Nicolò Basso	Approved by: Nicolò Basso
AURORA ROCKETRY	Document Type: Part	Status: APPROVED
	Title: S-PLD-02	Scale: A4 1:2
		Rev: 1 / Date of issue: XXXXXXX / Sheet: 1/1

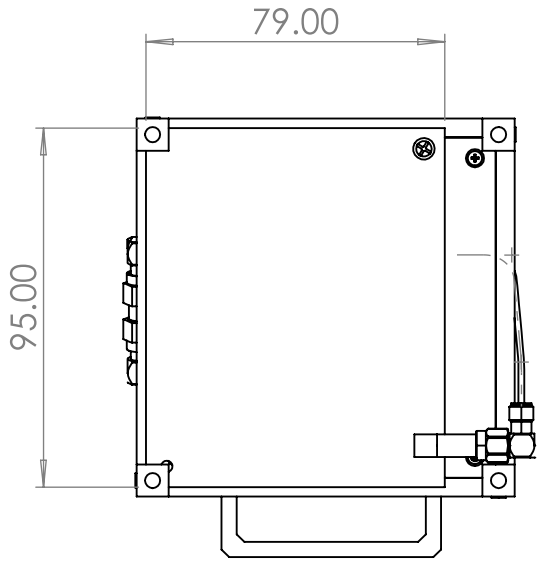

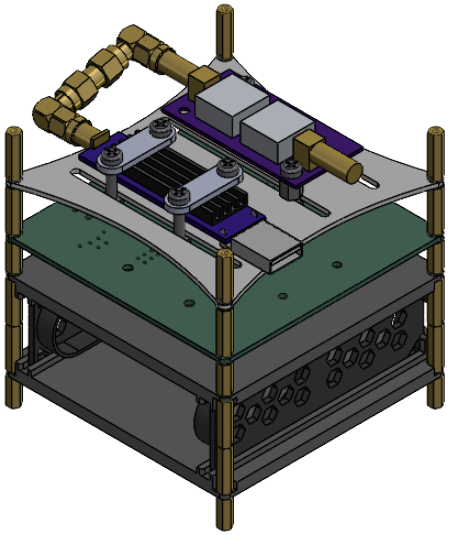

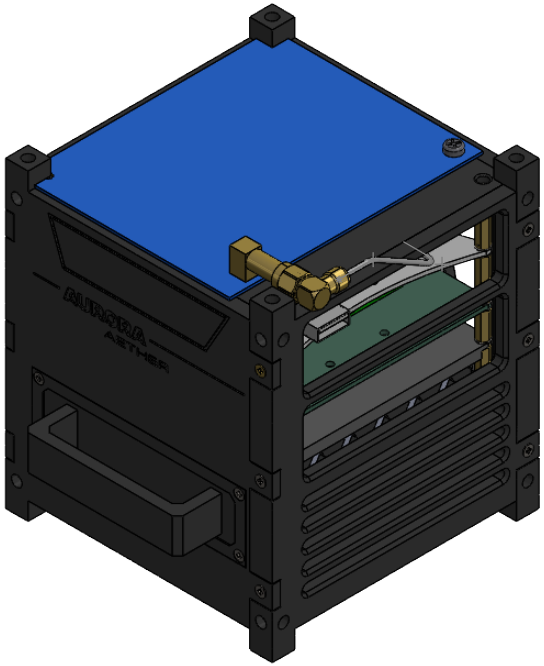

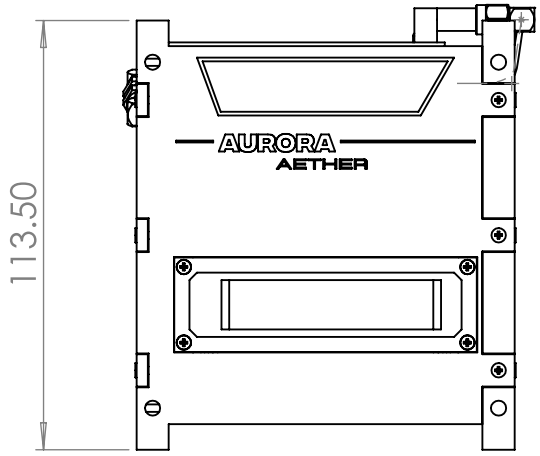

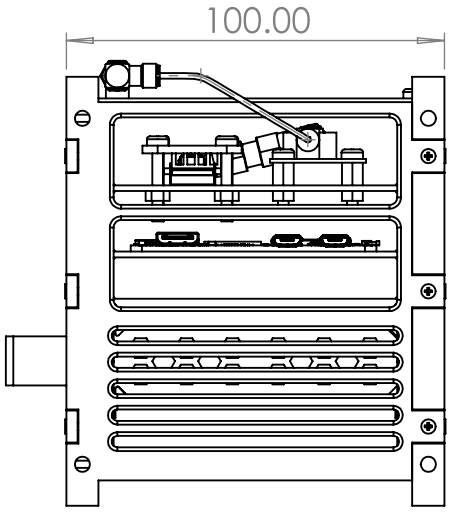

Project: Payload	Created by: Nicolò Basso	Approved by: Nicolò Basso
AURORA ROCKETRY	Document Type: Assembly	Status: APPROVED
	Title: S-PLD-AET	Scale: A4 1:2
		Rev: 1 / Date of issue: / Sheet: 1/1

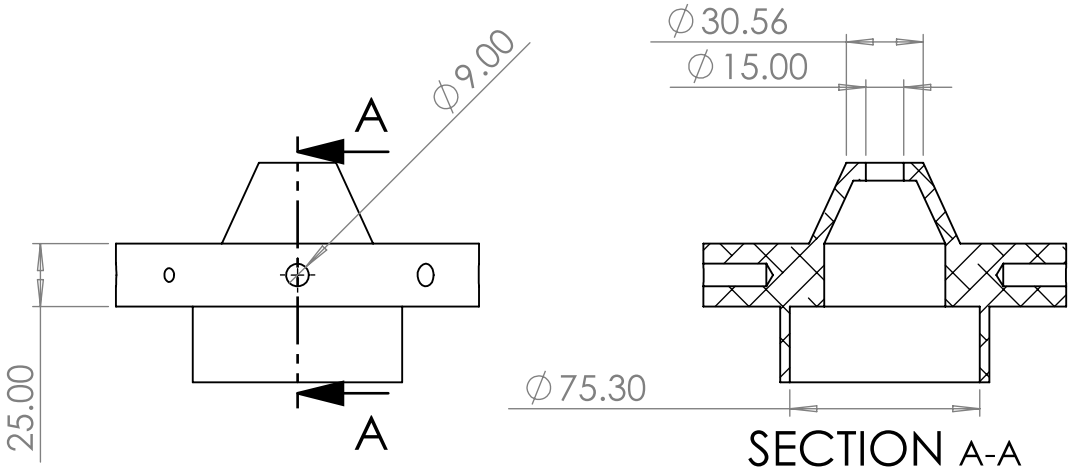

SECTION A-A

SCALE 1 : 3

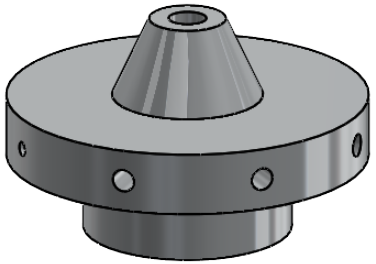

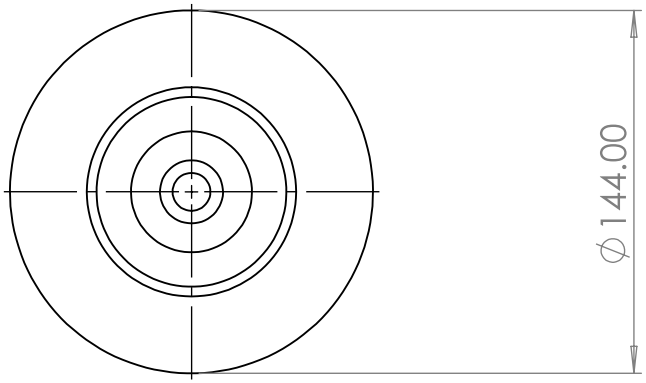

Project: Nemesis	Created by: Maurizio Romagnolo	Approved by: Daniele Bandini
AURORA ROCKETRY	Document Type: Part	Status: APPROVED
	Title: S-PRP-01	Scale: A4 1:3
		Rev: 1 / Date of issue: / Sheet: 1/1

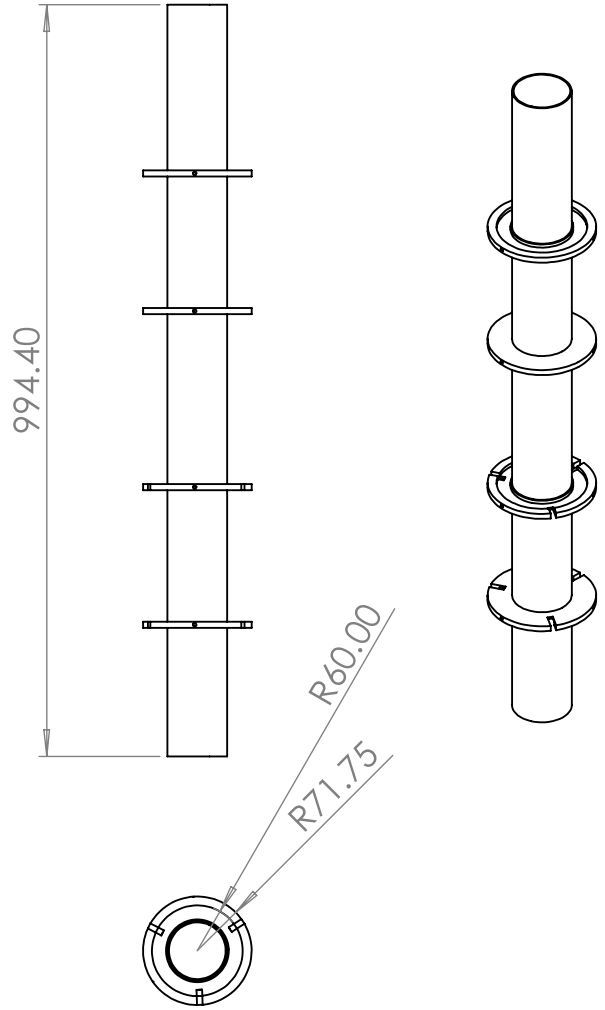

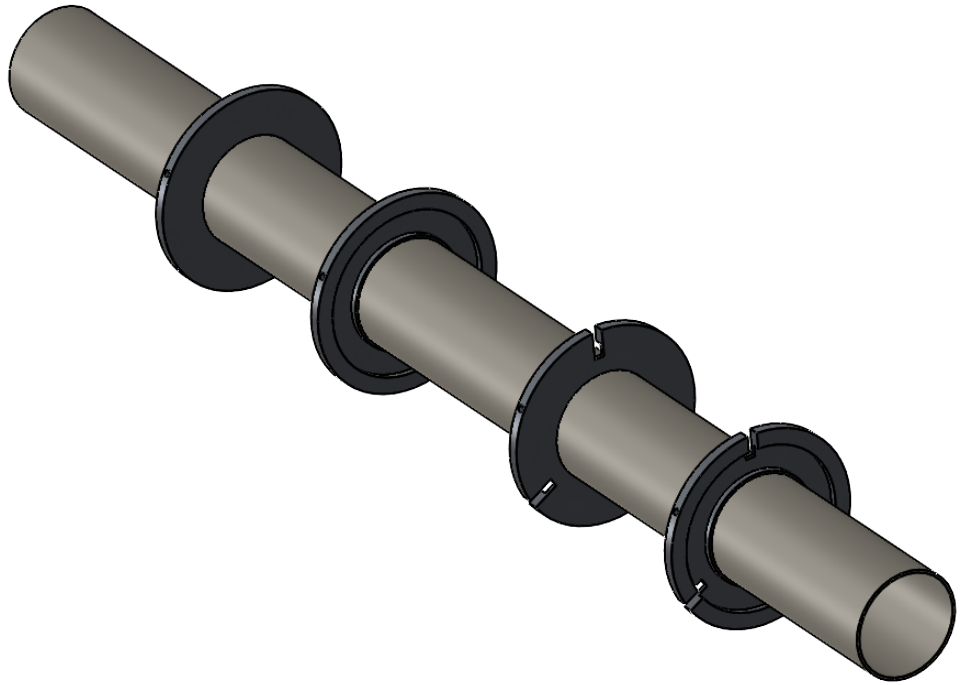

Project: Nemesis	Created by: Maurizio Romagnolo	Approved by: Lorenzo Piccinini
AURORA ROCKETRY	Document Type: Assembly	Status: APPROVED
	Title: S-PRP-02	Scale: A4 1:10
	Rev: 1	Date of issue:
		Sheet: 1/1

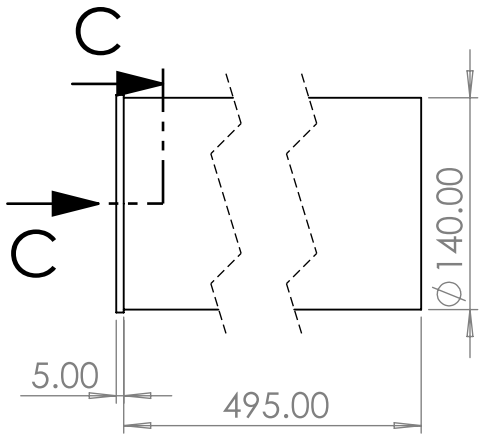

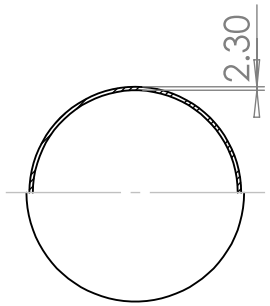

SECTION C-C

SCALE 1 : 5

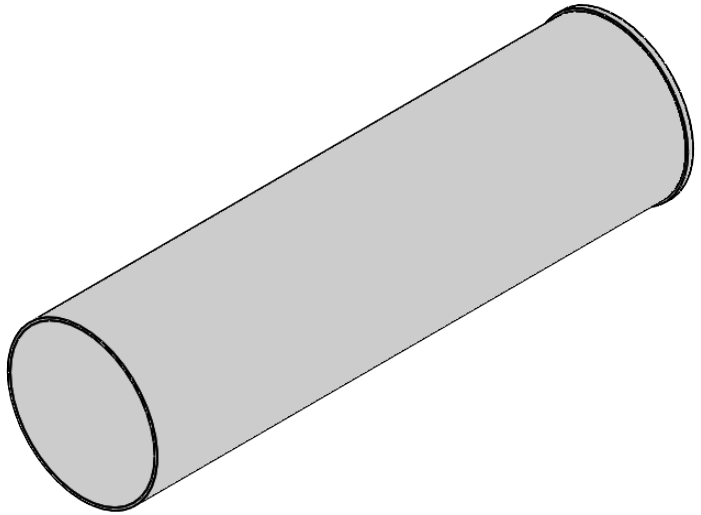

Project: Nemesis	Created by: Leonardo Olmi	Approved by: Lorenzo Piccinini
AURORA ROCKETRY	Document Type: Part	Status: APPROVED
	Title: S-REC-01	Scale: A4 1:3
		Rev: 1 / Date of issue: / Sheet: 1/1

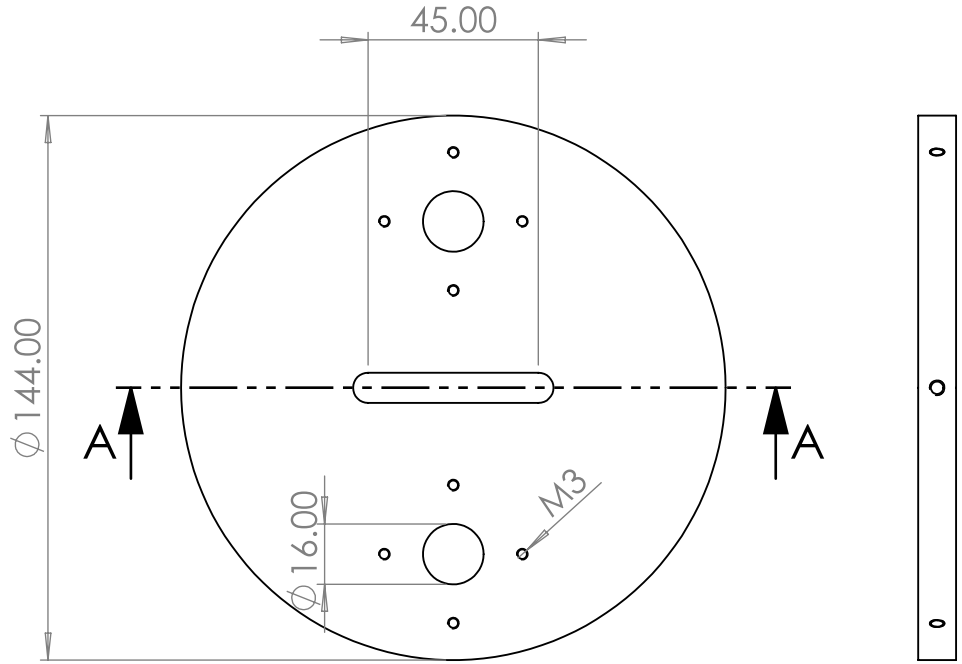

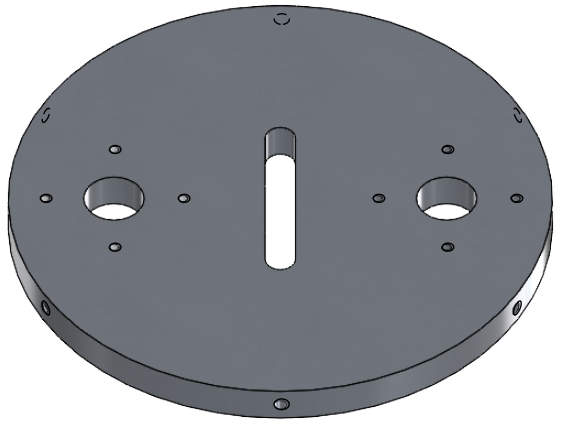

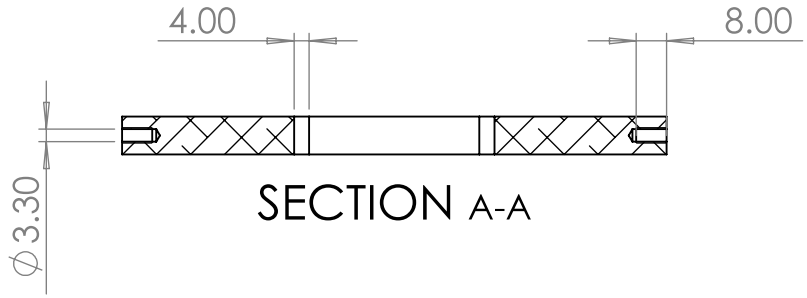

SECTION A-A

Project Nemesis	Created by Maurizio Romagnolo	Approved by Lorenzo Piccinini
AURORA ROCKETRY	Document Type Part	Status APPROVED
	Title S-REC-02	Scale A4 1:2
	Rev 1	Date of issue
		Sheet 1/1

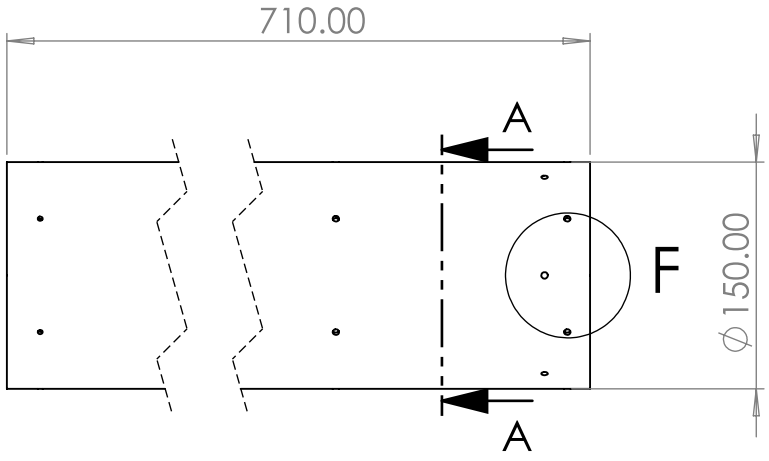

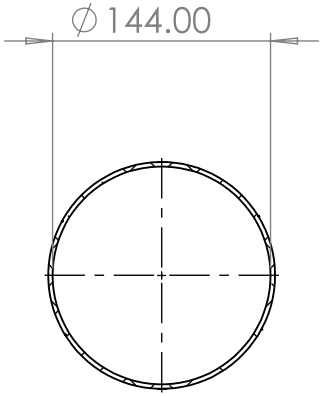

SECTION A-A

SCALE 1 : 5

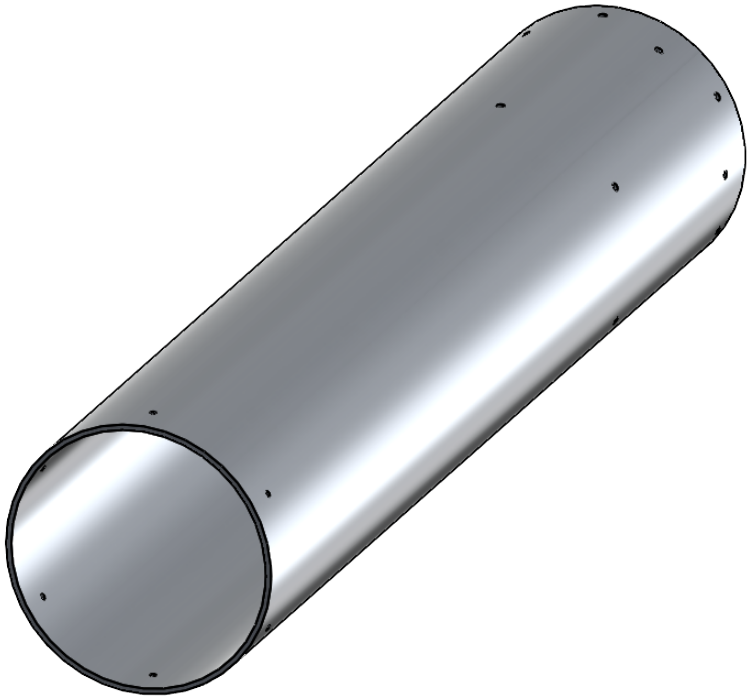

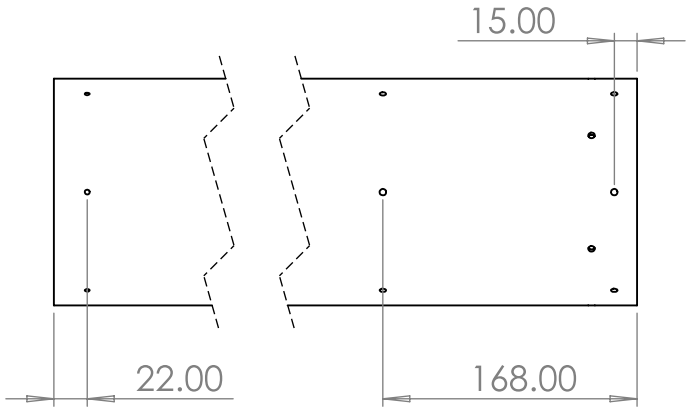

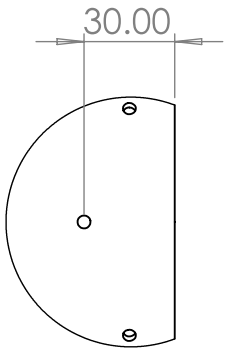

DETAIL F

SCALE 2 : 5

Project: Nemesis	Created by: Leonardo Olmi	Approved by: Lorenzo Piccinini
AURORA ROCKETRY	Document Type: Part	Status: APPROVED
	Title: β-01	Scale: A4 1:5
	Rev: 1	Date of issue:
		Sheet: 1/1

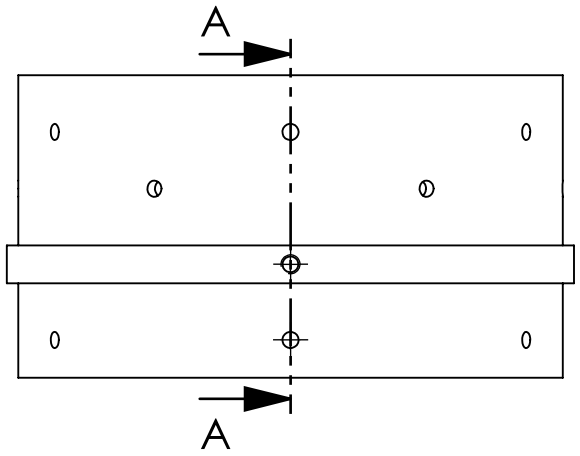

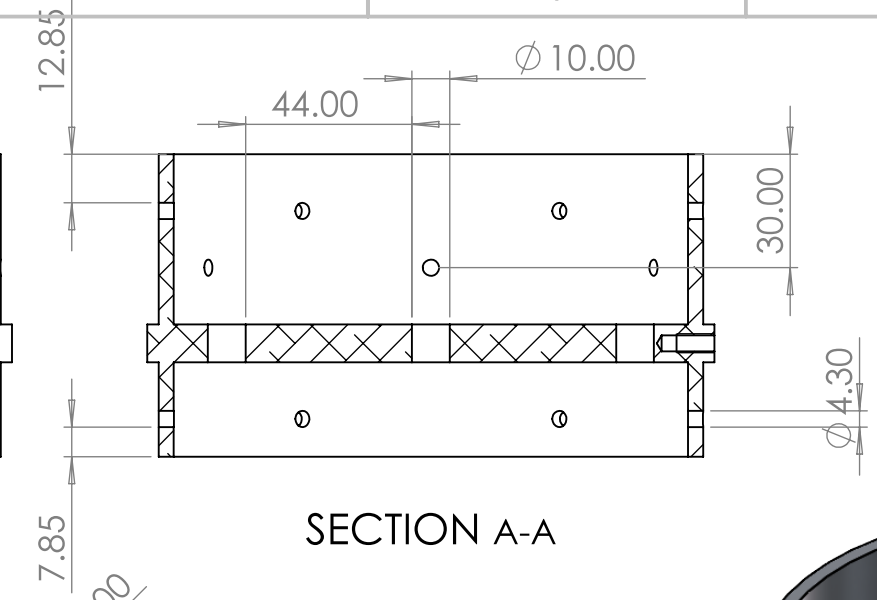

SECTION A-A

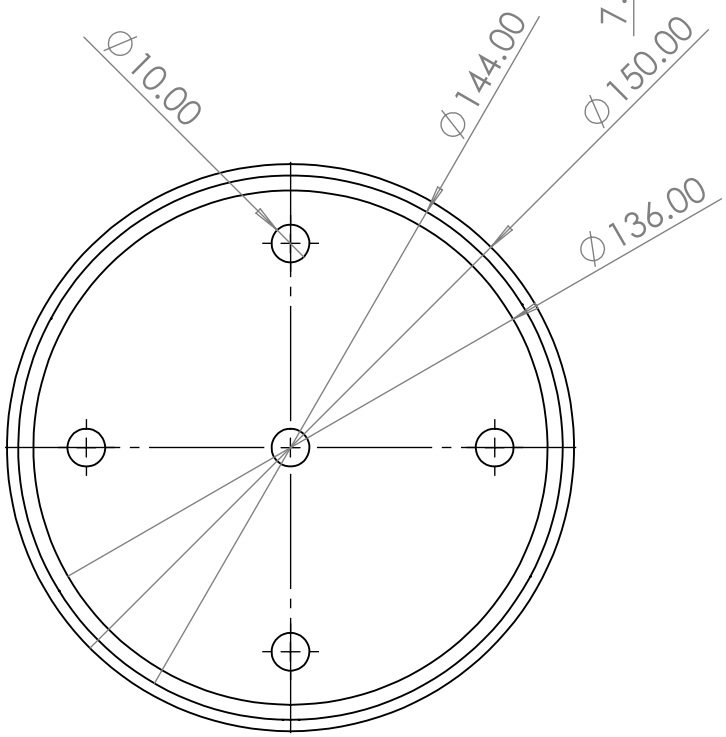

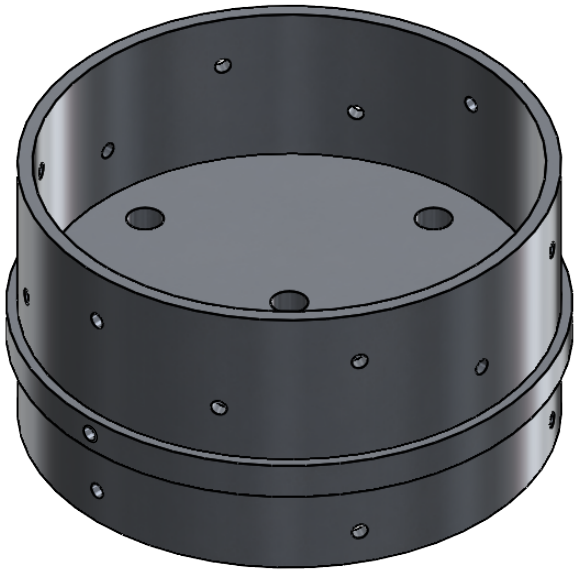

Project: Nemesis	Created by: Andrea Cecchini	Approved by: Nicolò Basso
AURORA ROCKETRY	Document Type: Part	Status: APPROVED
	Title: β-02	Scale: A4 1:2
	Rev: 1	Date of issue:
		Sheet: 1/1

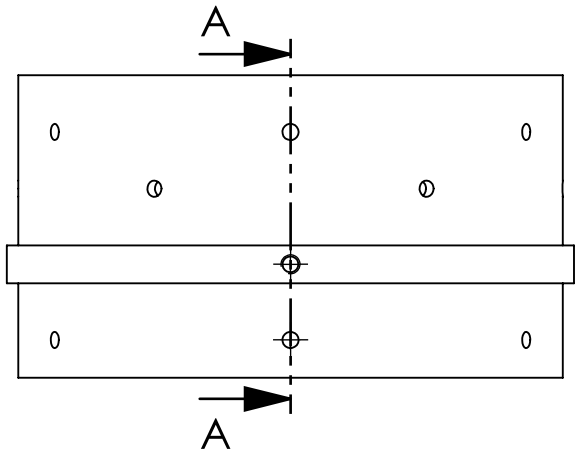

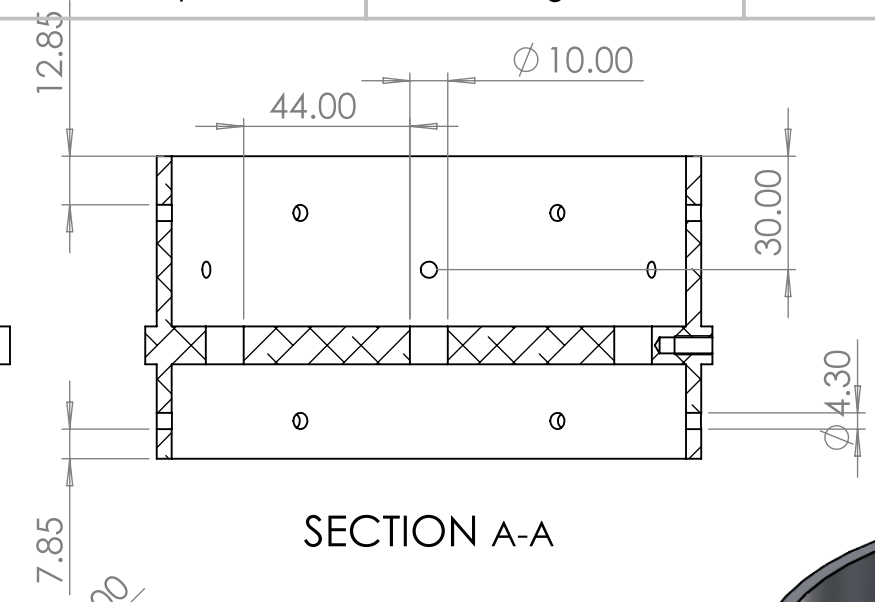

SECTION A-A

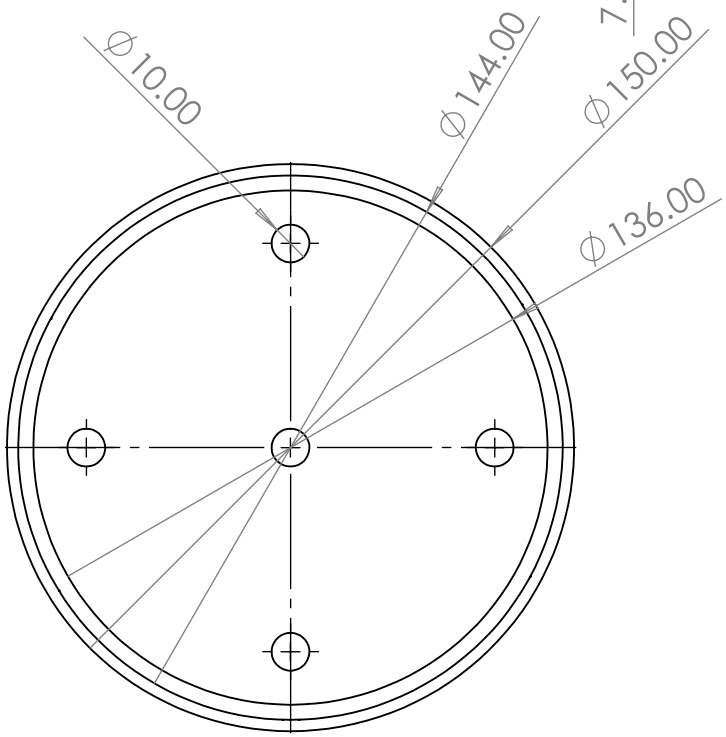

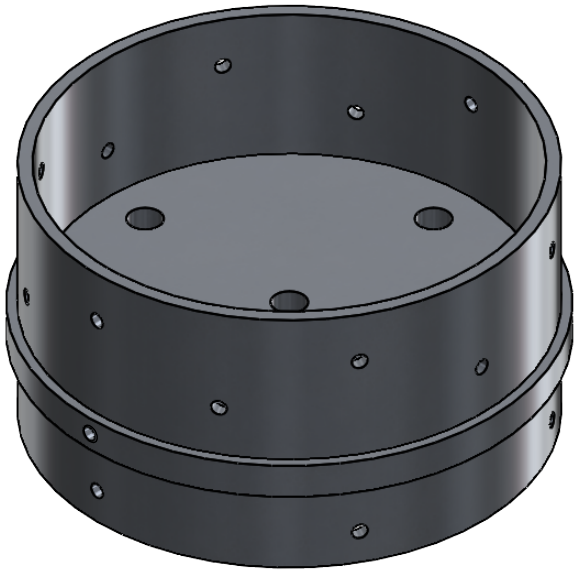

Project: Nemesis	Created by: Andrea Cecchini	Approved by: Nicolò Basso
AURORA ROCKETRY	Document Type: Part	Status: APPROVED
	Title: γ-01	Scale: A4 1:2
	Rev: 1	Date of issue:
		Sheet: 1/1

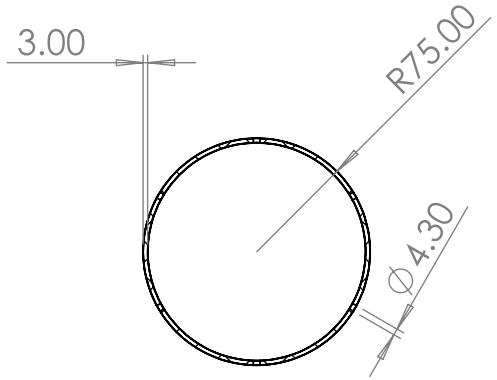

SECTION C-C

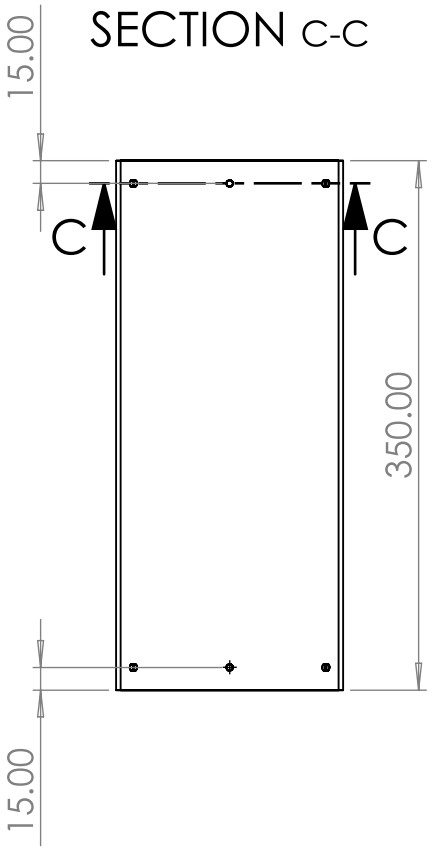

Project: Nemesis	Created by: Giammarco Perugini	Approved by: Lorenzo Piccinini
AURORA ROCKETRY	Document Type: Part	Status: APPROVED
	Title: γ-02	Scale: A4 1:5
		Rev: 1 / Date of issue: / Sheet: 1/1

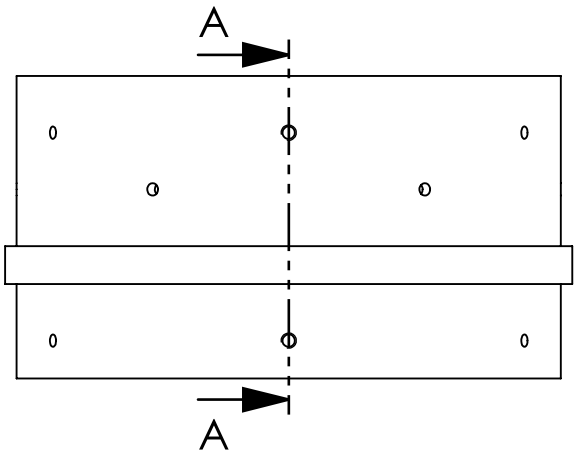

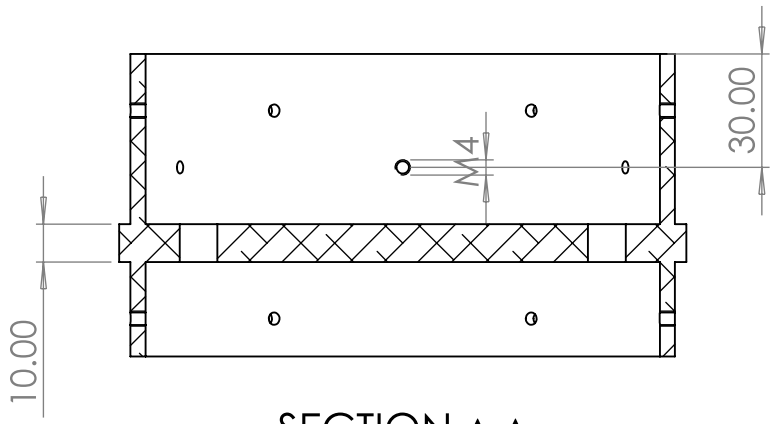

SECTION A-A

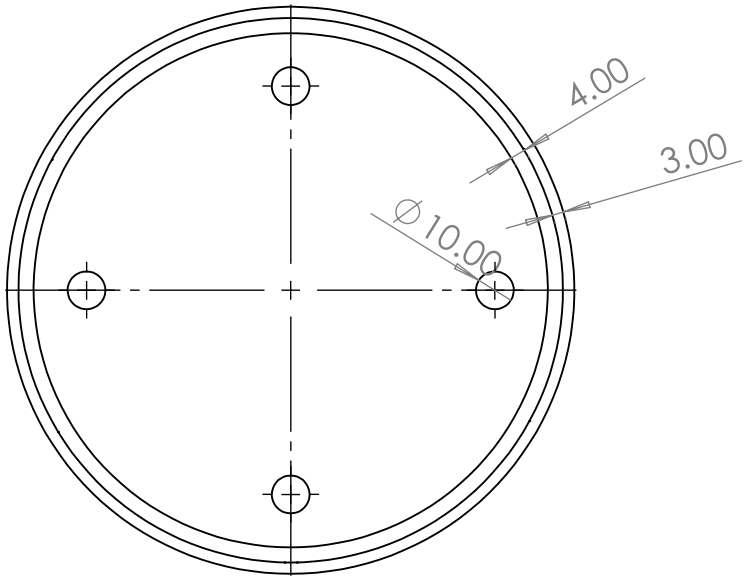

Project: Nemesis	Created by: Giammarco Perugini	Approved by: Lorenzo Piccinini
AURORA ROCKETRY	Document Type: Part	Status: APPROVED
	Title: γ-03	Scale: A4 1:2
	Rev: 1	Date of issue:
		Sheet: 1/1

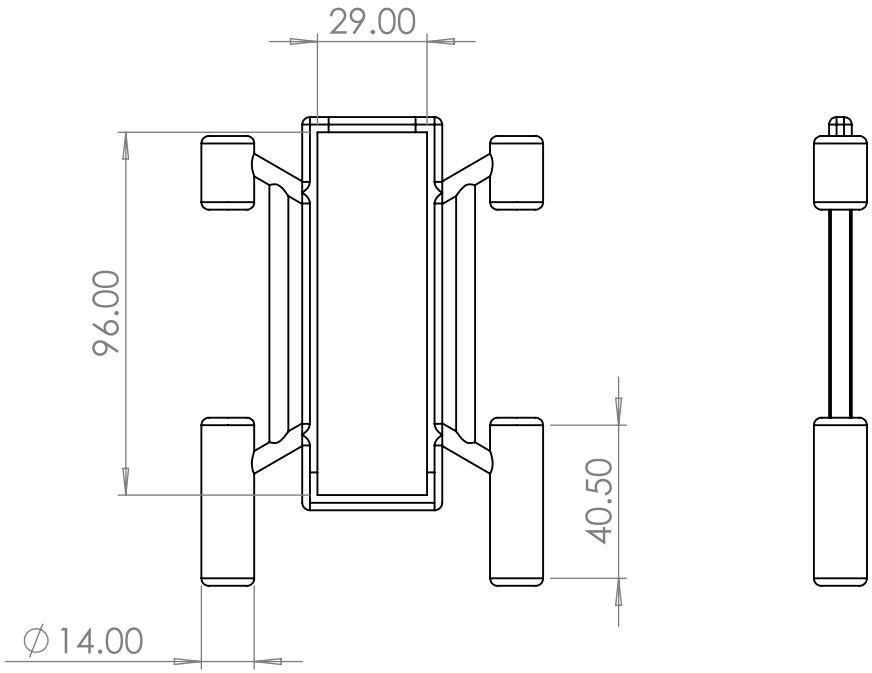

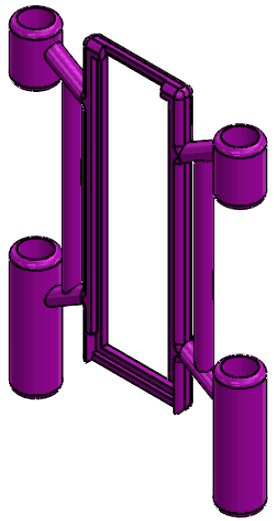

Project: Nemesis	Created by: Andrea Cecchini	Approved by: Nicolò Basso
AURORA ROCKETRY	Document Type: Part	Status: APPROVED
	Title: γ-04	Scale: A4 1:2
	Rev: 1	Date of issue:
		Sheet: 1/1

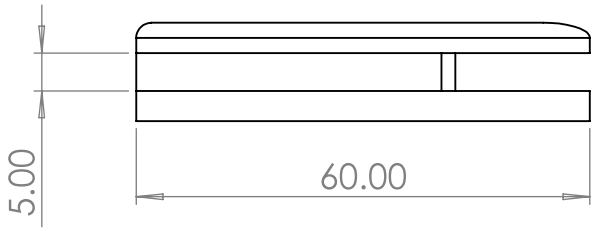

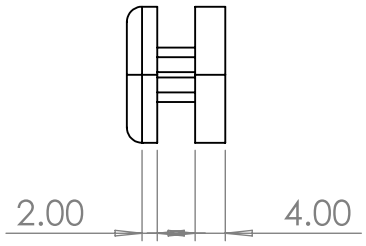

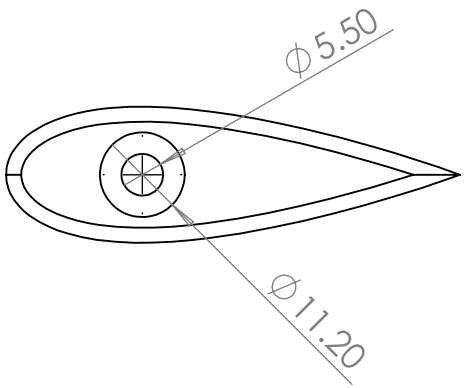

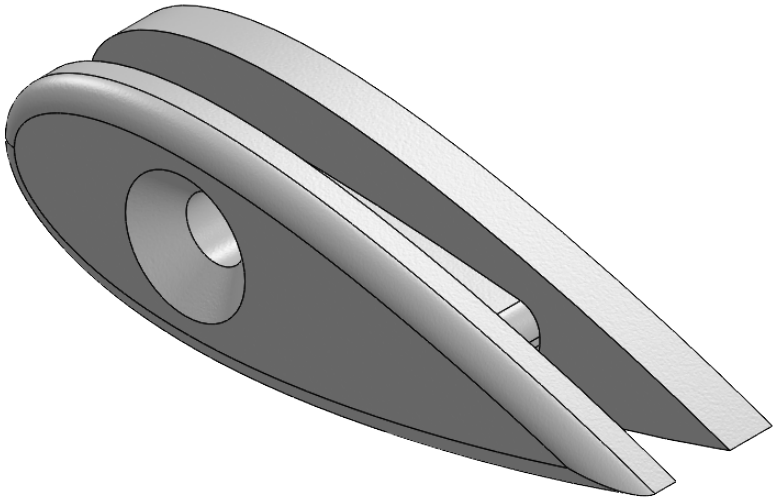

Project: Nemesis	Created by: Andrea Cecchini	Approved by: Daniele Bandini
AURORA ROCKETRY	Document Type: Part	Status: APPROVED
	Title: ω-01	Scale: A4 1:1
	Rev: 1 / Date of issue:	Sheet: 1/1

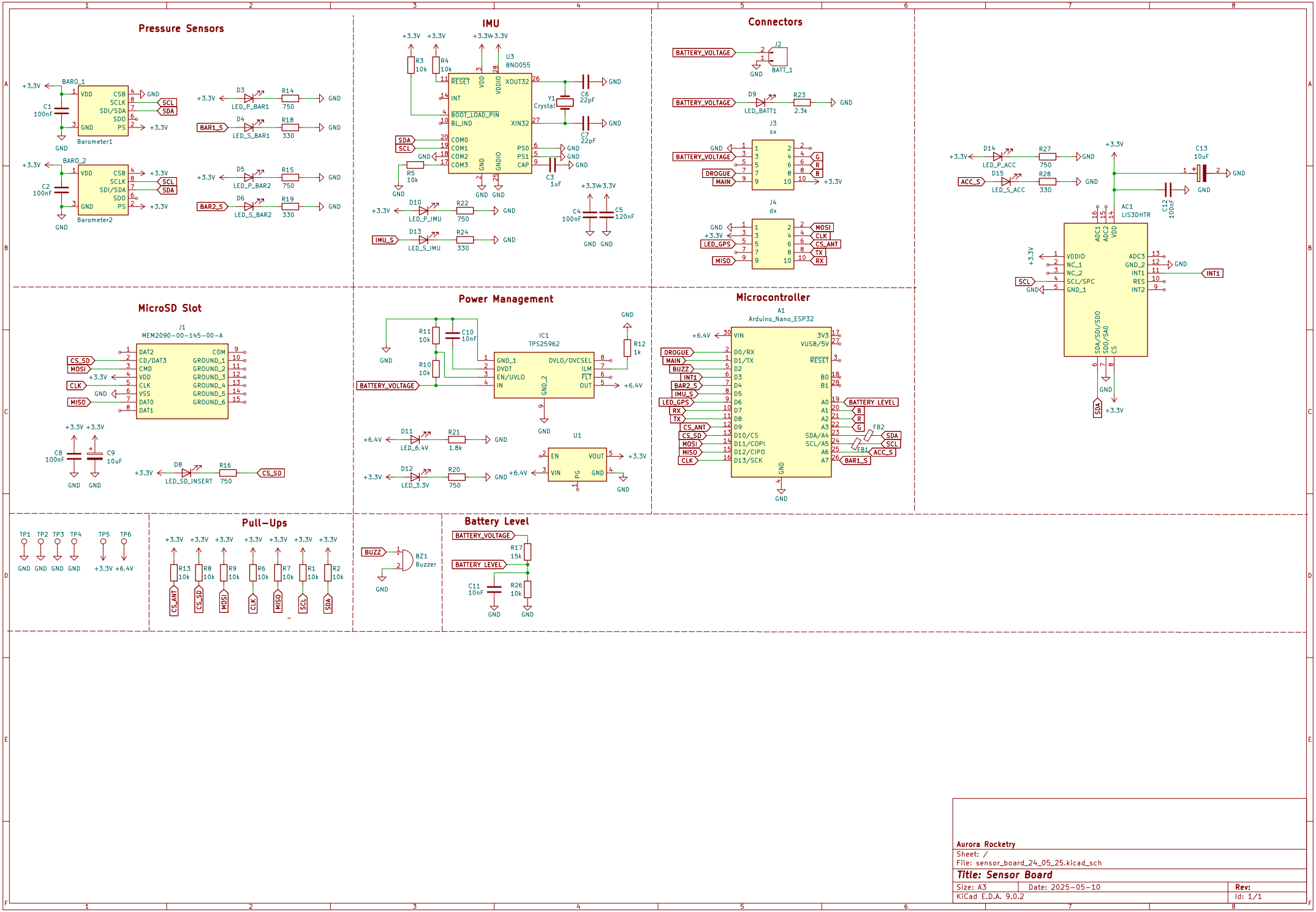

Aurora Rocketry	
Sheet: /	
File: sensor_board_24_05_25.kicad_sch	
Title: Sensor Board	
Size: A3	Date: 2025-05-10
KiCad E.D.A. 9.0.2	Id: 1/1
	Rev:

Radio Transceiver

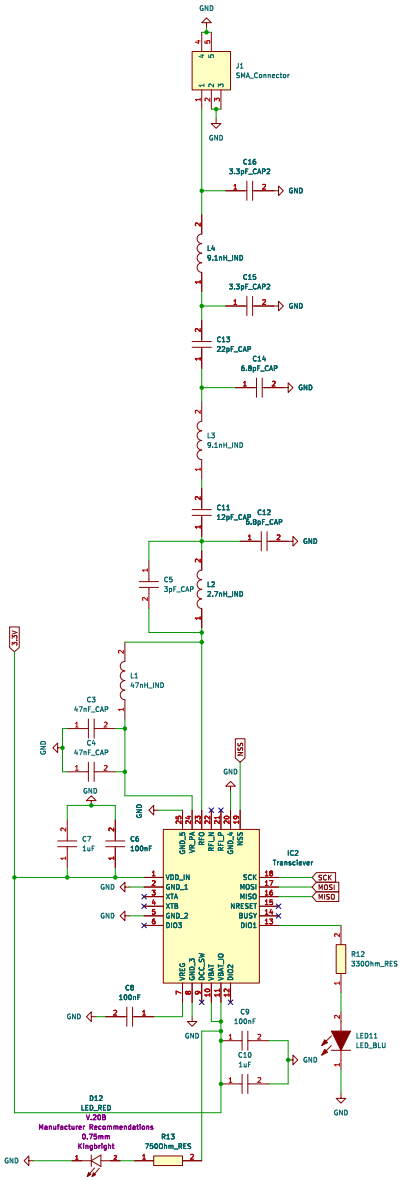

GPS

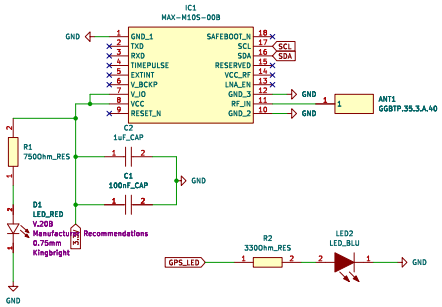

Switch

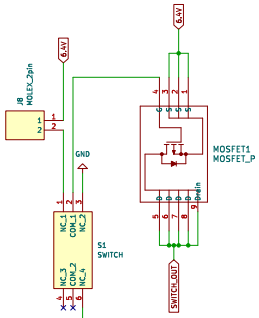

Actuators

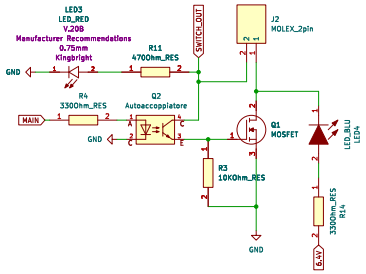

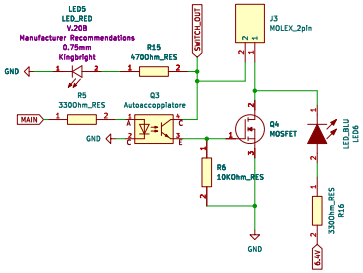

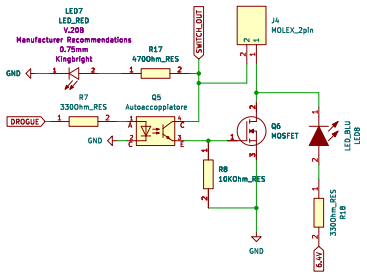

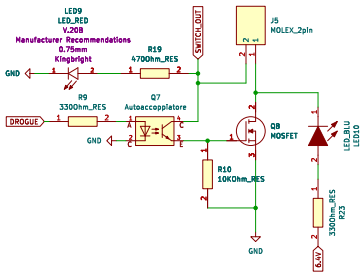

RGB LED

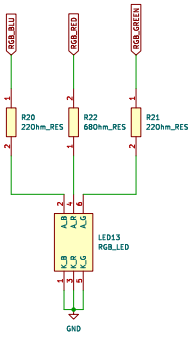

Connectors

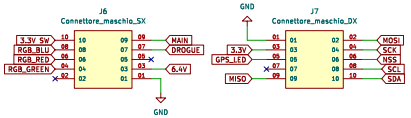

Sheet: /
File: Nemesis_antenna_board.kicad_sch
Title:
Size: A2 | Date: | Rev:
KiCad E.D.A. 9.0.0 | Id: 1/1

Appendix H

RocketPy Flight Simulation Results

H.1 Introduction

This appendix is dedicated to the discussion of the results of the RocketPy simulation. It was chosen to perform Monte Carlo simulations, in order to account for potential assembly inaccuracies, manufacturing defects, or uncertainties in weather conditions. The flights that were simulated all share the same launch rail of 12 m and rail inclination of 85 degrees.

H.2 Weather Condition

In the analysis of rocket flight, it is crucial to account for atmospheric conditions, with particular emphasis on wind speed and direction. The flight was simulated under three distinct wind scenarios.

The first scenario (a) (Figures 1 & 2) is customized using average atmospheric values computed over the time span October 10–15 for the years 2005 through 2024.

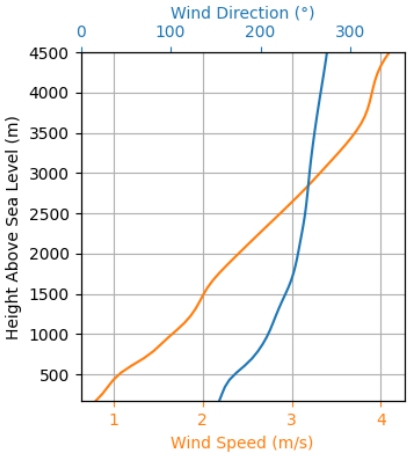

Fig. 1: Wind data for average wind conditions.

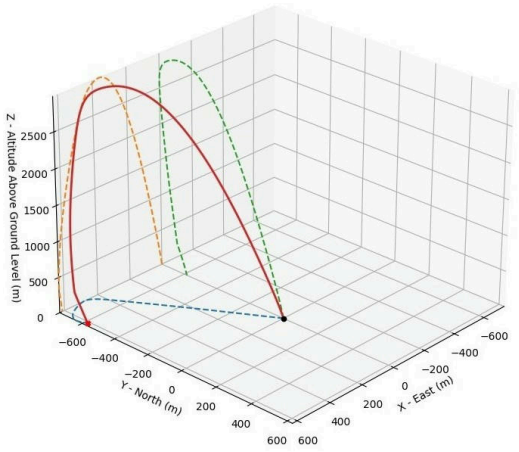

Fig. 2: Flight Trajectory for average wind conditions.

The second scenario (b) (Figures 3 & 4) considers the same time interval as the first; however, instead of averaging, it selects the day with the worst wind conditions observed within the analyzed period, which was found to be October 11, 2024.

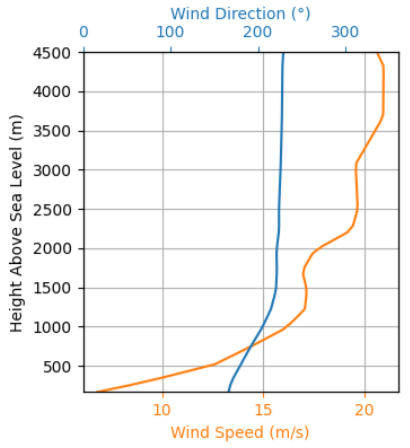

Fig. 3: Wind data for strong wind conditions.

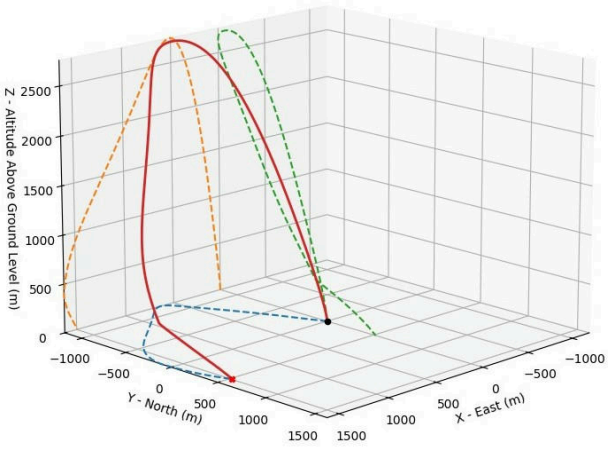

Fig. 4: Flight Trajectory for strong wind conditions.

The third scenario (c) (Figure 5 & 6) considers a constant wind intensity equal to the peak value of scenario (b), but with a direction opposite to that of the launch. This condition induces a sharp turn of the rocket during acceleration, followed by oscillations and the development of a bending moment (see Appendix H-4.3 Aereodynamics Forces). .

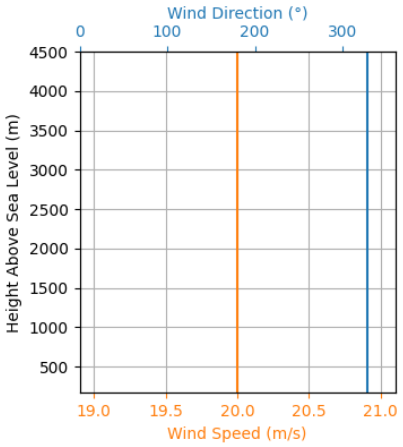

Fig. 5: Wind data for strong wind conditions.

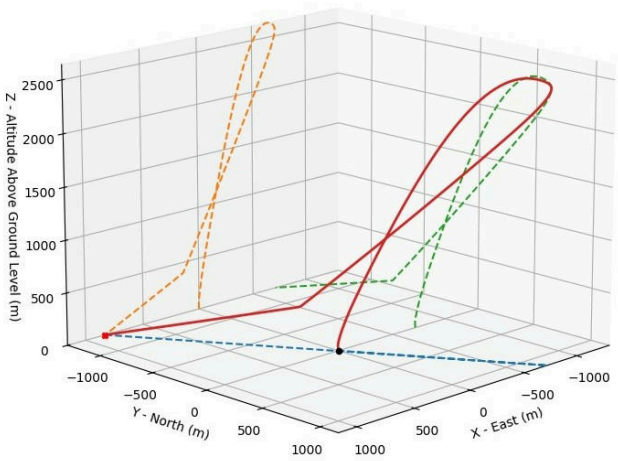

Fig. 6: Flight Trajectory for strong wind conditions.

H.3 Thrust Curve and Cd-Mach Curve

The motor's thrust and the aerodynamic drag coefficient of the rocket are definitely among the most relevant data required by RocketPy for its simulations. The thrust curve for the motor was taken from Thrustcurve.org [7] (Figure 7). The drag coefficient curve was determined by the Aerodynamics Team using a RASAero II analytical model that tries to take into account small protuberances, like those inevitably present on the rocket because of the screws that are used to link its components (Figure 8).

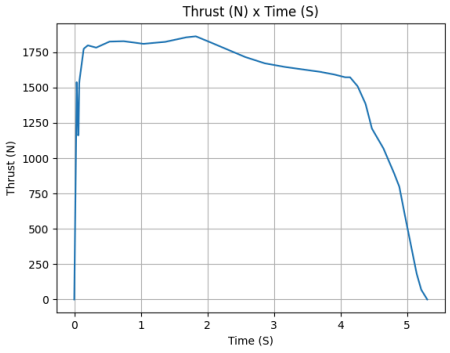

Fig. 7: Thrust curve of the M1545 rocket motor.

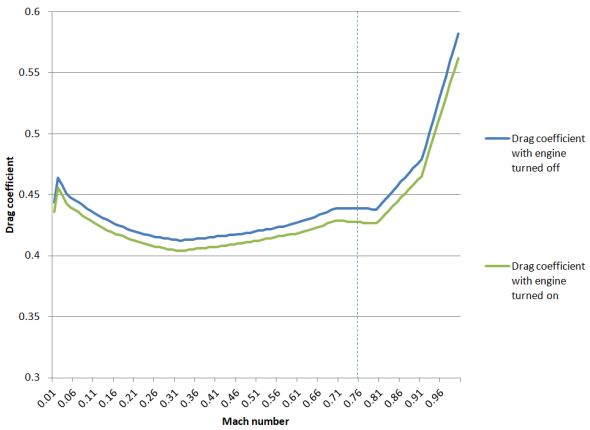

Fig. 8: CD as a function of Mach number.

Simulation Results

The following results were obtained from 150 simulations performed using the Monte Carlo method.

H.4 Out of Rail velocity

The exit velocity from the launch rail is consistently, though not significantly, higher than 30 m/s, in compliance with the EuRoC regulations (Figure 9).

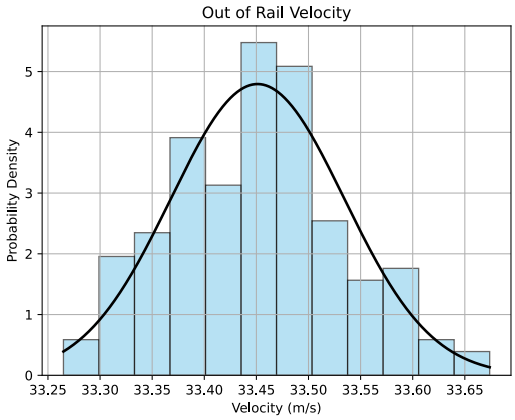

Fig. 9: Out of Rail Velocity.

H.5 Acceleration Profiles

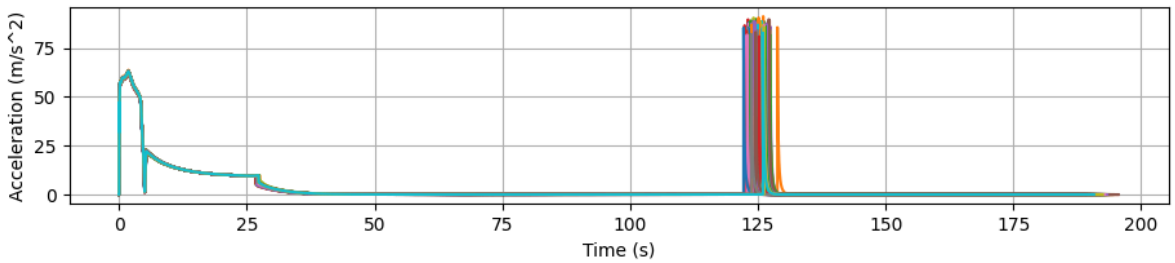

Fig. 10: Acceleration profiles.

By analyzing the acceleration graph, three significant peaks can be observed (Figure 10). The first, approximately 65 m/s², occurs at liftoff, while the second and third correspond to the deployment of the parachutes, Drogue and Main respectively. This led us to further investigate the aerodynamic forces.

H.6 Aerodynamics Forces

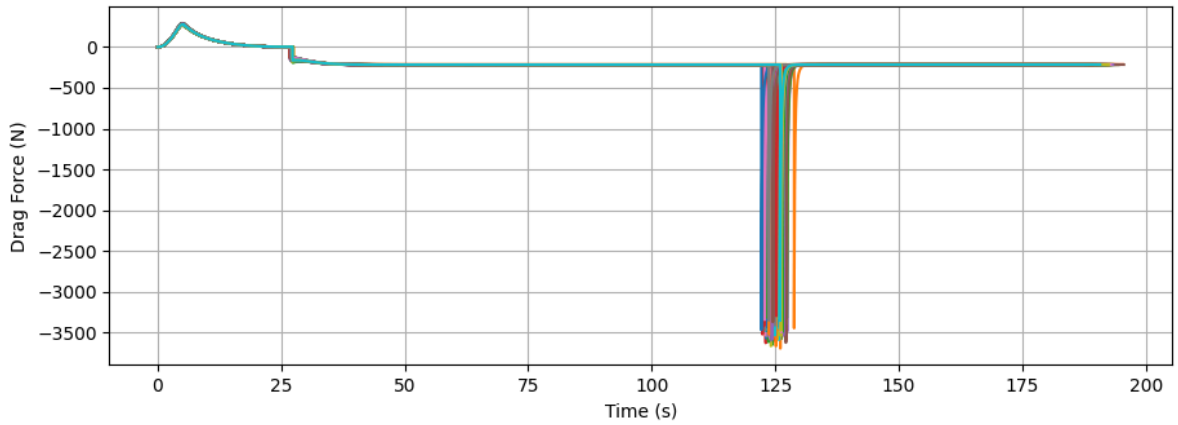

Fig. 11: Aereodynamics Forces.

Three peaks in the drag force experienced by the rocket mirror the acceleration profile, as expected (Figure 11). In particular, the second (approximately 250 N) and the third (approximately 3500 N) correspond to the deployment of the Drogue Chute and the Main Chute, respectively. These values were compared with the cord strength specifications provided by the manufacturer, ensuring that the system operates within a safe margin.

Aerodynamic moments were also analyzed in the three wind conditions, to evaluate their effect on structural integrity.

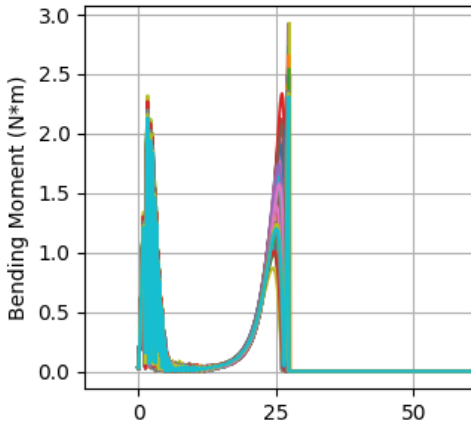

Fig. 12: Bending Moment in scenario (a).

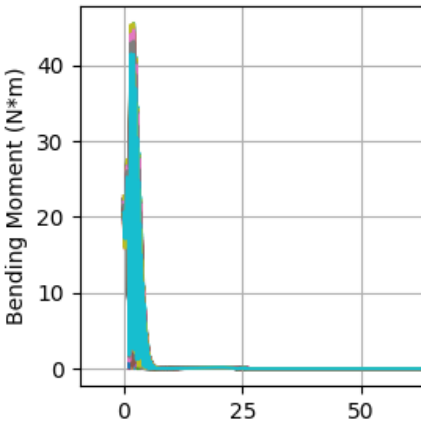

Fig. 13: Bending Moment in scenario (c).

It can be clearly seen (Figure 12 & 13) that in scenario (c) the bending moment is significantly higher than that calculated in scenario (a), due to the particularly disadvantageous direction and intensity of the wind: the rocket's inherent stability naturally tends to bend its trajectory against the direction from which the wind is blowing. If the wind is very strong and blowing in the direction of launch, the rocket fins are subjected to a significant angle of attack and generate lift that induces a bending moment on the structure. This process induces oscillating loads due to

overcompensation while the rocket is trying to stabilize itself. This led us to analyze the bending moment under the condition of maximum lateral lift (see Appendix x.x).

H.7 Velocity

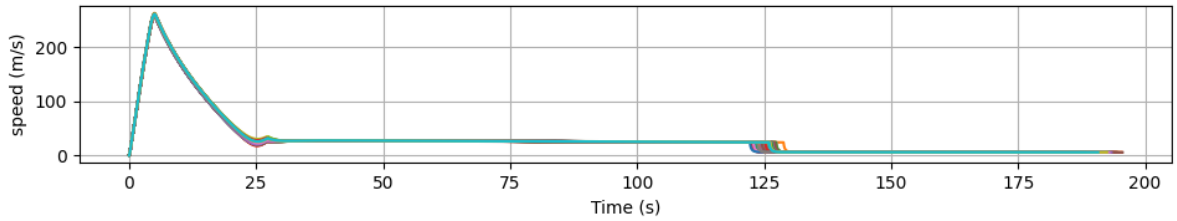

Fig. 14: Velocity profile.

The vertical velocity profile (Figure 15) shows that descent speeds lie within acceptable ranges: the rocket's vertical speed with the drogue parachute deployed averages at 25 m/s, while when the main is deployed it slows down to 6 m/s before hitting the ground.

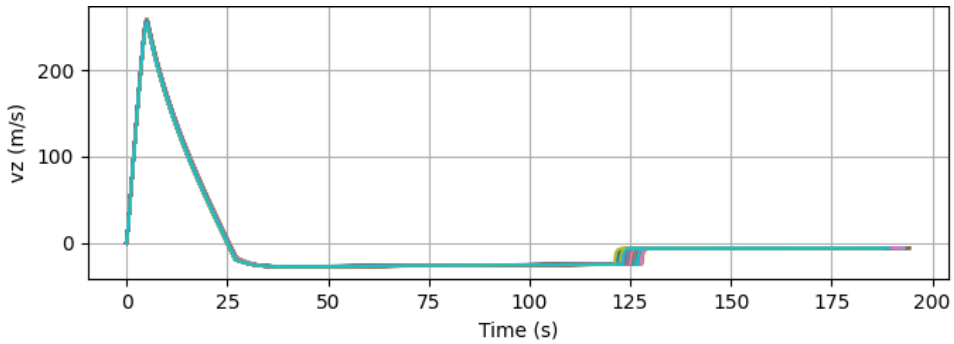

Fig. 15: Vertical Velocity.

The maximum velocity reached lies around 255 m/s (Figure 16), and it is attained during the ascent phase. Knowing this value was important in order to provide the Aerodynamics Team with a reference top speed, useful when interpreting CFD analyses on the matter (see Appendix I).

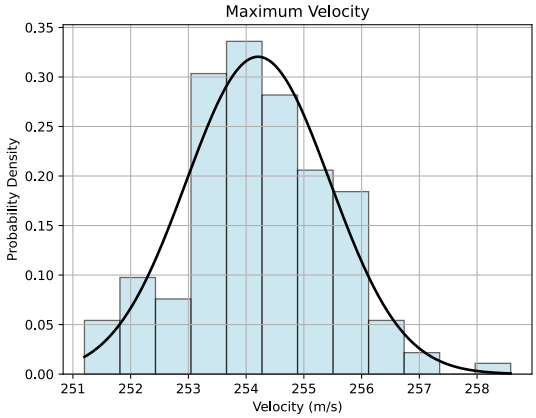

Fig. 16: Maximum Velocity.

H.8 Stability

The static stability margin of the rocket stays above 1.5 calibers for the whole duration of the flight in nominal conditions (Figure 17). In some cases of the Monte Carlo simulation, however, it happens to start from a lower value (around 1.4 calibers), but even in those cases it quickly rises above 1.5 calibers before leaving the launch rail due to fuel consumption.

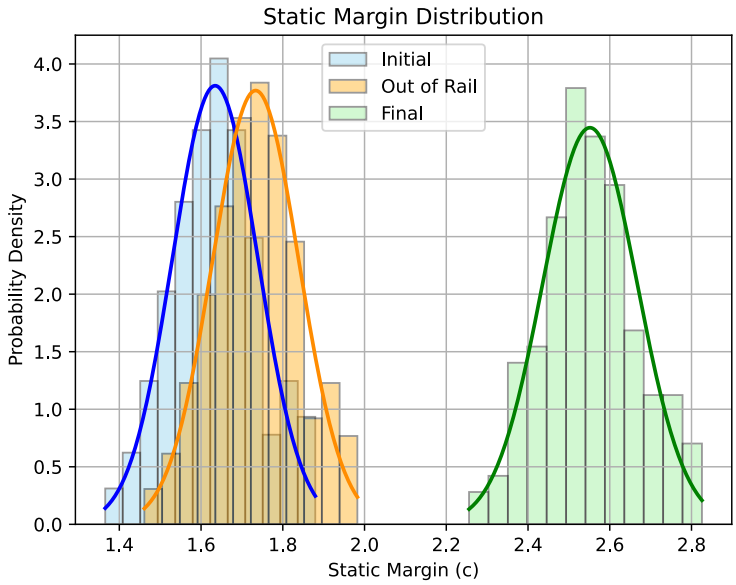

Fig. 17: Static Margin Distribution.

H.9 Apogee Altitude, Position and Landing Site

The average apogee altitude has slightly diminished compared to the results obtained from the flight simulation delivered with the Design Report. The main responsible for this change is the estimated drag coefficient of the rocket, which has increased due to the fact that protuberances like the heads of the M4 and M8 screws were not modeled correctly in the previous version of the flight simulation.

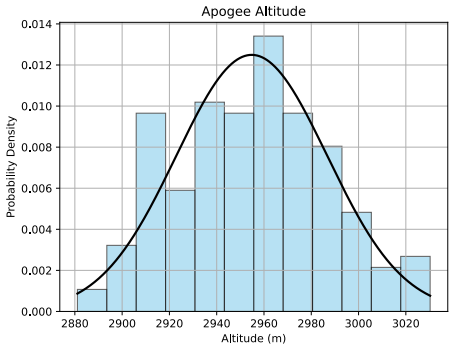

Fig. 18: Apogee altitude distribution over 150 iterations.

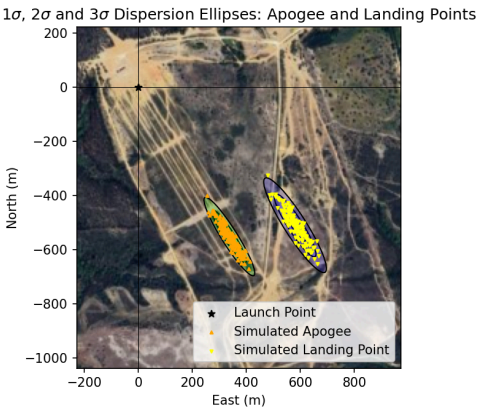

Fig. 19: Apogee and landing points distribution.

Appendix I

Structural analysis

This chapter verifies the structural integrity of Nemesis over the whole mission. The analysis is a verification, not an optimization: the objective is to show that the current configuration withstands the most severe loads the vehicle may face. A worst-case flight scenario combining maximum thrust and maximum aerodynamic loads is considered. This scenario does not occur operationally but provides an upper bound useful to guarantee structural robustness. The verification includes:

- determination of peak aerodynamic and propulsive loads;
- evaluation of internal resultants along the structure;
- local checks of the identified critical zones.

The computation method, numerical models, and simulation parameters are described in the next sections, followed by key results and conclusions.

Determination of Peak Aerodynamic and Propulsive Loads

Determination of Aerodynamic Loads

Aerodynamic loads are obtained with CFD simulations in ANSYS Fluent, using as inputs the velocity V and the static atmospheric parameters. The worst case is identified recalling:

$$L = \frac{1}{2}\rho S C_L V^2, \qquad D = \frac{1}{2}\rho S C_D V^2, \tag{8.1}$$

with maximum conditions linked to the maximum of $\rho C_X V^2$.

- Aerodynamic coefficients: In the linear regime, the coefficients C_X grow linearly with $|\alpha|$. RocketPy analyses give

$$|\alpha|_{\max} = 1.4^\circ \tag{8.2}$$

- Velocity and density: Maximizing ρV^2 over the trajectory data (191 s, 500 points) and using the ISA76 model yields:

$$\rho = 1.127 \frac{\mathrm{kg}}{\mathrm{m}^3}, \qquad V = 258.8 \frac{\mathrm{m}}{\mathrm{s}} \quad \rightarrow \quad \rho V^2 = 75.48 \text{ kPa} \tag{8.3}$$

Critical atmospheric conditions are:

$$P = 91.39 \text{ kPa}, \qquad \rho = 1.127 \frac{\mathrm{kg}}{\mathrm{m}^3}, \qquad T = 282.5\mathrm{K} \tag{8.4}$$

and the corresponding flight conditions are:

$$V = 258.8 \frac{\mathrm{m}}{\mathrm{s}}, \qquad M = 0.1691, \qquad |\alpha_{\max}| = 1.4^\circ \tag{8.5}$$

An additional critical flight condition is obtained by choosing the attitude that maximizes the torsional moment. For $\alpha \neq 0$, a torsional moment is generated; it is zero if the vehicle is

symmetric with respect to the wind plane and reaches a maximum for a 30° roll rotation (one fin normal to the plane), as shown in Figure 1.

Note. This statement is not quoted verbatim; it follows from Barrowman, J. S., "The Practical Calculation of the Aerodynamic Characteristics of Slender Finned Vehicles", NASA Goddard Space Flight Center, 1967.

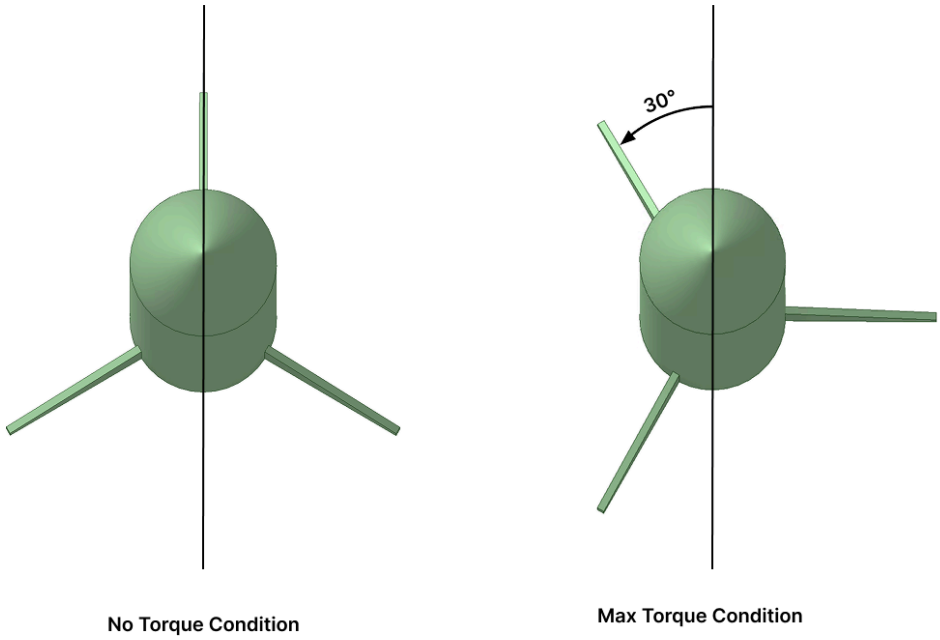

Fig. 1: Torsional moment as a function of roll angle.

This attitude was adopted in CFD, and the corresponding torsional moment is a target of the simulation.

Geometry

The Nemesis CAD model corresponds to that described in the aerodynamics chapter. According to the design assumptions, it matches the real external surfaces, except for local protrusions due to screws and fasteners. In this setup, the body is split into multiple surfaces to obtain, for structural purposes, local integral loads on specific surfaces. See Figure 2.

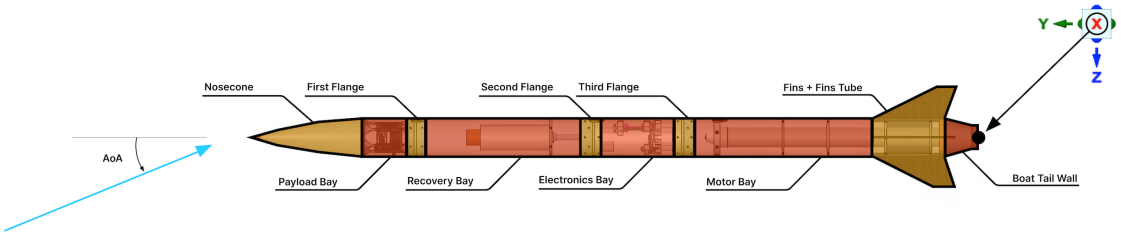

Fig. 2: Elements for aerodinamic loads calculation.

The load reference frame differs from that used during the aerodynamic analysis and is described below:

- origin: in the boat tail's base centroid;
- x axis: perpendicular to the wind plane, out of page;
- y axis: along the rocket longitudinal direction, from fins to boat tail;
- z axis: completes the right-handed set.

Mesh

The mesh is equivalent to that used for the aerodynamic-coefficient simulations, with the following adaptations:

- increased number of boundary-layer elements, consistent with a larger estimated boundary layer thickness, up to $\delta_{\max} = 4.8$ cm (vs. $= 3$ cm at zero α);
- extension to the full vehicle: given the angle of attack and fin configuration, symmetry-plane truncation is insufficient.

A Body of Influence is added around Nemesis to improve the transition from the last prism layer to the outer tetrahedral region. See Figure 3.

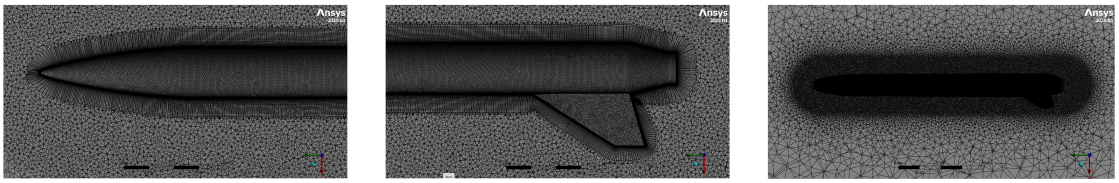

Fig. 3: Mesh for aerodynamic loads calculation.

Mesh quality criteria are maintained (with slightly different numerical values).

Setup

A pressure-based solver is retained. Assuming flow-development times shorter than attitude-variation times, a steady-state solution is used. Viscosity follows Sutherland's law. Turbulence parameters are adjusted to the larger boundary layer: $k = 10.05 \frac{\mathrm{m}^2}{\mathrm{s}^2}$, $\omega = 300.0 \mathrm{s}^{-1}$, with $I = 0.01$ and $\delta_{\max} = 4.8$ cm. Post-processing confirms the estimated maximum boundary-layer thickness and the y^+ range, consistent with the previous setup. Boundary conditions correspond to the altitude of maximum aerodynamic load from ISA76. A total of 1500 iterations is run.

Results and post-processing

For each element, aerodynamic loads are averaged over the last 250 iterations and shown in the Table below. Per-component contributions smaller than 1% are discarded to avoid numerical noise. Moments are reported about the full-mass rocket CG.

Element	F_x [N]	F_y [N]	F_z [N]	M_x [N m]	M_y [N m]	M_z [N m]
Nosecone	0.04123	−21.68	−32.36	−49.70	0	−0.0593
Payload Bay	0	−8.423	−1.179	−1.467	0	0
First Flange	0	−3.902	0	0	0	0
Recovery Bay	0	−28.59	−2.183	−1.570	0	0
Second Flange	0	−3.478	0	0	0	0
Electronics Bay	0.04496	−12.83	0	0	0	−0.006206
Third Flange	0	−3.379	0	0	0	0
Motor Bay	−0.3562	−29.35	−10.61	6.247	0	−0.2256
Fins	−3.265	−120.7	−171.4	154.4	−0.3849	−2.875
Fins Tube	−1.009	−13.46	−43.26	36.61	0	−0.9602
Boat Tail Wall	0.2499	−43.55	6.204	−5.974	0	0.3064
Total	−4.294	−289.4	−251.4	138.5	−0.3849	−3.813

The exhaust jet is not modeled and the nozzle is considered closed. This produces a base drag under the nozzle exit, which is excluded from the aerodynamic loads because it is non-physical. Mesh independence is verified by running a second case, halving the local mesh face sizing in the fins and boat tail region. The total load variations in the highlighted area are described in the Table below.

Load	Original sizing	1/2 Original Sizing	Acceptance	Effective
F_x [N]	−4.024	−4.350	$\lvert\Delta_{\%}\rvert < 10\%$	$\lvert\Delta_{\%}\rvert = 8.1\%$
F_y [N]	−177.7	−171.5	$\lvert\Delta_{\%}\rvert < 10\%$	$\lvert\Delta_{\%}\rvert = 3.6\%$
F_z [N]	−208.5	−212.1	$\lvert\Delta_{\%}\rvert < 10\%$	$\lvert\Delta_{\%}\rvert = 1.7\%$
M_x [N m]	185.0	187.4	$\lvert\Delta_{\%}\rvert < 10\%$	$\lvert\Delta_{\%}\rvert = 1.3\%$
M_y [N m]	−0.3849	−0.3581	$\lvert\Delta_{\%}\rvert < 10\%$	$\lvert\Delta_{\%}\rvert = 7.5\%$
M_z [N m]	−3.529	−3.780	$\lvert\Delta_{\%}\rvert < 10\%$	$\lvert\Delta_{\%}\rvert = 7.1\%$

Determination of Peak Propulsive Loads

Given the motor installed on Nemesis (Cesaroni Pro75 M1545), the maximum thrust from the documentation is 1.84 kN. The thrust acts as an axial load along the body axis.

Evaluation of Internal Stresses Along the Structure

This stage determines the internal resultants along the rocket structure: axial force, shear force, bendong moment and torsional moment. These quantities are obtained via structural analyses in ANSYS Static Structural using a beam model. The rocket is treated as a free body: external loads are balanced by inertia, not by fixed supports. Free–free analysis is enabled through Inertia Relief.

Note: constraining parts of the structure instead of using inertia as the reacting entity leads to errors in the evaluation of internal forces and moments.

Because mass distribution reacts against the loads, the beam model must reproduce mass,sectional properties, and inertias along the full length. The construction is described below.

Beam Model

A distinction is made between:

- **load-carrying masses**: structures that transmit load along the rocket (e.g., flanges, bulkhead, aluminum tubes);
- **non-load-carrying masses**: internal components not intended to carry global loads (electronics, recovery system, payload).

Load-carrying masses

These properties vary along the length, so the beam model is divided into multiple segments, each representing a specific physical span of Nemesis. The segmentation is shown below. Except for the through-rods in the electronics bay, all load-carrying sections are circular (solid or tubular). Given the outer diameter D_e and the inner diameter D_i of each section, the remaining geometric quantities are computed using the following relations:

$$A = \frac{\pi}{4}(D_e^2 - D_i^2), \qquad I_{xx} = I_{zz} = \frac{\pi}{64}(D_e^4 - D_i^4), \qquad J = I_{xx} + I_{zz} \quad (8.6)$$

The following Table shows the geometric parameters assigned to each segment.

Segment	y [mm]	D_e [mm]	D_i [mm]	A [mm^2]	$I_{xx} = I_{zz}$ [mm^4]	J [mm^4]
Nosecone	2313–2480	150	146	929.9	2.547×10^6	5.093×10^6
First Flange 1	2280–2313	150	136	3145	8.058×10^6	1.612×10^7
First Flange 2	2270–2280	150	0	1.767×10^4	2.485×10^7	4.970×10^7
First Flange 3	2233–2270	150	136	3145	8.058×10^6	1.612×10^7
Recovery Bay	1605–2233	150	144	1385	3.744×10^6	7.488×10^6
Sec. Flange 1	1560–1605	150	136	3145	8.058×10^6	1.612×10^7
Sec. Flange 2	1550–1560	150	0	1.767×10^4	2.485×10^7	4.970×10^7
Sec. Flange 3	1525–1550	150	136	3145	8.058×10^6	1.612×10^7
Electronics Bay	1225–1525	109.5	107.6	325.5	4.791×10^5	3.927×10^3
Third Flange 1	1200–1225	150	136	3145	8.058×10^6	1.612×10^7
Third Flange 2	1190–1200	150	0	1.767×10^4	2.485×10^7	4.970×10^7
Third Flange 3	1145–1190	150	136	3145	8.058×10^6	1.612×10^7
Motor Bay 1	1070–1145	150	144	1385	3.744×10^6	7.488×10^6
Bulkhead	1045–1070	150	0	1.767×10^4	2.485×10^7	4.970×10^7
Motor Bay 2	0–1045	150	144	1385	3.744×10^6	7.488×10^6

The rods across the electronics bay are modeled as an equivalent tubular section that preserves total area A and the geometric inertias $I_{xx} = I_{zz}$ (about suitable transverse axes through two rods). Instead, J is calculated as four times the torsional constant of a single rod along its longitudinal axis:

$$A = 4\left(\frac{\pi}{4}d^2\right) = \pi d^2 \qquad J = 4\left(\frac{\pi}{32}d^4\right) = \frac{\pi}{8}d^4 \tag{8.7}$$

No equivalent beam is defined for the boat tail and the nosecone. These are represented as concentrated masses at the end nodes.

Note: each beam segment was assigned its corresponding material: structural steel for the equivalent tube representing the rods in the electronics bay, and aluminum alloy for the rest (for material properties, see subsection Local Checks). However, the flanges were modeled with a fictitious aluminum that preserves stiffness and section properties but has zero mass. Their actual mass was instead applied as a concentrated mass at the centroid (with corresponding inertia moments), in order to also include screws, joints, and mechanical connections.

Non-load-carrying masses

Non-load-carrying masses are applied to the beam as concentrated masses (with principal inertias) or as distributed masses:

- Concentrated masses are indicated in red.
- Distributed masses are indicated by dark yellow lines and are accompanied by fictitious masses, shown as yellow dots of 0 kg. These are introduced to model the distribution of longitudinal moment of inertia, which cannot otherwise be represented by a single distribute mass along the longitudinal axis.

Figure 4 shows a comparison between Nemesis and the equivalent beam model.

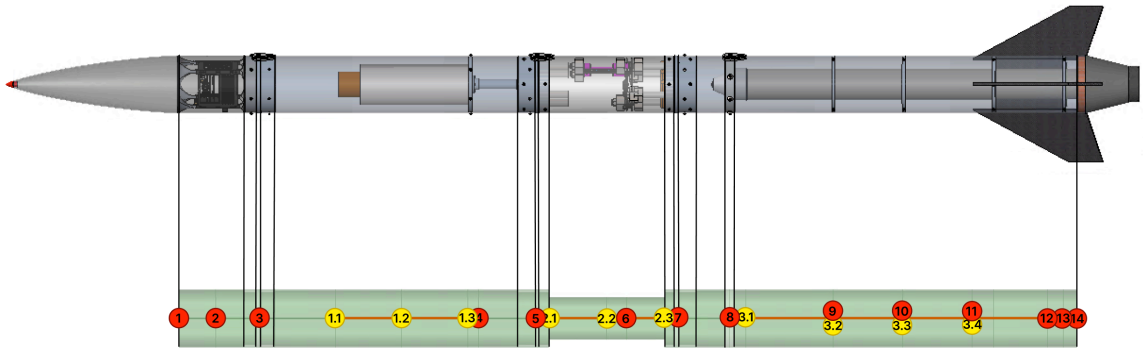

Fig. 4: Beam model representation.

Detailed lists of concentrated and distributed masses are provided in the two Tables below.

Note:

- The final concentrated mass BT+M (14) represents the boat tail and the portion of the motor inside it.
- The transfer of the concentrated masses of the nosecone (1) and BT+M (14) was accompanied by a correction of the inertia moments using the Huygens–Steiner theorem.
- The coordinates of the principal inertia axes are expressed in the reference basis defined in the technical report

Table of concentrated masses

Mass	y_{CG} [mm]	**Mass** [g]	**Axes**	**Inertias** [g mm^2]
1) Nosecone	2480	663.6	$p_1 = (0, 1, 0)$ $p_2 = (-1, 0, 0)$ $p_3 = (0, 0, 1)$	$I_{p_1} = 2.305 \times 10^{6}$ $I_{p_2} = 2.851 \times 10^{7}$ $I_{p_3} = 2.851 \times 10^{7}$
2) Aether (Payload)	2385	516.2	$p_1 = (0, 1, 0)$ $p_2 = (-0.74, 0, -0.67)$ $p_3 = (-0.67, 0, 0.74)$	$I_{p_1} = 1.264 \times 10^{6}$ $I_{p_2} = 2.012 \times 10^{6}$ $I_{p_3} = 2.075 \times 10^{6}$
3) First Flange	2273	852.9	$p_1 = (0.50, 0, 0.87)$ $p_2 = (0.87, 0, -0.50)$ $p_3 = (0, 1, 0)$	$I_{p_1} = 1.656 \times 10^{6}$ $I_{p_2} = 1.700 \times 10^{6}$ $I_{p_3} = 2.953 \times 10^{6}$
4) Peregrine System Assembly	1223	664.3	$p_1 = (-0.50, 0, 0.87)$ $p_2 = (0, -1, 0)$ $p_3 = (0.87, 0, 0.50)$	$I_{p_1} = 1.357 \times 10^{6}$ $I_{p_2} = 1.614 \times 10^{6}$ $I_{p_3} = 1.816 \times 10^{6}$
5) Second Flange	1560	832.5	$p_1 = (0.50, 0, 0.87)$ $p_2 = (0.87, 0, -0.50)$ $p_3 = (0, 1, 0)$	$I_{p_1} = 1.736 \times 10^{6}$ $I_{p_2} = 1.780 \times 10^{6}$ $I_{p_3} = 3.049 \times 10^{6}$
6) Electronics	1323	686.9	$p_1 = (0.03, 1, 0.01)$ $p_2 = (-1, 0, 0)$ $p_3 = (0, 0, 1)$	$I_{p_1} = 1.692 \times 10^{6}$ $I_{p_2} = 1.017 \times 10^{7}$ $I_{p_3} = 1.022 \times 10^{7}$
7) Third Flange	1190	820.8	$p_1 = (0.71, 0, 0.71)$ $p_2 = (0.71, 0, -0.71)$ $p_3 = (0, 1, 0)$	$I_{p_1} = 1.735 \times 10^{6}$ $I_{p_2} = 1.735 \times 10^{6}$ $I_{p_3} = 3.010 \times 10^{6}$
8) Bulk Head	1057	1110	$p_1 = (0.50, 0, 0.87)$ $p_2 = (0.87, 0, -0.50)$ $p_3 = (0, 1, 0)$	$I_{p_1} = 2.162 \times 10^{7}$ $I_{p_2} = 1.675 \times 10^{6}$ $I_{p_3} = 2.940 \times 10^{6}$
9) Centering 1	790	163.1	$p_1 = (0, 0, 1)$ $p_2 = (1, 0, 0)$ $p_3 = (0, 1, 0)$	$I_{p_1} = 3.017 \times 10^{5}$ $I_{p_2} = 3.017 \times 10^{5}$ $I_{p_3} = 6.017 \times 10^{5}$
10) Centering 2	610	163.1	$p_1 = (0, 0, 1)$ $p_2 = (1, 0, 0)$ $p_3 = (0, 1, 0)$	$I_{p_1} = 3.017 \times 10^{5}$ $I_{p_2} = 3.017 \times 10^{5}$ $I_{p_3} = 6.017 \times 10^{5}$
11) Centering 3	375	155.8	$p_1 = (0, 0, 1)$ $p_2 = (1, 0, 0)$ $p_3 = (0, 1, 0)$	$I_{p_1} = 2.869 \times 10^{5}$ $I_{p_2} = 2.869 \times 10^{5}$ $I_{p_3} = 5.721 \times 10^{5}$
12) Fins	236	418	$p_1 = (0, 0, 1)$ $p_2 = (1, 0, 0)$ $p_3 = (0, 1, 0)$	$I_{p_1} = 5.969 \times 10^{6}$ $I_{p_2} = 5.969 \times 10^{6}$ $I_{p_3} = 7.344 \times 10^{6}$
13) Centering 4	195.8	155.8	$p_1 = (0, 0, 1)$ $p_2 = (1, 0, 0)$ $p_3 = (0, 1, 0)$	$I_{p_1} = 2.869 \times 10^{5}$ $I_{p_2} = 2.869 \times 10^{5}$ $I_{p_3} = 5.721 \times 10^{5}$
14) BT + M	160	1478	$p_1 = (0, 1, 0)$ $p_2 = (0, 0, 1)$ $p_3 = (1, 0, 0)$	$I_{p_1} = 2.310 \times 10^{6}$ $I_{p_2} = 3.927 \times 10^{6}$ $I_{p_3} = 3.927 \times 10^{6}$

Table of distributed masses

Mass	y_{GC} [mm]	**Mass** [g]	**Axes**	**Inertias** [g mm^2]
1) Recovery	1734–2076	0.89	$p_1 = (0, 1, 0)$ $p_2 = (0, 0, 1)$ $p_3 = (1, 0, 0)$	$I_{p_1} = 0$ $I_{p_2} = 7.748 \times 10^{6}$ $I_{p_3} = 7.748 \times 10^{6}$
1.1)	2076	0	$p_1 = (0, 1, 0)$ $p_2 = (0, 0, 1)$ $p_3 = (1, 0, 0)$	$I_{p_1} = 3.828 \times 10^{5}$ $I_{p_2} = 0$ $I_{p_3} = 0$
1.2)	1905	0	$p_1 = (0, 1, 0)$ $p_2 = (0, 0, 1)$ $p_3 = (1, 0, 0)$	$I_{p_1} = 3.828 \times 10^{5}$ $I_{p_2} = 0$ $I_{p_3} = 0$
1.3)	1734	0	$p_1 = (0, 1, 0)$ $p_2 = (0, 0, 1)$ $p_3 = (1, 0, 0)$	$I_{p_1} = 3.828 \times 10^{5}$ $I_{p_2} = 0$ $I_{p_3} = 0$
2) Plexiglass Tube	1200–1550	0.5813	$p_1 = (0, 1, 0)$ $p_2 = (-0.71, 0, 0.71)$ $p_3 = (0.71, 0, 0.71)$	$I_{p_1} = 0$ $I_{p_2} = 7.495 \times 10^{6}$ $I_{p_3} = 7.495 \times 10^{6}$
2.1)	1550	0	$p_1 = (0, 1, 0)$ $p_2 = (-0.71, 0, 0.71)$ $p_3 = (0.71, 0, 0.71)$	$I_{p_1} = 1.047 \times 10^{6}$ $I_{p_2} = 0$ $I_{p_3} = 0$
2.2)	1375	0	$p_1 = (0, 1, 0)$ $p_2 = (-0.71, 0, 0.71)$ $p_3 = (0.71, 0, 0.71)$	$I_{p_1} = 1.047 \times 10^{6}$ $I_{p_2} = 0$ $I_{p_3} = 0$
2.3)	1200	0	$p_1 = (0, 1, 0)$ $p_2 = (-0.71, 0, 0.71)$ $p_3 = (0.71, 0, 0.71)$	$I_{p_1} = 1.047 \times 10^{6}$ $I_{p_2} = 0$ $I_{p_3} = 0$
Motor bay	195–1015	7208	$p_1 = (0, 1, 0)$ $p_2 = (0, 0, 1)$ $p_3 = (1, 0, 0)$	$I_{p_1} = 0$ $I_{p_2} = 4.805 \times 10^{8}$ $I_{p_3} = 4.805 \times 10^{8}$
3.1)	1015	0	$p_1 = (0, 1, 0)$ $p_2 = (0, 0, 1)$ $p_3 = (1, 0, 0)$	$I_{p_1} = 1.268 \times 10^{6}$ $I_{p_2} = 0$ $I_{p_3} = 0$
3.2)	790	0	$p_1 = (0, 1, 0)$ $p_2 = (0, 0, 1)$ $p_3 = (1, 0, 0)$	$I_{p_1} = 1.268 \times 10^{6}$ $I_{p_2} = 0$ $I_{p_3} = 0$
3.3)	610	0	$p_1 = (0, 1, 0)$ $p_2 = (0, 0, 1)$ $p_3 = (1, 0, 0)$	$I_{p_1} = 1.268 \times 10^{6}$ $I_{p_2} = 0$ $I_{p_3} = 0$
3.4)	375	0	$p_1 = (0, 1, 0)$ $p_2 = (0, 0, 1)$ $p_3 = (1, 0, 0)$	$I_{p_1} = 1.268 \times 10^{6}$ $I_{p_2} = 0$ $I_{p_3} = 0$
3.5)	195	0	$p_1 = (0, 1, 0)$ $p_2 = (0, 0, 1)$ $p_3 = (1, 0, 0)$	$I_{p_1} = 1.268 \times 10^{6}$ $I_{p_2} = 0$ $I_{p_3} = 0$

Applied Loads

For each aerodynamic element, the forces F_x, F_y, and F_z are applied as uniformly distributed loads over the corresponding beam span. For the nosecone and boat tail, the resultant forces are applied at the beam ends. This approach allows each beam element to be loaded with the exact resultant forces obtained from the CFD analysis. However, it does not guarantee that the induced moments are matched exactly. The reason is that applying a uniformly distributed force along an element automatically sets the element midpoint as the center of pressure, whereas in reality the actual center of pressure may not coincide with the midpoint. Moreover, shifting the application points of the aerodynamic loads of the nosecone and the boat tail to the beam extremities must be complemented by transport moments

$$\Delta M = M^{(\mathrm{CFD})} - M^{(\mathrm{beam})}, \tag{8.8}$$

with

$$M^{(\mathrm{beam})} = bF, \tag{8.9}$$

where

$$b = \pm\left(\frac{y_i + y_{i+1}}{2}\right) - y_{\mathrm{CG}}, \qquad \mathrm{CG} = 1160\ \mathrm{mm}, \tag{8.10}$$

and y_i, $y_i + 1$ are the endpoints of the $i - \mathrm{th}$ beam (coincident in the case of the nosecone and the boat tail extremities).

Corrective moments ΔM_x

The aerodynamic forces that can induce a moment about the x axis are, in general, F_y and F_z. However, all axial forces along y act directly on the beam, which lies on the y axis intersecting the x axis at the origin of the reference system. As a result, F_y does not produce any M_x, and the only contributing force is F_z. The Table below shows the corrective moments for M_x.

Element	$M_x^{(\mathrm{CFD})}$ [N m]	F_z [N]	b [mm]	$M_x^{(\mathrm{beam})}$ [N m]	ΔM [N m]
Nosecone	−49.70	−32.36	1320	−42.72	−6.985
Payload Bay	−1.467	−1.179	1237	−1.458	−0.00917
First Flange	0	0	1113	0	0
Recovery Bay	−1.570	−2.183	759.0	−1.657	0.08690
Second Flange	0	0	405.0	0	0
Electronics Bay	0	0	215.0	0	0
Third Flange	0	0	25.00	0	0
Motor Bay	6.247	−10.61	−372.5	3.952	2.295
Fins	154.4	−171.4	−875.0	150.0	4.425
Fins Tube	36.61	−43.26	−875.0	37.85	−1.243
Boat Tail Wall	−5.974	6.204	−1000	−6.204	0.230

Corrective moments ΔM_y

The forces that can induce a moment about the y axis are, in general, F_x and F_z. In this case, however, the application points of these aerodynamic forces lie on the beam itself, which coincides with the y axis. Therefore, the lever arm with respect to y is zero, and no moment is generated. It follows that the moment about y must be fully accounted for within the beam model. This contribution is summarized in the reduced Table below, since only the fins contribute significantly to M_y.

Element	$M_y^{(\mathrm{CFD})}$ [N m]	F_x/F_z [N]	b [mm]	$M_y^{(\mathrm{beam})}$ [N m]	ΔM [N m]
Fins	−0.3849	0	0	0	−0.3849

Corrective moments ΔM_z

The forces that can induce a moment about the z axis are, in general, F_x and F_y. Since their application points lie on the beam (aligned with the y axis, which intersects z at the origin), the forces F_y do not generate any M_z. The Table below shows the corrective moments for M_z.

Element	$M_z^{(\mathrm{CFD})}$ [N m]	F_x [N]	b [mm]	$M_z^{(\mathrm{beam})}$ [N m]	ΔM [N m]
Nosecone	−0.05930	0.04123	−1320	−0.05442	−0.004876
Payload Bay	0	0	−1237	0	0
First Flange	0	0	−1113	0	0
Recovery Bay	0	0	−759.0	0	0
Second Flange	0	0	−405.0	0	0
Electronics Bay	−0.006206	0.04496	−215.0	−0.009666	0.003460
Third Flange	0	0	−25.00	0	0
Motor Bay	−0.2256	−0.3562	372.5	−0.1327	−0.09292
Fins	−2.875	−3.265	875.0	−2.857	−0.01813
Fins Tube	−0.9602	−1.009	875.0	−0.8829	−0.07733
Boat Tail Wall	0.3064	0.2499	1000	0.2499	0.0565

Element Loads Applied to the Beam

The Table below lists the aerodynamic loads and corrective (transport) moments to be applied to each beam element. Forces are treated as uniformly distributed over the span of each element; moments are applied as uniformly distributed moments as well.

Segment	F_x [N]	F_y [N]	F_z [N]	ΔM_x [N m]	ΔM_y [N m]	ΔM_z [N m]
Nosecone	0.04123	−21.68	−32.36	−6.985	0	−0.004876
Payload Bay	0	−8.423	−1.179	−0.009167	0	0
First Flange	0	−3.902	0	0	0	0
Recovery Bay	0	−28.59	−2.183	0.08690	0	0
Second Flange	0	−3.478	0	0	0	0
Electronics Bay	0.04496	−12.83	0	0	0	0.003460

Segment	F_x [N]	F_y [N]	F_z [N]	ΔM_x [N m]	ΔM_y [N m]	ΔM_z [N m]
Third Flange	0	−3.379	0	0	0	0
Motor Bay	−0.3562	−29.35	−10.61	2.295	0	−0.09292
Fins	−3.265	−120.7	−171.4	4.425	−0.3849	−0.01813
Fins Tube	−1.009	−13.46	−43.26	−1.243	0	−0.07733
Boat Tail Wall	0.2499	−43.55	6.204	0.2300	0	0.05650

Results

The resulting internal resultants are illustrated in the Figure 5.

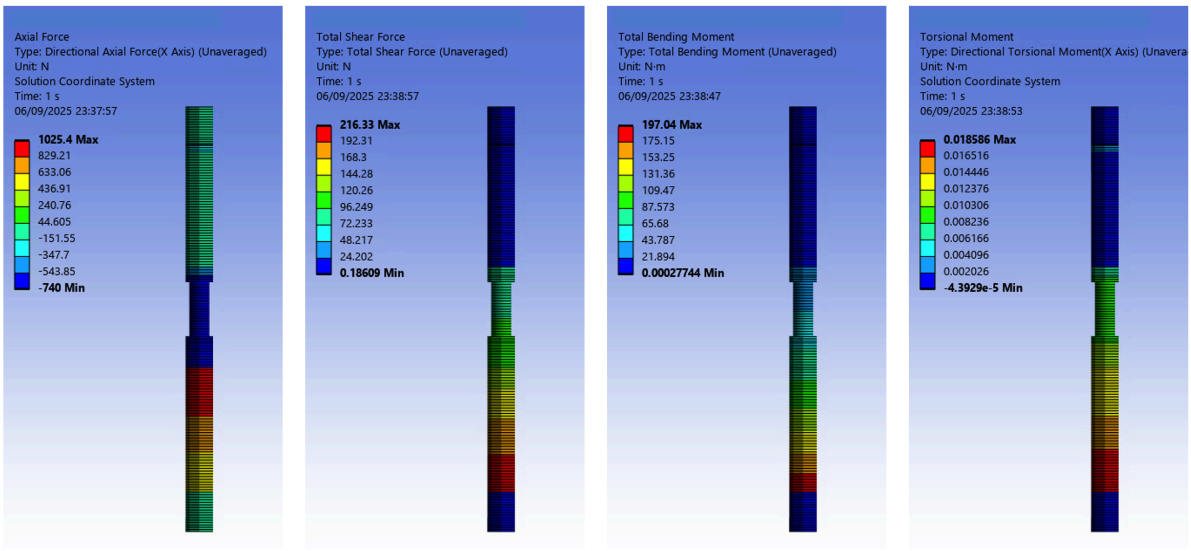

Fig. 5: internal resultants diagrams.

During the local analysis, each component is treated as an isolated free body. The internal resultants previously obtained correspond to the expected forces applied on it by the surrounding structure and are applied at the upper and lower interfaces that connect the element to the rest of the structure. The magnitude of each applied action equals the local value from the beam model and therefore depends on position. Consequently, the components are not in equilibrium in general, since the actions applied at the top may not equal those at the bottom in magnitude. This is consistent with the vehicle accelerating in the considered configuration. Equilibrium is closed by inertia (inertia relief); the solver balances the equations by introducing accelerations, which are outputs of the solution.

Axial Force

A discontinuity in axial force is observed at the bulkhead (motor attachment). Below the motor application point, the maximum tension is 1025N; immediately above, the maximum compression is -740N, propagating into the third flange and the electronics bay.

For each component, the axial resultant is represented by two axial forces applied at the interfaces that connect the element to the rest of the structure. N_a denotes the axial force acting

from above and N_b denotes the axial force actin from below. Sign convention: $N > 0$ tension, $N < 0$ compression.

Shear Force

Shear peak near the fins region, consistent with the lateral lift maximum. For each component, shear is represented by two transverse forces, T_a and T_b, acting in the beam's representation plane (as in the previous figures) and applied at the upper and lower interfaces with the surrounding structure. A shear force is positive if, taken alone, it induces a clockwise moment about the component centroid in the figure; negative otherwise. In the following, shear magnitudes are reported as positive.

Bending Moment

Bending peak near the fins region. For each component, the bending moment is applied by means of equivalent axial forces that vary linearly with the distance d from the neutral axis on the cross-section. The axial force follows the previously defined sign convention for axial forces (tension $N > 0$, compression $N < 0$).

Torsional Moment

Even under a worst-case torsional loading scenario, torsion remains minor compared to other actions, with the highest values again near the fins. Except for the body tube, torsion is neglected in local verifications.

Local checks of the identified critical zones

Critical items for local checks are

- bulkhead and its fasteners;
- third flange and its fasteners;
- body tube (motor tube);
- electronics bay rods.

The target safety factor is

$$\mathrm{SF} > 1.5, \tag{8.11}$$

which is consistent with aeronautical/aerospace practice. Materials used in the components below are listed with their properties in the following Table.

Property	Aluminum 6061	Structural Steel	PVC	ABS
Density [$\frac{\mathrm{kg}}{\mathrm{m}^{-3}}$]	2700	7850	1300	1020
Poisson's ratio [$-$]	0.330	0.3000	0.3400	0.394
Young's modulus [Pa]	6.900×10^{10}	2.000×10^{11}	3.000×10^{9}	2.000×10^{9}
Shear modulus [Pa]	2.594×10^{10}	7.692×10^{10}	7.463×10^{8}	7.170×10^{8}
Yield strength (tens./comp.) [Pa]	5.515×10^{7}	2.5×10^{8}	3.100×10^{7}	3.000×10^{7}
Ultimate strength (tens./comp.) [Pa]	1.241×10^{8}	4.6×10^{8}	5.200×10^{7}	4.000×10^{7}

,

Bulkhead

The aluminum bulkhead is part of the thrust structure and acts as the motor retention system, transferring the motor load to the fuselage. Axial action largely dominates over shear and bending, so only the axial force is considered in the check. From the beam diagrams, the axial force is:

$$N_a = -740.0\text{N}, \qquad N_b = -1025\text{N}, \tag{8.12}$$

N_a acts at the joint holes to the motor tube; N_b acts at the motor -bulkhead contact.

The bulkhead satisfies $\text{SF} > 1.5$ with margin, as shown in Figure 6. The negligible shear/ bending through the bulkhead would not change the conclusion.

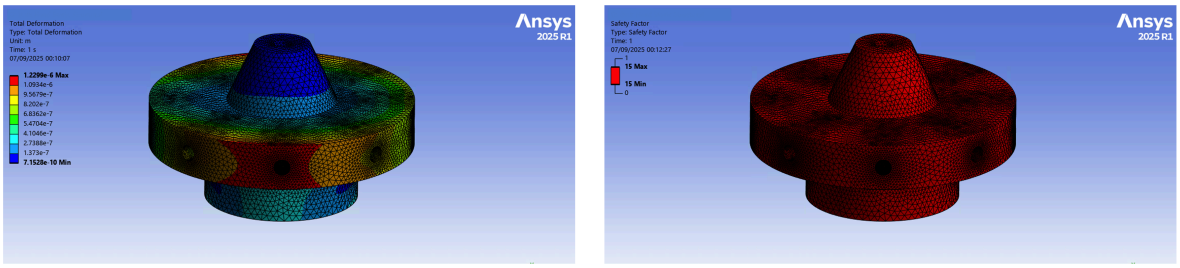

Fig. 6: Deformation and safety factor - Bulkhead.

M8 Screws

The bulkhead is connected to a 3 mm thick aluminum tube by seven M8 steel screws plus one M5 screw (the latter dedicated to the rail button). Screw capacity must cover the axial load transmitted by the beam. Forces on the screws are derived from the rocket axial force absorbed at the interface. The upper axial load acts on the shank over 3 mm (tube thickness) starting from the head side; the lower load acts over the remaining shank length inside the bulkhead. With 8 screws sharing the load:

$$N_a = -\frac{740.0}{8}\text{N} = 92.50\text{N}, \qquad N_b = -\frac{1025}{8}\text{N} = -128.1\text{N}. \tag{8.13}$$

As shown in Figure 7, the M8 screws meet the $\text{SF} > 1.5$ requirement.

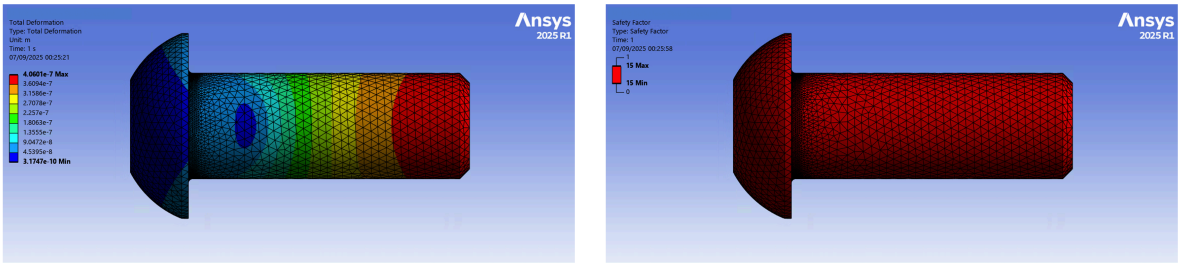

Fig. 7: Deformation and safety sactor - M8 screws.

Third Flange

The aluminum flanges are the elements that interconnect the three main segments of the rocket. The only simulation carried out on the interconnection flanges concerns the third flange, as it is the most heavily loaded. Verifying its structural integrity also demonstrates the integrity of the upper flanges.

Axial force

$$N_a \approx N_b = -740.0\text{N}. \tag{8.14}$$

Physically, $|N_a| < |N_b|$ is expected since the flange accelerates upward. Upper load is applied to the holes that host the connection with the rods of the electronics bay; lower load at the lower holes.

Shear Force

$$T_a \approx T_b = 120.3\text{N}, \tag{8.15}$$

applied to rods connections and lower holes, respectively.

Bending moment

$$M_a \approx M_b = 87.57\ \text{Nm}. \tag{8.16}$$

Bending is applied by equivalent axial forces given by

$$N_i = \frac{M d_i}{\sum_j d_j^2} \tag{8.17}$$

with d_i the distance of hole i from the neutral axis (mid-depth due to symmetry). The hole distances are modeled as follows, yielding the corresponding N_i in the rods connections (RC), and lower bolt circle (LBC).

RC equivalent axial forces and scheme

$\boldsymbol{d}$ [mm]	$\boldsymbol{N_i}$ [N]
± 54	± 0.8056
0	0

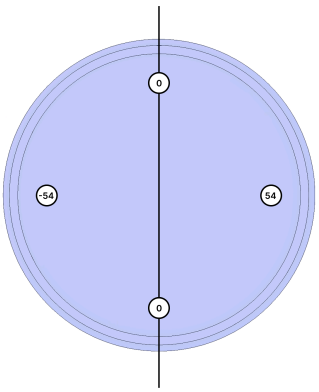

Fig. 8: RC: Scheme.

LBC equivalent axial forces and scheme

d [mm]	N_i [N]
± 70	± 0.2057
± 62	± 0.1822
± 34	± 0.1000

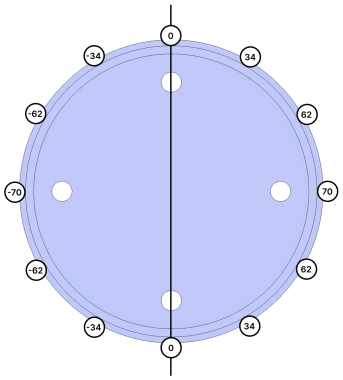

Fig. 9: LBC: Scheme.

Result

The flange sustains the loads. See Figure 10.

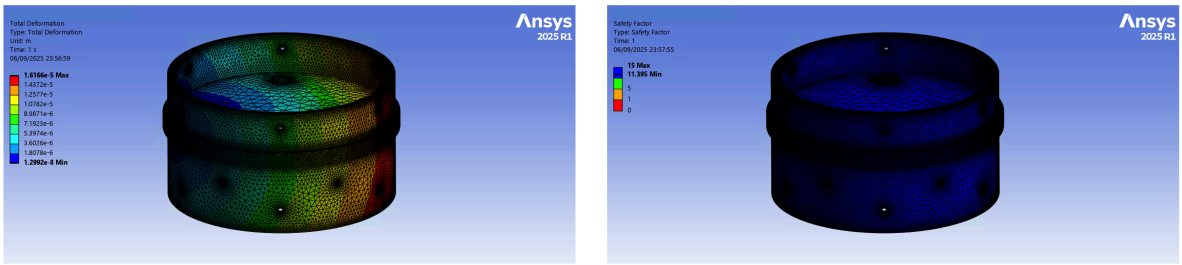

Fig. 10: Deformation and safety factor - Third Flange.

M4 Screws

The body tube is connected to the flange by 12 M4 screws. Given the strong compression in this region, the screws are verified by applying to one of them one twelfth of the local axial load from Nemesis. As in the case of the M8 screws, two offset axial forces are applied, consistent with the attachment configuration.

$$N_a \approx N_b = -\frac{740.0}{12}\text{N} = -61.67\text{N} \tag{8.18}$$

Result

The M4 screw also satisfies the required safety factor with ample margin. See Figure 11.

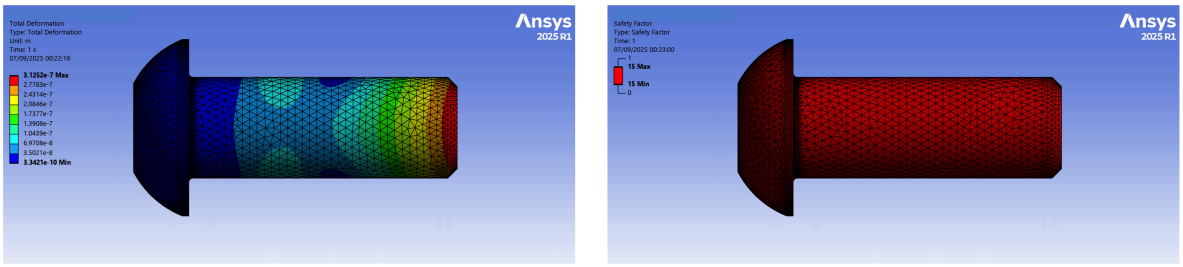

Fig. 11: Deformation and safety factor - M4 Screws.

Body Tube

From the beam model, the aluminum motor tube experiences maximum tension just below the bulkhead connection and, immediately above it, maximum compression. This reversal can be critical and is therefore checked.

Axial Force

Axial forces are applied at the tube–bulkhead and tube–flange connection holes.

$$N_a = -740\text{N}, \qquad N_b = -1025\text{N}. \tag{8.19}$$

Negative sign denotes compression in the tube segment between the bulkhead and the flange.

Shear Force

A single shear load of 120N is applied at the flange holes. No shear is applied at the lower, free end of the tube.

Bending Moment

Bending is applied at the tube–flange bolt pattern via equivalent axial forces, using the same distribution previously computed for the flange lower bolt circle, with opposite signs at the tube holes.

Torsional Moment and Fins Lateral Lift

A torsional action is included, although much smaller than other loads. It is modeled as a pure moment of $0.01850\ \text{Nm}$ distributed over the holes that host the fins. At the lower end (where no internal load transfer occurs) the external lateral lift of the fins is applied at the fin roots. This load alone induces the high local shear and bending observed in the area.

Result

The motor tube meets the requirement; no failure risk is indicated. See Figure 12.

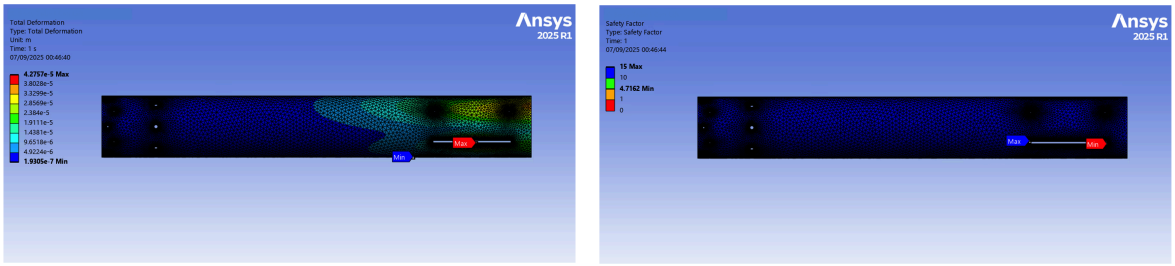

Fig. 12: Deformation and safety factor - Body tube.

Electronics Bay Rods

The four steel rods that transfer the load from the third flange to the second require verification. The rods are connected to the flanges through prevailing torque nuts, which guarantee structural integrity. The simulation includes both the rods and the flanges to which they are connected. Lock nuts are deliberately omitted, and the rods are rigidly tied to the flanges to demonstrate that, even under this conservative loading condition, they still satisfy the required safety factor. Recalling the low torsional stiffness of the rods, the torsional moment is not neglected.

Axial Force

At the twelve holes of the lower flange and the twelve holes of the upper flange, the following forces are applied (on the sides where the flanges connect with the rest of the structure).

$$N_a \approx N_b = -640\text{N}. \tag{8.20}$$

Shear

At the same holes, the following forces are applied:

$$T_a = 120\text{N}, \qquad T_b = 96\text{N}. \tag{8.21}$$

Bending Moment

In this case, the bending moment is not modeled as equivalent axial forces (as done for the flanges), but rather as pure moments applied at the flange holes:

$$M_a = 65.58\ \text{Nm}, \qquad M_b = 43.79\ \text{Nm}. \tag{8.22}$$

This simplification is justified by the fact that the flanges here only serve to transfer the action to the rods, and their detailed response is not of interest, having already been studied.

Torsional Moment

The torsional moment is applied as a pure moment at the same holes, with magnitude:

$$M_{ta} \approx M_{tb} = 0.1031\ \text{Nm}. \tag{8.23}$$

Result

It can be observed in Figure 13 that, even without the mechanical connections, the rods meet the required safety factor. The minimum values occur at the flanges, in the connections with the rods; in reality, these effects are further mitigated by the presence of the lock nuts.

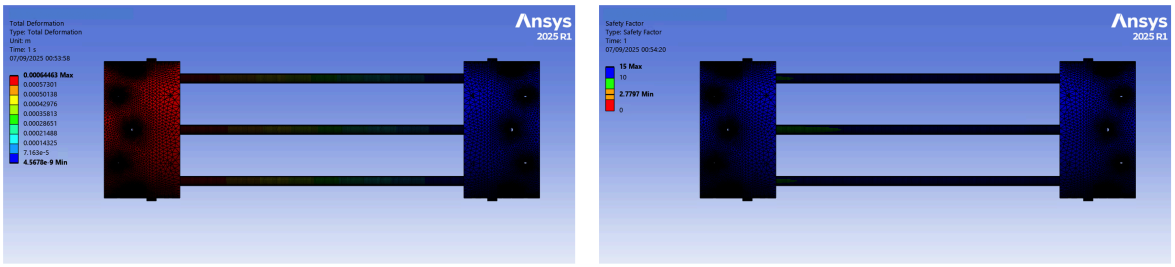

Fig. 13: Deformation and safety factor - Electronics bay rods.

Additional Analysis

Rail Buttons

On the launch rail, the rocket is supported by three PVC rail buttons connected to the fuselage through screw. A rigid constraint is set at the rail-contact point of one button (load path to ground). A load equal to one third of the rocket weight, 88.3N (26.9 kg total mass; 9 kg considered), is applied at the M5 screw hole that connects the rail button to the structure.

Result

The required safety factor is satisfied (slender margin but compliant). See Figure 14.

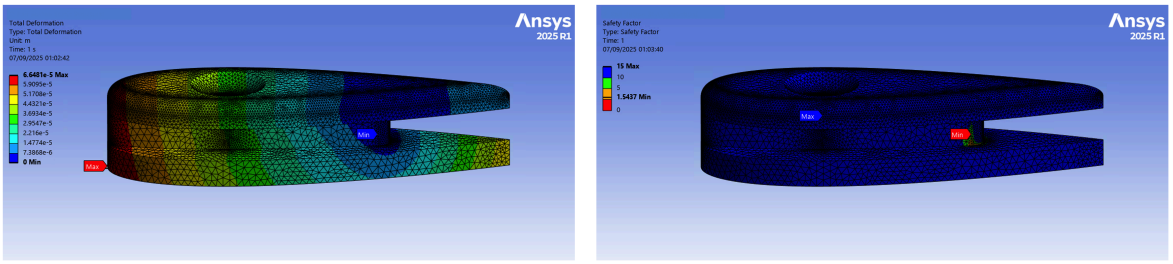

Fig. 14: Deformation and safety factor - Rail buttons.

Aether

Aether is supported by a ABS frame. Although not carrying the global structural loads from motor and aerodynamics, the frame must sustain inertial loads at high acceleration. The internal mass of 900g is lumped at the four inner corner nodes of the PVC cage (where it reacts on the structure). Additionally, the upper external attachments include the mass of the upper support, 80g, applied at the corresponding joints. With inertia relief active, the maximum estimated rocket acceleration of $65 \mathrm{m/s^2}$ is applied.

Result

The structure withstands the inertial load. See Figure 15.

Fig. 15: Deformation and safety factor - Aether.

Overview of Structural Tests

The structural tests carried out on Nemesis aimed to validate the design assumptions adopted during the analytical and numerical verification phases. In particular, the goal was to confirm that the thrust structure, the motor retention system, and the main load-bearing components withstand the most critical combinations of aerodynamic and propulsive loads expected during the mission.

The tests focused on:

- verifying the axial load transfer through the bulkhead and flanges;
- checking the integrity of the motor tube under combined compression and bending;
- assessing the contribution of the electronics bay rods in carrying shear and torsion;
- ensuring that fasteners (M8 and M4 screws) meet the required safety margins under local loads.

Results confirmed that all tested components satisfied the minimum safety factor of SF > 1.5, consistent with aerospace structural standards. Local minima were observed at the connections between rods and flanges in the electronics bay, but these effects are mitigated in the actual configuration by the presence of lock nuts. Similarly, torsional effects on the motor tube and fins region proved negligible compared to axial and bending stresses. Overall, the tests validate the robustness of the thrust structure and the load distribution strategy adopted in the beam model. The agreement between simulation predictions and test out-comes supports the reliability of the design assumptions and confirms that Nemesis is structurally adequate for its mission profile.

Appendix J

MatFins.m

The planform geometry was optimized with our in-house `MatFins` code through successive iterations to maximize apogee while meeting the prescribed static-margin and flutter-velocity constraints.

The main objective of the tool is to determine, through an iterative process, the geometric configurations (in planform) and the thicknesses of the fins that maximize the launch apogee, while meeting mission constraints. The code assesses aerodynamic stability (center of pressure and static margin) and aeroelastic safety (flutter speed of the fins), selecting only geometries that simultaneously meet the set requirements.

In each iteration, the program generates and evaluates a candidate geometry. If the geometry meets the static margin constraint and has a flutter speed higher than the maximum expected flight speed, it is considered admissible. Among admissible geometries, the code uses a weighting system based on the geometric parameters of the fins to estimate the impact of each geometry on the apogee. If the current geometry results in a higher apogee compared to the previous solution (according to the implemented evaluation criteria), it is recorded and printed as an improved solution.

Code

```
%% DATA - Imported from "data_###" functions
% NOSE
[nosecone, K1, Ln, Lntang] = data_nose();
% FINS
[ct0, cr0, taper, s0, sweep0, N, t, GE, ~, ~, dist_base, ~, ~, ~, l_panel] = data_fins();
% BOAT TAIL
[d1, d2, Lbt] = data_tail();
% TUBE
[~, ~, d, tube1, tube2, tube3] = data_tube();
% Total rocket length
L = Ln + Lntang + tube1 + tube2 + tube3 + Lbt;
% MISSION PARAMETERS
[tet0, p0, h_burnout, V_burnout, Mach, SM_min, SM_max] = data_mission();

i = 0;   % Counter for recorded improvements
j = 0;   % Counter for total iterations

%% ITERATIONS FOR OPTIMIZATION
for sweep1 = sweep0        % Try different sweep angles
    for s = s0             % Try different spans
        for cr = cr0       % Try different root chords
            for ct = ct0   % Try different tip chords (if taper is disabled)

                j = j + 1; % Count total iterations

                % Update tip chord if taper is applied
                if taper ~= 0
                    ct = taper * cr;
                end

                % Convert sweep angle to radians and compute sweep distance
                sweep = deg2rad(sweep1);
                x_r = s * tan(sweep);

                % Check longitudinal panel size limit
                if (ct + x_r) > l_panel
                    continue
                end

                %% CHECK STATIC MARGIN AND FLUTTER VELOCITY

                % Compute rocket center of gravity and total mass
```

```
                [CG, MTOT_carico] = Cg(L, ct, cr, s, x_r, N, t);

                % Compute center of pressure
                [Cp] = CP(d, N, cr, ct, s, x_r, dist_base, nosecone, K1, Ln, Lbt, d1, d2, L, Mach);

                % Calculate static margin
                SM1 = (Cp - CG) / d;

                % Verify static margin constraints
                if SM1 >= SM_min && SM1 <= SM_max
                    % Compute flutter velocity
                    Vflutter = Vf(x_r, cr, ct, s, t, tet0, p0, h_burnout, GE);

                    % Verify flutter constraints
                    if Vflutter < V_burnout
                        continue
                    end
                else
                    continue
                end

                %% OPTIMIZATION BASED ON FIN PARAMETER WEIGHTS
                % [1] Tola, C., & Yildirim, M. (2019). "Effects of Different Fin Shapes on Apogee and
Stability of
                % Model Rockets"

                % Initialize baseline geometry at first iteration
                if i == 0
                    S0     = s;
                    SWEEP0 = sweep;
                    T0     = t;
                    SXT0   = s * t;
                    CR0    = cr;
                    CT0    = ct;
                end

                % Current geometry for comparison
                S1     = s;
                SWEEP1 = sweep;
                T1     = t;
                SXT1   = s * t;
                CR1    = cr;
                CT1    = ct;

                % Apply literature-derived weights to normalized parameter changes
                DIFF_NORM = -(S1 - S0) * 0.15 / S0 ...
                            + (SWEEP1 - SWEEP0) * 0.271 / SWEEP0 ...
                            - (T1 - T0) * 0.45 / T0 ...
                            - (SXT1 - SXT0) * 0.019 / SXT0 ...
                            + (CR1 - CR0) * 0.023 / CR0;

                % Skip if no improvement
                if DIFF_NORM < 0
                    continue
                else
                    % Update baseline to improved geometry
                    S0     = s;
                    SWEEP0 = sweep;
                    T0     = t;
                    SXT0   = s * t;
                    CR0    = cr;
                    CT0    = ct;
                end

                % Log parameters for configurations that yield improvements
                stampa(CG, MTOT_carico, SM1, Cp, Vflutter, t, s, cr, ct, x_r, rad2deg(sweep), j);

                % Increment counter for recorded improvements
                i = i + 1;
```

```
            end
        end
    end
end
function [ct0,cr0,taper,s0,sweep0,N0,t0,GE,density_carbonfiber,density_nomex,dist_base,t_cf_ext,t_cf_int,t_nomex,l_panel]
= data_fins()

% GEOMETRY - lengths in meters
sweep0 = 55:0.5:70;         % sweep angle if iterating fins type 3

cr0 = 0.35:-0.02:0.25;      % Root chord length
ct0 = 0;                    % Tip chord length
taper = 0.3;

s0 = 0.16:-0.005:0.155;     % Span
N0 = 3;                     % Number of fins [3/4]
t0 = 0.0076;                % Thickness

l_panel = 0.34;             % Maximum panel width for fin (x-direction)

% STRUCTURE
E_cf = 33500000;            % Tensile modulus in psi - Epoxy/Carbon Fiber Composite
nu_cf = 0.3;                % For Carbon Fiber AS4 3k
G_cf = E_cf/(2*(1+nu_cf));  % Shear modulus in psi

% G_nomex = 24 MPa = 3481.4 psi
G_nomex = 3481.4;           % Shear modulus in psi (shear resistance modulus)
t_nomex = 3;                % mm (2 plies)
t_cf_ext = 0.6;             % mm (2 plies, external layers)
t_cf_int = 0.4;             % mm (1 ply, internal layer)

% Equivalent shear modulus of the sandwich structure [psi]
GE = (2*G_nomex*t_nomex + 2*G_cf*t_cf_ext + G_cf*t_cf_int) / ...
     (2*t_nomex + 2*t_cf_ext + t_cf_int);

density_carbonfiber = 1.78;           % g/cm^3
density_nomex = 48;                   % kg/m^3
density_nomex = density_nomex / 1000; % g/cm^3
dist_base = 0;                        % cm distance from tube base
end


function [nosecone0, K10, Ln0, Lntang] = data_nose()
%% NOSECONE GEOMETRY
% The nosecone geometry is determined by the variable "nosecone" and a
% specific parameter K1, which has a meaning depending on the selected geometry.

nosecone0 = 6; % Type identifier
K10       = 0; % Geometry-specific parameter

% Nosecone type options:
% 1 = Conical
% 2 = Ogive, K1 ranges from 0 to 1
%        K1 = 0 -> cone
%        K1 = 1 -> tangent
% 3 = Hemispherical/Elliptical
% 4 = Parabolic, K1 ranges from 0 to 1
%        K1 = 0.5 -> half parabola
%        K1 = 0.75 -> three-quarters parabola
%        K1 = 1 -> full parabola
% 5 = Power-law
%        K1 = 0.5 -> n-power law
% 6 = Haack Series
%        K = 0 -> Von Karman
%        K = 1/3 -> LV_Haack

%% NOSECONE DIMENSIONS - lengths in meters
Lntang = 0.2;  % Tangent section length along the tube
```

```
Ln0    = 0.45; % Curved nosecone length (including tip)

% The nose tip is always approximated as a continuation of the main curve
end


function [d1, d2, Lbt] = data_tail()
% Boat Tail Parameters
% Lbt0 = 0.10;   % Boat tail length [m]
% d1 = d;       % Initial diameter of boat tail [m]
% d2 = 0.058;   % Final diameter of boat tail [m]

d1 = 0.15;      % Initial diameter [m]
d2 = 0.092;     % Final diameter [m]
Lbt = 0.116;    % Boat tail length [m]
end

function [xCG_Tubo_carico, M_Tubo_carico, d, tubo1, tubo2, tubo3] = data_tube()
%% TUBE AND ROCKET DIMENSIONS - in meters
d = 0.15;       % Diameter [m]
tubo1 = 0.72;   % Length of external tube sections [m]
tubo2 = 0.36;
tubo3 = 1.06;

%% PREVIOUSLY COMPUTED TUBE CENTER OF GRAVITY
% Center of gravity of the tube alone (without fins)
xCG_Tubo_carico = 176;  % cm, CG of the tube without fins
M_Tubo_carico  = 26824; % g, mass of the tube without fins
end

function [tet0,p0,h_burnout,V_burnout,Mach,SM_min,SM_max] = data_mission()
% Mission parameters
tet0 = 15;          % Ground temperature [°C]
p0 = 101.325;       % Ground pressure [kPa]
h_burnout = 750;    % Burnout altitude [m]
V_burnout = 258;    % Burnout velocity [m/s]

% Temperature at burnout (converted to Kelvin)
tet = tet0 - (0.0065 * h_burnout) + 273.15;

% Speed of sound at burnout altitude [m/s]
Vs = sqrt(401.8 * tet);

% Mach number at burnout
Mach = V_burnout / Vs;

% Stability margin objectives
SM_min = 1.55;
SM_max = 1.80;
end

function [XCGm_carico, MTOT_carico] = Cg(L, ctm, crm, sm, x_rm, N, tm)
%% STRUCTURAL DATA
[~,~,Lbt] = data_tail();
[~,~,~,~,~,~,~,~,density_carbonfiber, density_nomex, dist_base, tmm_cf_est, tmm_cf_int, tmm_nomex, ~] =
data_fins();
[xCG_Tubo, M_Tubo, ~, ~, ~, ~] = data_tube();

%% CONVERT INPUTS TO CENTIMETERS
ct = ctm * 100;      % Tip chord [cm]
cr = crm * 100;      % Root chord [cm]
s  = sm * 100;       % Span [cm]
x_r = x_rm * 100;    % Longitudinal sweep distance [cm]
t  = tm * 100;       % Fin thickness [cm]

t_cf_est = tmm_cf_est / 10;  % External carbon layer thickness [cm]
t_cf_int = tmm_cf_int / 10;  % Internal carbon layer thickness [cm]
t_nomex  = tmm_nomex / 10;   % Nomex layer thickness [cm]
```

```
%% FINS MASS AND CENTER OF GRAVITY
A_fin = (ct + cr) * s / 2;                    % Fin surface area [cm^2]

% Mass of carbon fiber panel
V_fins_carb = (t_cf_est*2 + t_cf_int) * A_fin;
M_fins_carb = V_fins_carb * density_carbonfiber;

% Mass of Nomex panel
V_fins_nomex = t_nomex * 2 * A_fin;
M_fins_nomex = V_fins_nomex * density_nomex;

% Mass of fin side panels (approximation)
V_fins_lato = t * t_cf_est * (cr + ct + 2*s);
M_fins_lato = V_fins_lato * density_carbonfiber;

% Center of gravity of a single fin panel [cm]
xCG_fins_panel = (cr^2 + cr*ct + ct^2 + x_r*(cr + 2*ct)) / (3*(ct + cr));

% Total fin mass and CG position along rocket axis
M_TOT_fins = N * (M_fins_carb + M_fins_nomex + M_fins_lato);
xCG_fins = L*100 - Lbt - dist_base - cr + xCG_fins_panel;

%% TOTAL ROCKET (WITH MOTOR)
MTOT_carico = M_Tubo + M_TOT_fins;                    % Total mass [g]
XCG_carico = (xCG_Tubo*M_Tubo + xCG_fins*M_TOT_fins) / MTOT_carico;  % Weighted CG [cm]
XCGm_carico = XCG_carico / 100;                       % CG in meters

end


function [CP] = CP(d, N, cr, ct, s, x_r, dist_base, nosecone, K1, Ln, Lbt, d1, d2, L, Mach)
% Reference:
% [2] J. S. Barrowman, "The Practical Calculation of the Aerodynamic Characteristics of Slender Finned
Vehicles," NASA Technical Paper.
% [3] Crowell, "Descriptive Geometry of Nosecones," 1996.
% [4] "Calculating the Centre of Pressure of a Model Rocket," Rocketry Handbook.

%% FIN PARAMETERS
% Sweep angle of fin leading edge
sweep = atan((1/s) * (x_r + 0.5*(ct - cr)));

% Mean aerodynamic chord
l = s / cos(sweep);

% Tube radius
R = d/2;

% Factor depending on number of fins
if N == 3 || N == 4
    f = 1;
elseif N == 6
    f = 0.5;
end

% Normal force coefficient slope for fins at alpha = 0
CN_f = (1 + (f * R)/(s + R)) * ( (4 * N * ( (s/d)^2 )) / ...
       (1 + sqrt(1 + ((2*l)/(cr+ct))^2)) );

%% MACH < 0.5 - FIN CENTER OF PRESSURE
% Distance from rocket tip to fin leading edge
x_f = L - cr - Lbt - dist_base/100;  % dist_base converted from cm to m

% Barrowman method chord terms
CAM  = 2/3 * (cr + ct - (cr * ct)/(cr + ct));
xCAM = (x_r * (cr + 2*ct)) / (3*(cr + ct));

% Fin center of pressure position from rocket tip
Xf = x_f + xCAM + CAM*0.25;
```

```
%% NOSE CONE
% Normal force coefficient for nose at alpha = 0
CN_n = 2;  % Assumed constant for all nose types

% Nose cone center of pressure depends on geometry type
switch nosecone
    case 1  % Conical [3][4]
        Xn = 2/3 * Ln;
    case 2  % Ogive [3][4]
        Xn = 0.466 * Ln;
    case 3  % Hemispherical/Elliptical [3]
        Xn = 0.333 * Ln;
    case 4  % Parabolic [3][4]
        Xn = 0.5 * Ln;
    case 5  % Power-law [3], formula from RASAero tests
        Xn = (K1*10)/(5 + K1*10) * Ln;
    case 6  % Von Karman / Haack [3]
        if K1 == 0
            Xn = 0.5 * Ln;   % Von Karman
        else
            Xn = 0.437 * Ln; % Haack
        end
end

%% BOAT TAIL
% Normal force coefficient slope for boat tail at alpha = 0
CN_b = 2 * ( (d2/d)^2 - (d1/d)^2 );

% Distance from rocket tip to boat tail start
x_cs = L - Lbt;

% Boat tail center of pressure position
Xb = x_cs + (Lbt/3) * (1 + (1 - d1/d2)/(1 - (d1/d2)^2));

%% OVERALL CENTER OF PRESSURE
% Weighted average using normal force coefficients
CP = (CN_n*Xn + CN_b*Xb + CN_f*Xf) / (CN_n + CN_b + CN_f);
end


function Vf = Vf(x_r, cr, ct, s, t, tet0, p0, h_burnout, GE)
% Reference:
% [5] NACA TN 4197, "Summary of Flutter Experiences as a Guide to the Preliminary Design of Lifting
Surfaces on Missiles"
    % Calculate temperature in Celsius at altitude h
    tet = tet0 - (0.0065 * h_burnout);  % Temperature in Celsius at altitude h

    % Define sea-level standard pressure in psi
    p0_psi = 14.696;  % Sea-level standard pressure in psi

    % Calculate atmospheric pressure at altitude
    p = 101.29 * ((tet + 273.1) / 288.08) ^ 5.256;  % Atmospheric pressure in KPa

    % Calculate geometric mean aerodynamic chord area
    A = 0.5 * (cr + ct) * s;  % Geometric mean aerodynamic chord area
    AR = (s^2) / A;           % Aspect ratio (unitless)
    lamda = ct / cr;          % Taper ratio (unitless)

    % Calculate speed of sound at altitude
    a = 20.05 * sqrt(273.16 + tet);  % Speed of sound in m/s

    % Calculate aerodynamic center location
    Cx = ((2 * ct * x_r) + ct^2 + (x_r * cr) + (ct * cr) + cr^2) / (3 * (cr + ct));  % Aerodynamic
center location
    eps = (Cx / cr) - 0.25;  % Distance from aerodynamic center to quarter chord (unitless)

    % Define air properties
    k = 1.4;  % Ratio of specific heats (unitless)
```

```
    % Calculate dynamic pressure at sea level
    DN = (24 * eps * k * p0_psi) / pi;  % Dynamic pressure at sea level in psi

    % Calculate flutter velocity
    Vf = a * sqrt(GE / ((DN * (AR^3) / (((t / cr)^3) * (AR + 2))) * ((lamda + 1) / 2) * (p / p0)));
end
```

Nosecone and Fin-Set simulation results

The following simulations were carried out using outdated configurations, which did not take into account surface roughness or the presence of rail guides and screws. Since then, the rocket's mass has changed, while the position of the center of gravity has remained largely unchanged. Since the optimization results depend only on the center of gravity, and not on the mass or aerodynamic drag coefficient, they remain valid, as do the conclusions derived from these analyses.

The results presented below in Table 1 to 3 show the configurations tested for the nosecone and fins, obtained using RASAero and the optimization software MatFins. The tables include key parameters such as apogee (outdated but useful for visualizing the code's functionality), static margin, center of pressure, final velocity, and geometric dimensions, and they guided the selection of the final configuration adopted for the Nemesis rocket.

Table 1: Nosecone comparison.

Parameter	Von Kármán	Tangent Ogive
Apogee (m)	3204	3190
Static Margin (cal.)	1.566	1.557
CP (m)	2.007	2.006
Chord Root (cm)	29.00	31.00
Tip Chord (cm)	8.30	9.30
Span (cm)	16	16
Sweep (°)	57.50	57.00
Thickness (cm)	0.76	0.76

Table 2: Apogee check in RASAero for fin iterations.

Iter	Apogee (RASAero) (m)
2	3176.03
14	3176.65
26	3177.57
39	3190.23
51	3190.85
64	3203.50

Table 3: Fin iterations.

Iter	Mass (g)	SM (cal.)	CP (m)	Flutter vel. (m/s)	Thickness (mm)	Root chord (cm)	Tip chord (cm)	Span (cm)	Sweep dist (cm)	Sweep (°)
2	27165	1.581	2.010	827.769	7.6	33.00	9.90	16.00	22.85	55.00
14	27165	1.579	2.010	822.163	7.6	33.00	9.90	16.00	23.28	55.50
26	27165	1.577	2.009	816.530	7.6	33.00	9.90	16.00	23.72	56.00
39	27145	1.587	2.010	799.127	7.6	31.00	9.30	16.00	24.17	56.50
51	27145	1.582	2.010	793.427	7.6	31.00	9.30	16.00	24.64	57.00
64	27125	1.566	2.007	775.384	7.6	29.00	8.70	16.00	25.11	57.50